National Centre for Nuclear Research
Andrzeja Sołtana 7 Str.
05-400 Otwock, Poland
Radiation Detectors Division (TJ3)

PhD dissertation

Photofission of nuclear materials and fission signatures detection with application in border monitoring

Paweł Sibczyński

The PhD dissertation supervised
by Prof. dr hab. Jan Kownacki
and dr Agnieszka Syntfeld-Każuch

15 July 2015

Mojej małżonce Emilii, rodzicom i bratu
For my wife Emilia, parents and brother

Podziękowania

Poniższa rozprawa doktorska jest efektem pracy wielu osób, które przyczyniły się do jej końcowej formy. Pragnę szczególnie gorąco podziękować promotorowi tej pracy, prof. dr hab. Janowi Kownackiemu oraz dr Agnieszce Syntfeld-Każuch, pełniącej rolę promotora pomocniczego, za okazane wsparcie w dążeniu do sfinalizowania tego materiału. Szczere podziękowania należą się również prof. Markowi Moszyńskiemu, który zawsze służył swoim doświadczeniem i cennymi radami w dziedzinie materiałów scyntylacyjnych. Dziękuję również za zaufanie, jakim mnie obdarzyliście, przyjmując mnie do grona grupy naukowej Zakładu TJ3. Podziękowania kieruję również kolegom i koleżankom z Zakładów TJ2 - w szczególności Panu Krzysztofowi Winclowi i Pani Barbarze Zarębie za przeprowadzone symulacje Monte Carlo wydajności detektora ^{3}He, TJ3 (szczególne podziękowania dla Joanny Hanke-Iwanowskiej za współpracę w ogólnym tego słowa znaczeniu) oraz TJ4 (głównie Michałowi Gierlikowi za wsparcie podczas pomiarów aktywacji neutronowej scyntylatora BaF_2).

Wyrazy wdzięczności należą się również kolegom i koleżankom z CEA LIST w Saclay we Francji, w szczególności Frédérickowi Carrel oraz Matthieu Hamel za fantastyczną współpracę w tematyce fotorozszczepienia oraz produkcji organicznych materiałów scyntylacyjnych, jak również Fredericowi Lainé za poświęcony czas w obiekcie SAPHIR przy operowaniu akceleratorami liniowymi. Również chciałbym podziękować Pauline Blanc, Adrien Sari, Marion Ledieu oraz Evie Montbarbon za udaną współpracę w ramach programu wymiany osobowej POLONIUM.

A spoza pracy, chcę podziękować mojej żonie Emilii, rodzicom, bratu oraz przyjaciołom - za to, że jesteście i wspieracie mnie na każdym kroku, który pokonuję.

Thanks

The PhD dissertation is a result of work of many people, whose contributed to the final form of the thesis. Primarily, I would like to thank my supervisor prof. dr hab. Jan Kownacki and Agnieszka Syntfeld-Każuch, who had a role as a supportive supervisor, for thorough support during preparation of the thesis. Warm thanks should be also directed to prof. Marek Moszyński, who served his experience and knowledge in the matter of scintillation materials. I also thank you for the confidence you bestowed to me, inviting me to the Radiation Detectors Division (TJ3) scientific group. Moreover, I am very thankful to my teammates from the TJ2 Department (especially to Mr. Kszysztof Wincel and Mrs. Barbara Zaręba for performing the MCNPX simulations of gaseous ^{3}He detector), TJ3 (especially to Joanna Hanke-Iwanowska) as well as TJ4 (principally to Michał Gierlik for support in activation measurements of BaF_2 scintillator).

Special thanks are also directed to my colleagues from CEA LIST, Saclay France, especially to Frédérick Carrel and Matthieu Hamel for the fruitful collaboration in the field of photofission and development of organic scintillators, as well as to Frederic Lainé for taking time to operate the LINAC in SAPHIR facility. I would also thank to Pauline Blanc, Adrien Sari, Marion Ledieu and Eva Montbarbon for the effective collaboration within the frame of POLONIUM staff exchange program.

And outside of work, I want to thank my wife Emilia, parents, brother and friends - for the fact that you are and you support me in every step I take.

Streszczenie

Motywacją przedstawionej pracy doktorskiej jest przeprowadzenie badań nad nowymi technikami oraz materiałami scyntylacyjnymi do detekcji promieniowania charakterystycznego powstałego w wyniku fotorozszczepienia materiałów jądrowych (zarówno rodnych jak i rozszczepialnych), jako jeden z celów nierozprzestrzeniania materiałów rozszczepialnych i bezpieczeństwa wewnętrznego. Fotorozszczepienie materiału jądrowego polega na jego wzbudzeniu za pomocą wysokoenergetycznych fotonów o energii powyżej 6 MeV. Wzbudzone jądro rozpada się na dwa fragmenty (produkty fotorozszczepienia) po czasie 10^{-15} s, jednocześnie emitując natychmiastowe promieniowanie w postaci neutronów i promieniowania γ. Ponadto, wzbudzone jądra atomowe ulegają rozpadowi β^-, emitując neutrony opóźnione z czasem połowicznej emisji od kilkuset ms aż do około minuty, a także opóźnione promieniowanie γ. W rozprawie doktorskiej zawarto dokładną analizę linii γ emitowanych z materiału rozszczepialnego (100 g U, wzbogaconego do 93% ^{235}U) po naświetleniu fotonami o energii maksymalnej 15 MeV z akceleratora liniowego (LINAC). Co więcej, wykonano po raz pierwszy pomiary wydajności detekcji prędkich neutronów z ^{252}Cf za pomocą scyntylatorów zawierających ^{19}F, takich jak EJ-313 oraz BaF_2, stosując metodę aktywacji progowej (ang. Threshold Activation Detection - TAD). Powyższe scyntylatory zostały zastosowane do detekcji natychmiastowych neutronów powstałych w wyniku fotorozszczepienia materiału jądrowego. W ramach pracy doktorskiej, pomiary przeprowadzone zostały w NCBJ oraz w CEA LIST w Saclay we Francji. Ponadto, wytworzono całkowicie nowy scyntylator plastikowy na bazie pentafluorostyrenu (F-plastic). Zawartość fluoru w tym scyntylatorze wynosi 3,73 $\times 10^{22}$ atomów/cm^3 i jest to obecnie największa ilość atomów fluoru, jaką udało się uzyskać w przypadku scyntylatora plastikowego. Celem produkcji takiego scyntylatora jest znalezienie alternatywy o dobrym stosunku ceny do wydajności na neutrony na łatwopalny i toksyczny ciekły scyntylator fluorokarbonowy EJ-313, który posłużyłby do rejestracji natychmiastowych neutronów techniką TAD z fotorozszczepienia materiału jądrowego.

Abstract

The motivation of this PhD dissertation is the research of novel techniques and scintillation materials for photofission signature detection from nuclear materials (both fertile and Special Nuclear Materials (SNM)), as an element of non-proliferation and safety. Photofission relies on the fission of heavy nuclei using photons carrying energy above 6 MeV. The induced heavy nuclei decay into two fragments (photofission products) and then, within 10^{-15} s, prompt radiation in the form of neutrons and γ-rays are emitted. The photofission products undergo the β^- decay, emitting delayed neutrons with a half-life from hundred ms up to about one minute and delayed γ-rays, as well. The PhD dissertation contains precise analysis of γ lines emitted from SNM (100 g U, enriched to 93% ^{235}U) excited by high energy Bremsstrahlung photons with energy endpoint of 15 MeV, produced by a linear accelerator (LINAC). For the first time, the efficiency of fast neutron detection from ^{252}Cf with scintillators containing ^{19}F, such as the fluorocarbon EJ-313 and BaF_2, was measured using a Threshold Activation Detection (TAD) technique. Next, the above mentioned scintillators were applied to the detection of prompt neutrons from photofission of nuclear materials. The measurements were carried out at NCBJ and CEA LIST, Saclay, France. Furthermore, a new type of plastic scintillator based on pentafluorostyrene was developed (F-plastic). The amount of fluorine is about 3.73 $\times 10^{22}$ F atoms/cm^3 and currently it is the highest amount of fluorine atoms obtained for plastic scintillators. The F-plastic is considered a cost-efficient alternative to liquid fluorocarbon scintillators, such as the toxic and flammable EJ-313, also possible to use in TAD technique for prompt neutrons detection from nuclear materials.

The PhD dissertation is based on the following papers:

1. P. Sibczynski, J. Kownacki, A. Syntfeld-Kazuch, M. Moszynski, M. Kisielinski, W. Czarnacki, K. Kosinski, M. Matusiak, M. Klimasz, M. Kowalczyk, T. Abraham, J. Mierzejewski, J. Srebrny, "Decay chains and photofission investigation based on nuclear spectroscopy of highly enriched uranium sample", Applied Radiation and Isotopes, vol. 82, pp. 170-174, 2013.

2. W. Klamra, P. Sibczynski, M. Moszyński, W. Czarnacki, V. Kozlov, "Extensive studies on light yield nonproportional response of undoped CeF_3 at room and liquid nitrogen temperatures", Journal of Instrumentation, vol. 8, pp. P06003, 2013.

3. M. Hamel*, P. Sibczynski*, P. Blanc, J. Iwanowska, F. Carrel, A. Syntfeld-Każuch, S. Normand, "A fluorocarbon plastic scintillator for neutron detection: Proof of concept", Nuclear Instruments and Methods in Physics Research Section A: Accelerators, Spectrometers, Detectors and Associated Equipment, vol. 768, pp. 26-31, 2014 (* these authors have contributed equally)

4. P. Sibczynski, J. Kownacki, M. Moszyński, J. Iwanowska, A. Syntfeld-Każuch, A. Gójska, M. Gierlik, Ł. Kaźmierczak, E. Jakubowska, G. Kędzierski, Ł. Kujawiński, F. Carrel, M. Ledieu, F. Lainé, "Verification of threshold activation detection (TAD) technique in prompt fission neutron detection using scintillators containing ^{19}F", Journal of Instrumentation 010T_0215, Accepted Manuscript, 2015.

Other publications which partially contributed to the PhD dissertation:

1. J. Iwanowska, L. Swiderski, M. Moszynski, T. Szczesniak, P. Sibczynski, N. Z. Galunov, N. L. Karavaeva, "Neutron/gamma discrimination properties of composite scintillation detectors", Journal of Instrumentation, vol. 6, no. 07, pp. P07007, 2011.

2. P. Sibczynski, M. Moszyński, T. Szczęśniak, W. Czarnacki, "Study of NaI(Tl) scintillator cooled down to liquid nitrogen temperature", Journal of Instrumentation, vol. 7, no. 11, pp. P11006, 2012.

3. W. Klamra, P. Sibczynski, M. Moszyński, V. Kozlov, "Light yield nonproportionality of doped CeF_3 scintillators", Journal of Instrumentation, vol. 9, pp. P07013, 2014.

4. J. Iwanowska-Hanke, M. Moszynski, L. Swiderski, P. Sibczynski, T. Szczesniak, T. Krakowski and P. Schotanus, "Comparative study of large samples (2" $\times$ 2") plastic scintillators and EJ309 liquid with pulse shape discrimination (PSD) capabilities", Journal of Instrumentation, vol. 9, no. 06, pp. P06014, 2014.

5. S. Korolczuk, S. Mianowski, J. Rzadkiewicz, P. Sibczyński, Ł. Świderski, I. Zychor, "Digital approach to high count rate gamma-ray spectrometry", Submitted to IEEE Trans. Nucl. Sci., 2015.

Contents

List of Figures

List of Tables

Chapter 1

Introduction

Nuclear fission is a nuclear reaction in which a heavy atomic nucleus (A $>$ 200) splits into two lighter nuclei. This type of reaction is known as binary fission. Much more rarely, in 0.2 - 0.4 % of events, the fission can lead to decay into three fragments; this type of reaction is called ternary fission. In the two-fragment decay, the mass distribution of the heavier and lighter nuclei, created due to disintegration, is slightly different for each type of heavy atom. Disintegration is associated with the release of huge amount of energy, which is about 200 MeV per one event. The fission process is especially associated with the very heavy nuclei, which comprise more neutrons than protons. It can occur either spontaneously or due to inducing the nuclei using high energy photons or neutrons (fast or thermal, depending on the induced nuclear material) as well as heavy ion. The fission results in the emission of prompt and delayed radiation, which takes a significant amount of energy. The former is emitted within 10^{-14} - 10^{-15} s, the latter are emitted some time after disintegration.

Nuclear fission phenomenon was discovered in 1938 by Lise Meitner, her nephew Otto Frisch and two radiochemists: Otto Hahn and Fritz Strassman [1]. Hahn and Strassman introduced the term "uranium fission" for the first time. Lise Meitner was the first who used the term "nuclear fission" and correctly interpreted the results previously obtained by Hahn [2]. Fission was observed due to the bombardment of the uranium sample with neutrons and the registration of barium nuclei. Hahn received the Nobel prize in 1944, but, unfortunately, the committee omitted the contribution

of Lise Meitner to this discovery. In fact, some historians believe that Meitner should have been awarded the Nobel prize together with Hahn.

On the basis of the liquid drop model of atomic nucleus, few groups from scientific laboratories predicted the photofission process [3, 4]. Feenberg concluded that the energy required to enable the uranium isotope to pass through the potential energy hill was relatively low (only a few million volts). He calculated that nucleus deformation parameter $2E_s/E_c$ was equal to 1.20 for the ^{238}U, where E_s and E_c stand for surface and Coulomb contribution in the drop model, respectively. This means that if the surface barrier E_s is low, then the additional energy provided to the Coulomb contribution E_c - by γ-rays or particles - may overcome the surface potential E_s and, finally, result in fission of the nucleus. Thus, natural uranium and other heavy nuclei could easily become fissile after interaction with high-energy γ-rays or particles.

Three years later, in 1941, Haxby et al. measured thw photofission signatures from uranium and thorium [5]. Photofission was observed due to irradiation of the samples with 6.1 MeV γ-rays from fluorine-based target (CaF_2 and AlF_3 metals) bombarded with protons having an approximate energy of about 3.5 MeV. The photofisson products from the irradiated uranium foil were registered by ionization chamber and visualized on oscilloscope, 41 fission events were observed during a 295 s measurement run at a geometrically solid angle of 1.31%. In this paper [5], the number of fissions per unit of γ-ray intensity was measured with a Geiger counter. The proton energy was 3.4 MeV at a beam current of 0.5 μA.

The discovery of neutron fission opened the way not only for the development of nuclear power plants, but also for a nuclear weapon. On August the 2^{nd}, 1939, Leó Szilárd - Hungarian–American physicist - wrote a letter of caution and persuaded Einstein to sign it and forward it to US President, F. D. Roosevelt. The letter contained the information that Germany could have the knowledge and capability to produce a nuclear bomb. This led to the establishment of the US Manhattan Project in 1942, on which Meinter refused to work. The Manhattan Project led to development of the nuclear bombs. Two of them were dropped on Hiroshima and Nagasaki in 1945, resulted in death toll of several hundred thousands people.

In the present day, in order to induce photofission of nuclear materials, high energy

linear accelerators (LINACs) are used, offering the dose rate of several Gy × min at 1 meter and energies of Bremsstrahlung photons reaching even 30 MeV at the endpoint energy, e.g. the LINAC at Intense Resonance Neutron Source (IREN) in Dubna, Russia. This LINAC is used as a time-of-flight, high resolution neutron spectrometer [6]. For safety reasons, only the LINAC offering the Bremsstrahlung endpoint energy at 9 MeV can be applied to border monitoring. On the one hand, Bremsstrahlung photons of high energy from the LINAC are very penetrative and large amounts of photoneutrons are also produced, on the other hand. Specifically, photoneutrons can be a serious problem in medical applications, because they can cause secondary cancers for patients and also expose hospital staff to deactivation γ-rays after the irradiation. All nuclear materials can undergo photofission after irradiation with high energy photons of above 6 MeV. In general, the LINAC-based approach can be applied in many fields of industry, such as:

1. Homeland Security and border monitoring, for non-intrusive inspection (NII) of cargo containers aiming at the prevention of illicit trafficking of nuclear materials - this field of application will be thoroughly discussed in this dissertation.

2. Application in the transmutation of nuclear materials for fission of long living nuclei into those having a shorter half-life [7].

3. Characterization of bulky nuclear waste packages in order to classify the storage method [8].

4. Fundamental physics, such as the above mentioned IREN source [6].

The fissionable materials (named also nuclear materials) are divided into two categories:

1. Fertile materials - ^{234}U, ^{238}U or ^{232}Th can be classified as natural fertile materials. In general, they are nuclei capable of undergoing fission - even with low probability - after capturing a high energy neutron. They are unable to undergo fission by slow neutrons and are not capable of sustaining a nuclear fission chain reaction. Their reaction cross section becomes significant for the neutrons carrying the energy above 1 MeV, and thus, cannot be used for the critical mass in a nuclear bomb. According to the International Atomic Energy Agency (IAEA) glossary, the above mentioned materials are Indirect Use Nuclear Materials. The amount

of 10 t of natural ^{238}U or 20 t of the depleted ^{238}U or ^{232}Th are considered to be a "Significant Quantity" from the point of view of security aspects. Moreover, 75 kg of U enriched to below 20% is also considered to be an Indirect Use Nuclear Material.

2. Fissile materials (known as Special Nuclear Materials (SNM)) - these materials are a subset of the fissionable materials. Due to the significant fission cross section (582 b for ^{235}U, according to [9]) and the capability of sustaining a nuclear fission chain reaction with neutrons of any energy, they can be used as a material creating the critical mass in a nuclear bomb. It is worth pointing out that about 50 kg of highly enriched uranium is sufficient to produce a nuclear bomb (the enrichment value of 80% is considered military grade). Thus, particular monitoring of such materials is strictly required in order to prevent their illicit trafficking. According to the IAEA specifications, 25 kg of ^{235}U (enriched to above 20%), 8 kg of ^{233}U or 8 kg Pu (less than 80% of ^{238}Pu) are assigned as a "Significant Quantity" of the SNM and are considered to be Direct Use Nuclear Materials.

Since 11 September 2001, when the World Trade Center accident took place, the term "terrorism" has become more important than ever before. The act changed the world and accelerated further investigation in the field of Homeland Security and border monitoring in order to find an efficient and precise way of identifying possible threats, such as the illegal transfer of drugs, explosives, chemical weapons, radioactive and nuclear materials through the border via trucks, ports and airports.

The motivation of this PhD dissertation is the investigation of novel techniques and scintillation materials for photofission signatures detection from nuclear materials, as an element of non-proliferation. The current political situation, especially the uncontrolled establishment of the Islamic State of Iraq and the Levant (ISIS), requires that we pay particular attention to this aspect. As an example, in 2014 several kilograms of uranium were stolen in Mosul city, Iraq [10]. Thus, the interest in the illegal possession of such a material is observed. Although small quantities of nuclear materials are useless and production of a nuclear bomb is an exceptionally complex problem, the above mentioned topic should not be ignored. Moreover, additional potential risk is related to the production of dirty bombs (radiological dispersal devices (RDD)), which

are based on conventional explosives coupled to nuclear material. Such types of bombs are impractical for several reasons: due to the long half-life of nuclear materials and some radioactive materials the environmental contamination would be rather low. Nevertheless, fear generated in the community after such an attack could be a real problem - thus, some people call such a bomb "psychological". In the case of measurable radioactive contamination, removal of local construction materials could be required and this could then be exceptionally expensive. The most critical case related to the theft of the radioactive material (^{137}Cs) from a hospital occured in Goiânia city, Brasil. During the theft the ^{137}Cs source had an activity of 50.9 TBq and was transferred between many people. After this accident 4 people died and 22 were exposed to the risk of loss of life or health. A few buildings had to be demolished due to the contamination. It was the most serious radiation accident related with improper storage of a radioactive material.

This PhD dissertation describes techniques applied to the detection of nuclear materials at the borders, including delayed [11] and prompt radiation detection. An important part of the work was aimed at the precise characterization of decay chain γ-rays at an EAGLE array [12] and delayed γ-rays emitted from a 100 g uranium rod (enrichment of 93%) in the energy range from 0.25 MeV to 4 MeV [13]. Particular effort was put into prompt neutrons detection by means of the threshold activation detection (TAD) technique with organic and inorganic scintillators [14]. Moreover, in collaboration with CEA LIST, Saclay, France, a novel plastic scintillator based on pentafluorostyrene ($C_8F_5H_3$) was developed, containing a large amount of fluorine (3.73×10^{22} F atoms/cm^3) [15], which can be considered for detection of prompt photofission neutrons by means of fluorine activation. Additionally, it is highly probable that this is the densest plastic scintillator ever produced (density of 1.56 g/cm^3), even denser than the plastic scintillators based on bismuth, reaching up to 1.40 g/cm^3 [16]. This is due to the lower availability of the Bi doping in the scintillator base solution (about 17% by weight). Details about the conducted work are presented in Chapters 3-6. Summarizing conclusions were introduced in Chapter 7. In order to familiarize a reader with abbreviations, the Glossary, Chapter 8, was introduced. During the PhD dissertation several scientific programs were realized, which I gratefully acknowledge in Chapter 9. Currently,

within the C-BORD project in the frame of Horizon 2020 Program (accepted by the European Commission, stared at 06.2015), an advanced system for a threat detection will be developed. The National Centre for Nuclear Research (NCBJ) participates in this project in development of a novel system for nuclear material detection by means of prompt neutron registration. The work performed in this PhD dissertation provided strong background in this field, which resulted in participation in further development of nuclear materials detection techniques in the C-BORD project.

Chapter 2

Photofission physical processes and fission signatures of nuclear materials

2.1 Neutron fission and photofission signatures of nuclear materials

Detection of nuclear materials potentially hidden inside bulk cargo requires an efficient method which can unequivocally detect the signatures of the material's presence. Naturally emitted radiation from nuclear materials, while abundant, has rather low energy and can be easily shielded. Thus, the detection efficiency of passive methods are becoming insufficient. Therefore, active inspection methods are emerging as efficient solutions for nuclear materials detection with the use of a penetrating radiation, such as neutrons, photons or other particles [17]. Fortunately, nuclear materials exposed to fission-inducing radiation yield very unique and often strong characteristic signatures. Some of the most important photofission signatures are delayed γ-rays and neutrons as well as prompt signatures, emitted in the range of femtoseconds after the fission, such as neutrons and γ-rays. They vary significantly in magnitudes, signal-to-noise ratio, attenuation in various shieldings and applied methods of detection. As an example, delayed γ-rays have a high emission factor. However, delayed γ-rays posses drawbacks such as a significant contribution of low energy photons overlapping with a strong natural background and the fact that γ-rays can be emitted from other activated materials.

Moreover, strong contribution can rise from scattered photons generated on LINAC tungsten converter. On the other hand, delayed neutrons are very unique signatures, but are scarce, have low abundance and carry a low amount of energy, thus, they can be easily attenuated in low-Z content of a cargo container. Fission specific signatures will be described in the Subsections 2.1.1, 2.1.2, 2.1.3 and 2.1.4. They are the consequence of a nuclear fission reaction induced by Bremsstrahlung photons or neutrons. After the absorption of the probing radiation the nucleus is highly excited, it then splits into two nuclei having different atomic masses (A) between 80 - 160 [18, 19]. The fragments separate and fly-apart after $\sim 10^{-15}$ s, but before this occurs, they are "glued" by their nuclear mass, which releases part of the excitation energy by the emission of prompt neutrons and γ-rays. These fission fragments are unstable and undergo β^- decay, emitting characteristic γ-rays till the last nucleus in the β-decay chain reaches a stable state. Depending on the nucleus, the deexcitation time varies from nanoseconds up to many hours, as presented in [13]. In a few cases - when the excitation energy is especially high - the nucleus can emit not only a delayed γ-ray, but also a so-called delayed neutron. A simplified scheme of the fission process is shown in Figure 2.1.

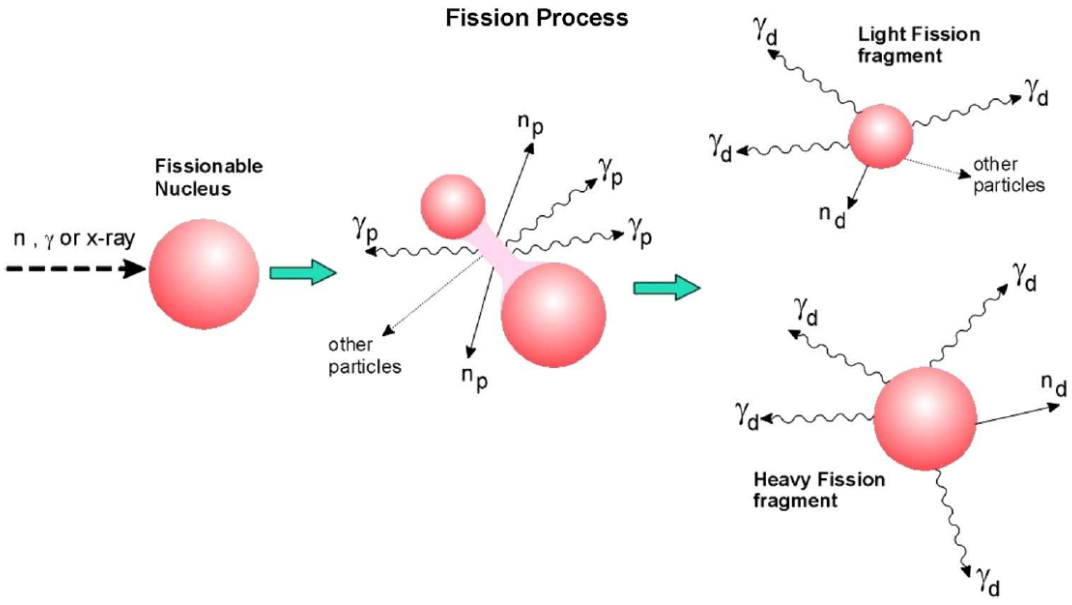

Figure 2.1: Schematics of the fission process [17].

The key parameter for the fission-based inducing technique is the fission cross section (expressed in barns, where 1 b = 10^{-24} cm^2), responsible for the interrogation rate efficiency. It depends on the probing radiation used in order to induce the fission process in nuclear materials. The fission cross section varies from 600 b for the thermal neutrons, a few hundred barns for the resonance region between 0.4 - 10 keV, and 1.2 b for fission neutrons of 2.2 MeV energy. Cross sections for the photofission process are much lower than that of neutrons, although the Bremsstrahlung flux from a LINAC is usually 5-6 orders of magnitude higher than the neutron flux from D+T and D+D neutron generators. Typically, the photofission cross section is 0.001 b for 6 MeV and rises with the energy to about 0.1 b for 10 MeV Bremsstrahlung photons. Neutron induced fission and photofission cross section scheme is shown in Figure 2.2. The cross section for materials present in the environment is presented in Figure 2.3.

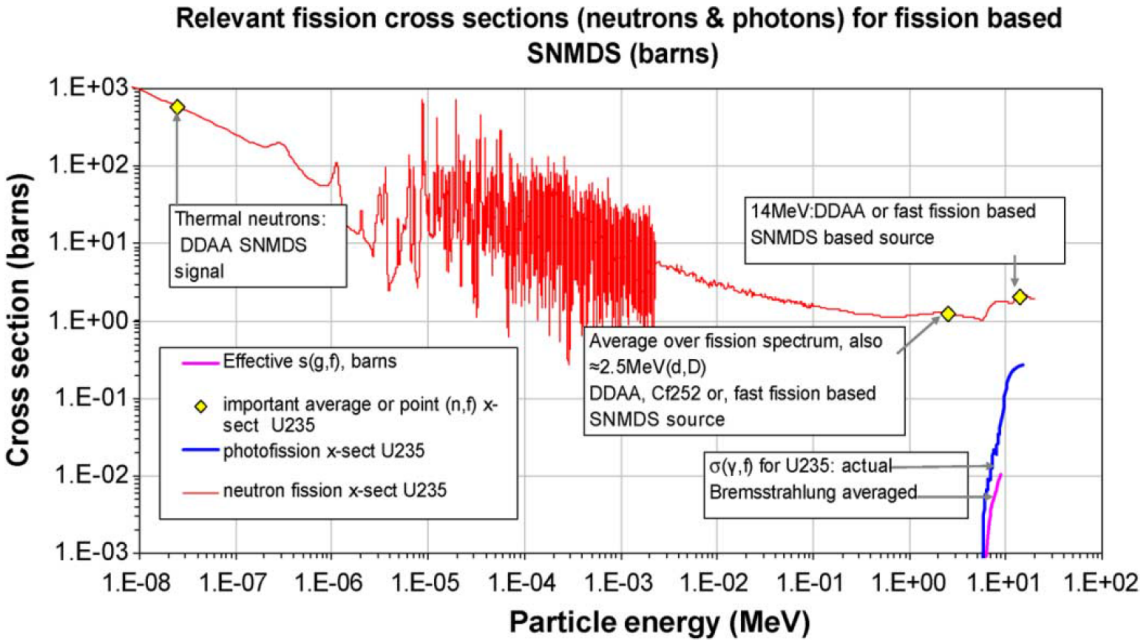

Figure 2.2: The cross section for fission and photofission of ^{235}U, taken from [17].

Besides fission specific signatures, non-fission specific signatures are also available in order to detect or characterize nuclear materials:

1. Detection of γ-rays, originated from nuclei decaying along the specific decay chain,

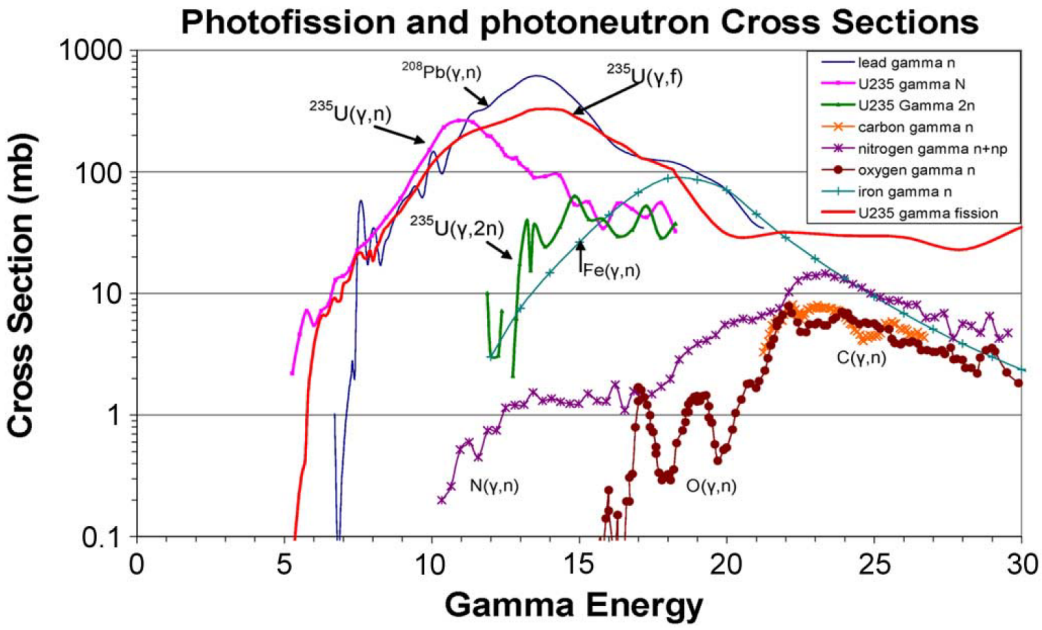

Figure 2.3: The cross section for fission and photofission of ^{235}U as well as for reactions with elements present in environment, taken from [17].

detected with use of high resolution detectors, such as high-purity germanium (HPGe) [8, 13]. These γ-rays can be also detected with plastic scintillators, showing the excess of events over natural background.

2. X-rays scattering on nuclei having a high atomic number (Z). Detection is based on use portals or cars with installed pencil-beam X-ray lamps. The X-rays backscatter on an inspected object, then, basing on the scattering angle and photon energy, it is possible to reconstruct the image with use of advanced algorithms. For example, this technique was applied in the Z-Backscatter Van (ZBV), offered by the American Science & Engineering (AS&E) company [20].

3. Muon tomography, based on the detection of muons passing through some layers of scintillators (usually plastics), providing information about angular distribution and position of the interaction. Finally, knowing the initial angular distribution of the muons before scattering on the materials inside an inspected cargo container, it is possible to determine the scattering angle by the final layer of the scintillators

and perform an image reconstruction of the cargo content [21]. Currently the method offers rather poor energy resolution in comparison with the X-ray imaging and the time required for the inspection is relatively long.

4. Nuclear Resonance Fluorescence (NRF) - is a nuclear process in which the nucleus absorbs high energy γ-rays, resulting excitation of the nucleus. Then, the nucleus releases a cascade of discrete γ photons, which are characteristic for a specific nucleus. As a source of high energy photons, a LINAC emitting Bremsstrahlung photons or laser Compton scattered (LCs) γ-rays can be used. The latter technique was proposed by [22] and further evaluated by [23] and [24] for the characterization of spent fuel. Thanks to the very good energy resolution of the scattered γ-rays exciting the analyzed nuclear material, the material emits very characteristic cascades of γ-rays to the ground state, which are recorded with HPGe detectors.

The high energy photons are obtained from a LINAC conversion target (usually tungsten (W) or tantalum (Ta)), which is bombarded by electrons of fixed energy in the range of several MeV. The energy loss of electrons on the conversion target results in emission of the Bremsstrahlung photons. As showed in Figure 2.4 [25], the energy

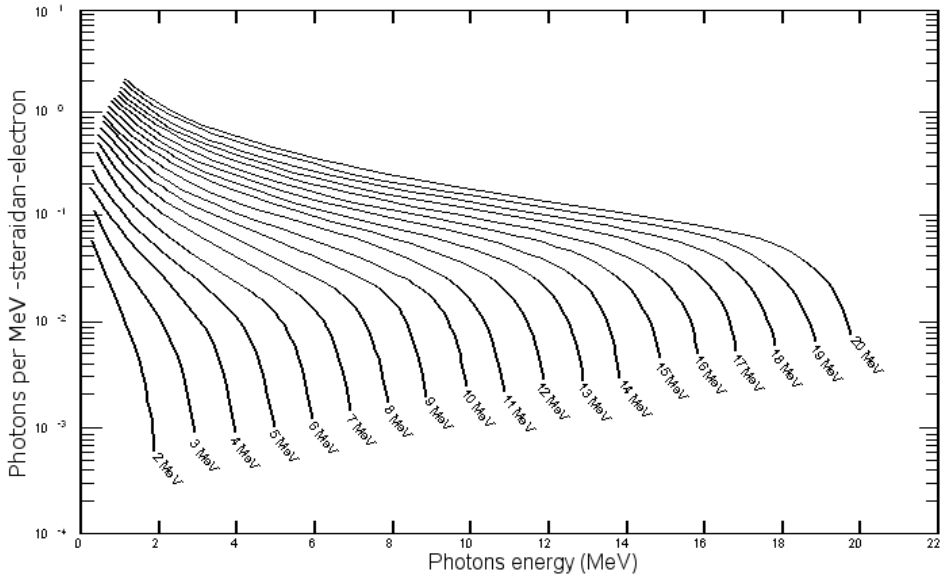

Figure 2.4: Distribution of Bremsstrahlung photons as a function of electrons [25].

distribution of the Bremsstrahlung photons is a continuum, with the photons energy endpoint close to the energy of electrons hitting the conversion target. As showed in Figure 2.5, the photofission of nuclear material can occur only between the reaction threshold E_{thr} and the Bremsstrahlung photons energy endpoint E_{max}.

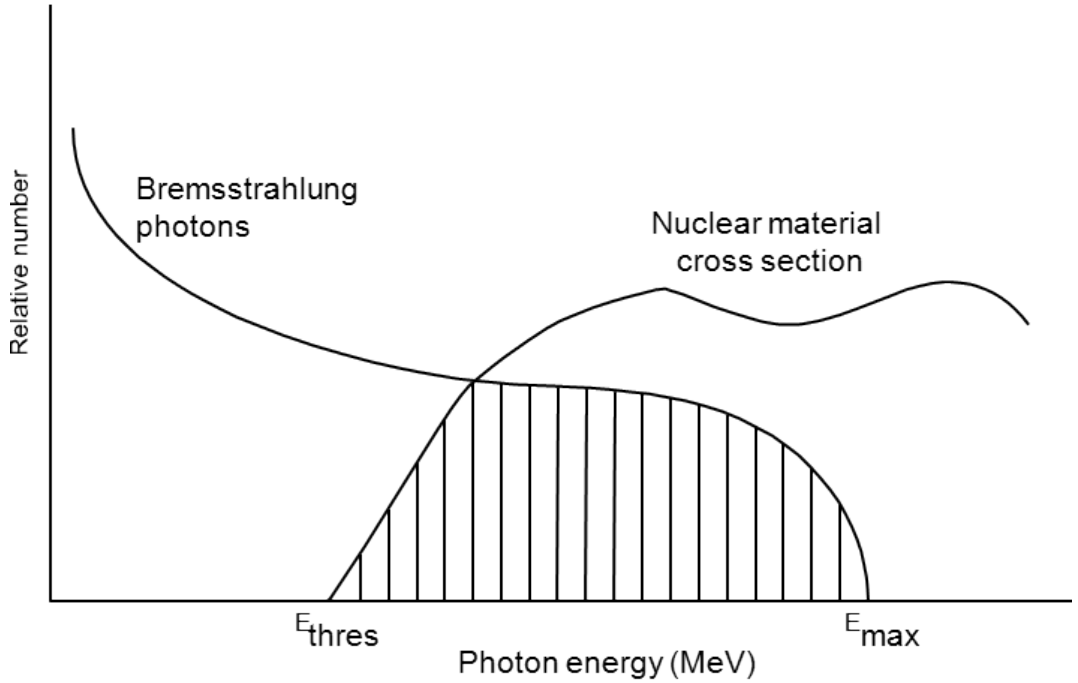

Figure 2.5: Scheme of effective energy region, in which the induced nuclear material can undergo photofission, based on [25].

2.1.1 Delayed γ-rays

The delayed γ-rays, emitted from fissionable materials, are very firm signatures indicating their presence in bulk cargo, especially for unshielded nuclear material. Currently two methods can be considered for the excitation of suspected material and the emission of delayed γ-rays. The method based on a LINAC emitting Bremsstrahlung radiation with an endpoint of 9 MeV as well the method called differential die away analysis (DDAA), requiring a deuterium-deuterium (D+D) or deuterium-tritium (D+T) neutron generator, depending on the application, can be considered for detection of special nuclear materials at the border [26]. The dissertation will be focused solely on

the former method, the latter will be shortly described in this Chapter. The DDAA method for delayed γ-ray detection is based on a D+D neutron generator working in pulse mode, emitting neutrons with E = 2.5 MeV, respectively, due to the fusion reaction. The neutrons have to be thermalized in order to induce Special Nuclear Material (SNM), which possess a high cross section for neutrons with a thermal energy of about 0.025 eV. Thus, either the cargo content must be hydrogenous or the neutron generator should be covered by high density polyethylene (HDPE) or a similar hydrogenous material working as the neutron moderator. The thermalized neutrons, reaching the inspected cargo and its content, can induce the potentially hidden SNM, which undergoes fission, and then, emits characteristic radiation, including delayed γ-rays. Compared to delayed γ-rays, the population of neutrons from the neutron generator decays much faster, allowing their measurements between neutron beam pulses, many milliseconds after shut off of the interrogation beam, when the γ-rays from the thermal neutron capture disappear. However, between the beam pulses, natural radiation and that emitted from cargo constitutes the main source of background radiation. The thermalized D+D generator is recommended for this application in order to avoid the activation of ^{16}N and other elements. Measuring the delayed γ-rays of energy above 3 MeV still provides one of the most efficient means for SNM detection [17].

The emission time of the delayed γ-rays from fission fragments varies significantly - from μs to many hours - however, the averaged half-life of emission was estimated to be 30 s for ^{235}U and ^{239}Pu and 80 s for ^{238}U [17]. Walton et al. reported in [27] the absolute intensities of early delayed γ-rays (emission time between 1.0×10^{-5} and 7×10^{0} s and energy E_γ>0.511 MeV) for ^{235}U, ^{238}U and ^{232}Th. The estimated absolute intensity $I_{\gamma\ del}$, described in γ photons/(fission $\times$ s), is presented in Table 2.1.

Table 2.1: Absolute intensities $I_{\gamma\ del}$ of early delayed γ-rays for $E_\gamma > 0.511$ MeV, according to [27]. Details were described in the text.

Emission time	$I_{\gamma\ del}(^{238}\mathrm{U})$	$I_{\gamma\ del}(^{235}\mathrm{U})$
$7\ \mu s - 7 s$	2.86	1.25
0.1 s - 7 s	2.71	1.11
$<$ 1 ms	0.04	0.09
$<$ 10 ms	0.06	0.11
$<$ 100 ms	0.21	0.15

The results presented in Table 2.1 showed that the delayed γ-rays are rather abundant and can be detected by large volume organic, inorganic scintillators and HPGe detectors. Photofission delayed γ-rays detection is an efficient means of revealing nuclear material in cargo equipment. The technique is more efficient when the nuclear material is unshielded with high-Z materials due to the low attenuation of the γ-rays in low-Z materials, like polyethylene (PE), water, wood or textiles. Moreover, it can also be the cheapest solution applied to detect them due to the fact that even low-cost plastic scintillators can be successfully applied for delayed γ-rays detection. For high precision measurements, like the estimation of material composition, fundamental research, and the scanning of bulky nuclear waste packages, the best solution is a high purity germanium detector (HPGe) due to its outstanding energy resolution of about 2.1 keV at 1333.5 keV emitted from ^{60}Co, which is unreachable even with the best inorganic scintillators, such as $LaBr_3$:Ce [28]. However, due to the required cooling of the HPGe to the liquid nitrogen (LN_2) temperature, its application for border monitoring is more complex than the solution based on scintillation detectors. According to [29], the estimated number of delayed γ-rays per fission is 7 and is significantly greater than the number of delayed neutrons per fission event, which is around 0.01.

2.1.2 Delayed neutrons

Delayed neutrons are the most unique signatures of nuclear material presence. Excepting a very few types of reactions, like ^{17}O(n,p)^{17}N with neutron energy threshold of 10.4 MeV or ^{18}O(γ,p)^{17}N for electromagnetic photon energy of 15.9 MeV there is no other source of delayed neutrons. The latter reaction yields a delayed neutron with a half-life of 4.1 s and can be observed only in a laboratory-grade LINAC facility operating with very high Bremsstrahlung photon energy. Such (γ,n) reactions will not be observed at the border-grade facility due to lower energy of Bremsstrahlung radiation applied. The easiest method of delayed neutron detection is based on the use of ^{3}He gaseous detectors due to the high cross section for neutrons of low energy and low sensitivity to γ radiation. More details concerning the measurement method will be presented in Chapter 5. The ^{3}He gaseous detector was used for the first time for the detection of delayed neutrons from fission by Batchelor et al. [30]. An example of the

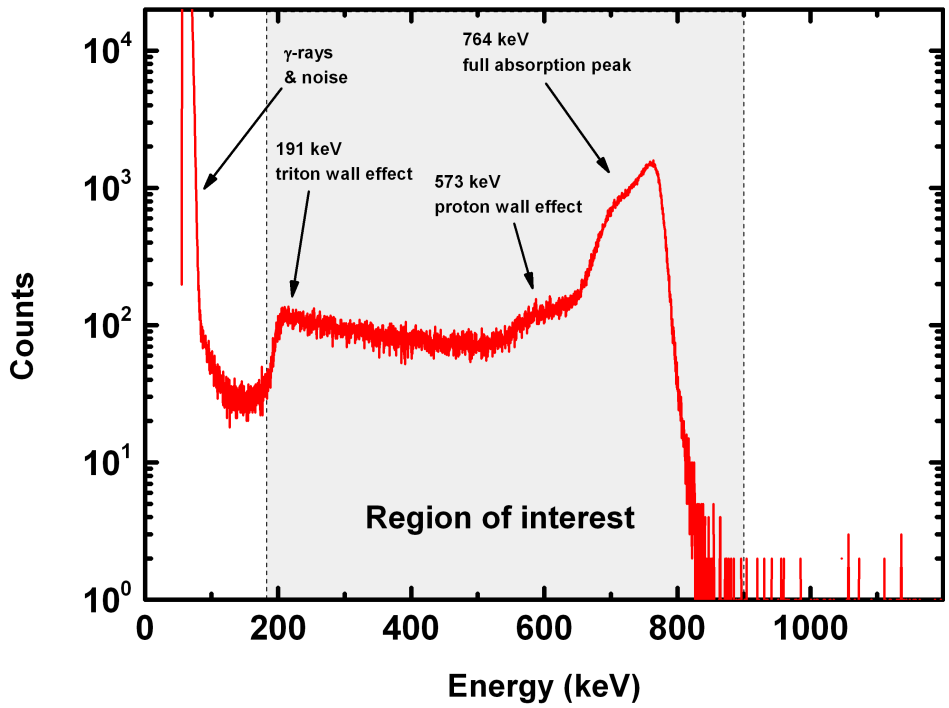

Figure 2.6: An example of the ^{252}Cf spectrum recorded with a ^{3}He detector.

^{3}He response to neutrons from a ^{252}Cf source is shown in Figure 2.6.

Particularly, delayed neutrons were extensively studied during the US. Manhattan Project (1942-1946). For the first time, their half-lives, energies and yield divided into several groups were shown in 1948 by Hughes et al. [31] for ^{235}U. Further study was performed in order to gather more detailed information about the energy distribution [32]. Measurements showed that delayed neutrons can carry energy of up to 2.4 MeV, however, their intensity in this range of energy is around 200 times lower than that with energy of around 0.5 MeV. In order to register the delayed neutrons, a cloud chamber registering recoiled protons was applied. Only the energy distribution of neutrons above 300 keV was plotted because the track of the recoiled protons was too short to provide reliable results. In this reference, the mechanism of the delayed neutrons emission was described as well.

The delayed neutrons are emitted after fission or photofission in the following process: the fission fragment (precursor) ${}_{Z}{}^{A}\mathrm{B}$, which undergoes β^{-} decay to ${}_{Z+1}{}^{A}\mathrm{C}$ (neutron emitter), leaves the emitter in either the ground state or in one of the excited states.

If the ${}_{Z+1}{}^{A}\mathrm{C}$ nucleus is in the excited state above the neutron separation energy E_n, delayed neutron emission occurs resulting in the final excited nucleus ${}_{Z+1}{}^{A-1}\mathrm{D}$. An example of the decay scheme was shown in Figure 2.7. As reported in [33], many delayed neutrons precursors with 27<Z<63 have been identified.

The delayed neutrons emitted from nuclear materials due to photofission usually carry an energy between 0.25 - 0.62 MeV [31]; their half-lives can be divided into several groups, as showed in Table 2.2 taken from [34]. The ν_a^d stands for the number of delayed neutrons emitted per 100 photofission events, β_i^c for the intensity for selected group. In the Ref. [34], the samples were irradiated with 15 MeV Bremsstrahlung photons obtained from a betatron, when the irradiation was finished, the sample ^{232}Th, ^{238}U, ^{235}U, ^{239}Pu were transported within 0.1 s to the measurement site with a neutron detector.

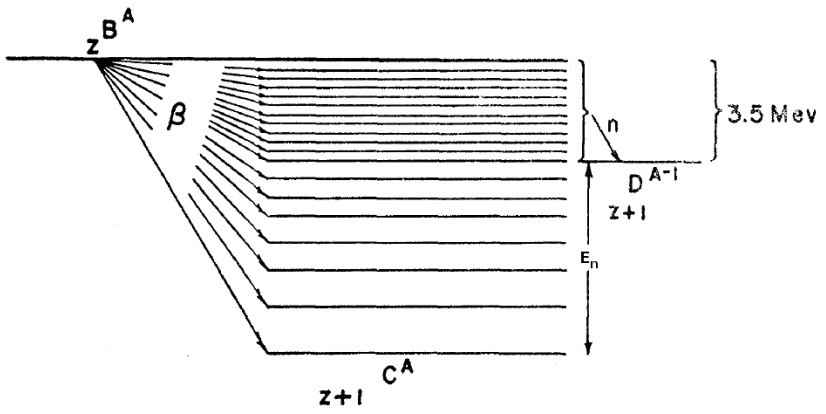

Figure 2.7: Decay scheme showing the fission fragment ${}_{Z}{}^{A}\mathrm{B}$ (precursor) decaying to excited ${}_{Z+1}{}^{A}\mathrm{C}$ nucleus (neutron emitter). The ${}_{Z+1}{}^{A}\mathrm{C}$ in the state above the neutron separation energy E_n decays to final nucleus ${}_{Z+1}{}^{A-1}\mathrm{D}$ by delayed neutron emission [32].

At the present times, a high pressure ^{3}He is the most efficient medium for photofission delayed neutron detection. Unfortunately, due to a of ^{3}He the prices of such detectors have increased by a factor of 3-4 per liter ^{3}He in the last decade. This fact has motivated many scientific groups to start searching for cheaper solutions, based on ^{10}B or ^{6}Li. Alternatives to ^{3}He detectors were presented in [35] and are listed below:

- liquid or plastic scintillators containing ^{10}B and having pulse shape discrimination (PSD) capability for γ-ray and neutron signal discrimination [36]
- boron-coated straws (BCS) [37,38],
- BF_3 proportional counters - unfortunately not widely used in Homeland Security due to toxicity of that gas [39] and requirement of high voltage (>2000 V), which is problematic in humid environment [40],
- ^{10}B lined proportional counter [41],
- gadolinium glass such as gadolinium oxyorthosilicate (GSO) [42] or plastic [43],

Table 2.2: Delayed neutrons abundance and half-life times divided into groups [34].

Isotope	$\nu_d{}^a/100$	Group i	$T_{1/2}$ (s)	β_i^c
^{232}Th	3.8 ± 0.6	1	55.6 ± 1.5	4.40 ± 0.20
fissionable		2	20.3 ± 0.8	16.3 ± 1.0
material		3	5.45 ± 0.50	15.9 ± 1.5
		4	1.98 ± 0.20	37.5 ± 3.0
		5	0.43 ± 0.10	17.2 ± 2.0
		6	0.18 ± 0.03	8.7 +2.0 -4.0
^{235}U	0.96 ± 0.13	1	54.7 ± 2.5	5.4 ± 0.5
SNM		2	20.3 ± 1.0	20.0 ± 2.0
		3	5.45 ± 0.60	15.2 ± 2.0
		4	2.01 ± 0.25	36.9 ± 4.0
		5	0.50 ± 0.10	13.9 ± 2.0
		6	0.19 ± 0.04	8.6 +2.0 -5.0
^{238}U	3.1 ± 0.4	1	56.2 ± 0.8	1.98 ± 0.08
fissionable		2	21.3 ± 0.3	15.7 ± 0.5
material		3	5.50 ± 0.20	17.5 ± 0.7
		4	2.15 ± 0.10	31.1 ± 0.8
		5	0.70 ± 0.06	17.7 ± 0.9
		6	0.19 ± 0.02	16.1 +2.0 -5.0
^{239}Pu	0.36 ± 0.06	1	54.0 ± 3.0	6.05 ± 0.60
SNM		2	20.6 ± 1.0	20.6 ± 2.0
		3	5.7 ± 0.7	18.3 ± 3.0
		4	1.94 ± 0.30	29.5 ± 4.0
		5	0.58 ± 0.10	14.9.± 3.0
		6	0.20 ± 0.04	10.6 +2.0 -5.0

- ^{6}Li based detectors, for example $LiCaAlF_6$:Eu (LiCAF:Eu) or LiCAF:Ce scintillators in form of crystal [44, 45] or rubber [46],
- inorganic scintillators, such as ^{6}LiI:Eu [47] or Cs_2LiYCl_6:Ce (CLYC) [48],
- ^{6}LiF/ZnS:Ag layers covering wavelength shifting (WLS) fibers [49].

From the point of view of delayed neutrons detection, the most important challenge is to produce a detector having γ-ray absolute rejection ratio for neutrons $\epsilon_{abs\ \gamma n}$ of 10^{-6} at 1.33 MeV or better in order to achieve the required low level of false alarms for the monitoring systems [50]. Moreover, together with a good $\epsilon_{abs\ \gamma n}$ parameter, the neutron detector should provide considerable absolute detection efficiency, allowing for application in Radiation Portal Monitors (RPM).

Concerning the boron based detectors, the reaction of neutrons in ^{10}B results in such a reaction (2.1):

$$n +^{10} B \rightarrow \alpha +^{7} Li + \gamma(480keV). \tag{2.1}$$

The main limitation of ^{10}B scintillators is the low deposition energy of the reaction products, resulting in the appearance of the deposition peak at about 60 keVee for BC523A and 110 keVee for EJ309B5, see [36]. Moreover, in the 2D plots, the peak appears between the structures related with γ and neutrons, as showed in Figure 2.8. During operation with a LINAC, significant amount of X- and γ-rays results in large amount of counts in a low energy region, drastically degrading the signal-to-background ratio of these scintillators.

The ^{10}B lined proportional counters can also be used for neutron detection, however, they still offer lower absolute sensitivity than the proportional counter based on ^{3}He, including boron coated straws.

The solution based on thin LiCAF scintillators doped with Ce or Eu also seems not to be useful for the delayed neutron detection due to their quite high price per volume. Currently it is possible to obtain an $\varnothing$4" scintillator 1 mm thick. However, the scintillators are still sensitive to γ radiation. Due to a thermal neutron absorption peak appearing below $<$2 MeV, the detection of delayed neutrons in the presence of γ-rays

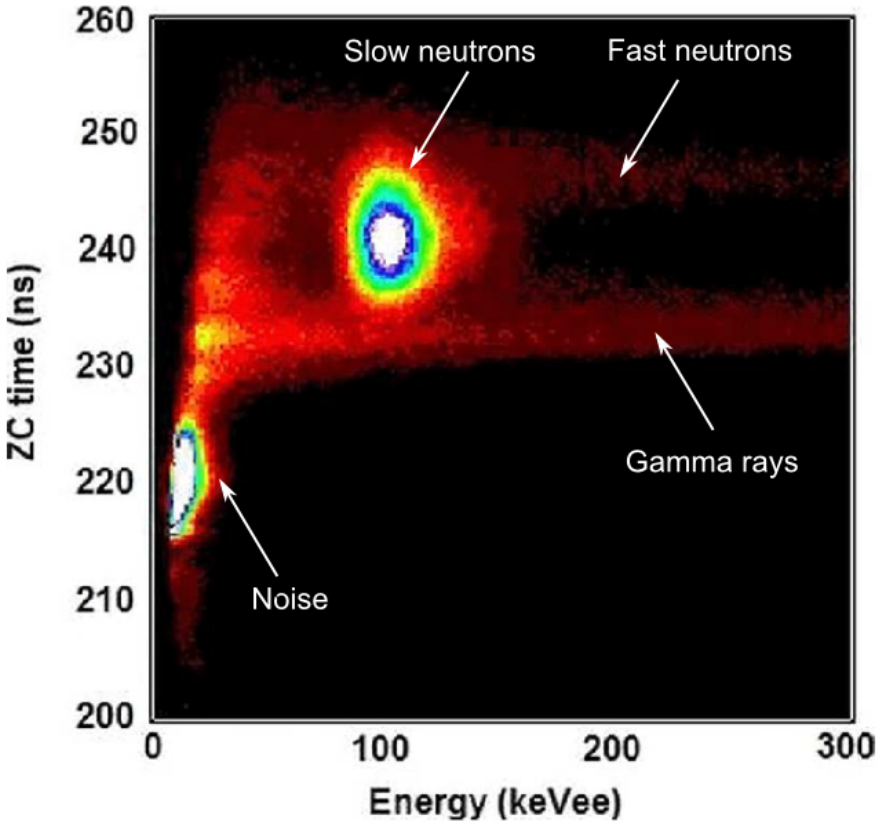

Figure 2.8: A 2D plot of Zero Crossing time versus energy measured with ⌀3" × 3" EJ309B5 scintillator irradiated with the Pu-Be source shielded with lead and paraffin [36].

from nuclear material photofission and background will hardly be possible. The same issue occurs with the gadolinium based scintillators. The possibility of pulse shape discrimination (PSD) was showed preliminarily in [44] where specially designed electronic filters were applied. However, the PSD capability was not observed in [45] with use of zero-crossing technique and the later paper [46], comparing the performance of the LiCAF scintillators in form of crystal and rubber.

Of all the available ^{3}He-free solutions, the most robust seems to be the ^{6}LiF/ZnS(Ag) detector [49]. The detector is based on a ^{6}LiF and ZnS:Ag mixture coating a plastic PVT scintillator, acting as the wavelength shifter. Such detectors are currently manufactured by Symetrica Ltd. and Saint-Gobain, and can be offered in

large sizes. For example, in 2010 R. Kouzes et al. [51] performed tests of the 1.0 m long × 0.1 m wide × 0.2 m thick ^{6}LiF/ZnS(Ag) detector, encased in a polyethylene moderator. The test were based on the requirements presented in [50]. A ^{252}Cf neutron source was used for testing the ^{6}LiF/ZnS(Ag) neutron detector sensitivity:

- To reduce the γ-ray flux, the source shall be surrounded by at least 0.5 cm of lead. To moderate the neutrons, 2.5 cm of polyethylene shall be placed around the source.

- The absolute detection efficiency for such a ^{252}Cf source, located 2 m perpendicular to the geometric midpoint of the neutron sensor, shall be greater than 2.5 cps/ng of ^{252}Cf [52]. 10 nanograms of ^{252}Cf is equivalent to 5.4 micro-Ci or 2.1 $\times 10^{4}$ n/s, since ^{252}Cf has a 3.092% spontaneous fission (SF) branch and 3.757 neutrons/SF.

- The neutron detector shall not generate alarms due to the presence of strong γ-rays sources. The ratio of neutron detector γ-ray detection efficiency to neutron detection shall be less than 0.001.

Finally, to evaluate the performance of the ^{6}LiF/ZnS:Ag detector (and, in general, all types of neutron detectors [50]), the following parameters are crucial to measure them:

- Absolute neutron detection efficiency ($\epsilon_{abs\ n}$) - defines the required efficiency for neutron detection in a specific geometry. It should be at least $\epsilon_{abs\ n} \geq 2.5$ cps/ng ^{252}Cf at 2m for a source in a defined moderated form.

- Intrinsic efficiency of γ-rays detected as neutrons ($\epsilon_{int\ n\gamma}$) - it is defined as a response of a neutron detector to the presence of a γ-ray field when no neutron source is present. As a result, it is the net number of counts registered as neutrons, which in fact were γ-rays, divided by the number of photons striking the neutron detector. This reasonable $\epsilon_{int\ n\gamma}$ value was defined to be $\leq 10^{-6}$ at the exposure of 10mR/h. With an optimized ^{3}He detector, it is possible to obtain an $\epsilon_{int\ n\gamma}$ better than 10^{-8}.

- Gamma Absolute Rejection Ratio in the presence of neutrons (GARRn) of 0.9 $\leq$ GARRn $\leq$ 1.1 at 10 mR/h dose rate. It is defined as the number of events

that are counted as neutrons ($\epsilon_{abs\ \gamma n}$) in the presence of both γ-ray and neutron sources, divided by the number of neutrons recorded without the γ-ray source ($\epsilon_{abs\ n}$).

For the ^{6}LiF/ZnS:Ag detector designed by Symetrica Ltd., the neutron efficiency was estimated to be 3.5 cps/ng of ^{252}Cf, the exposure rate of 5 mR/h under irradiation with ^{60}Co was obtained at 521 cm and the calculated $\epsilon_{int\ n\gamma}$ value was estimated to be of the order of 10^{-8} for dose rates up to 40 mR/hr and was similar to that for ^{3}He detectors. The GARRn value for the ^{60}Co exposure rate of 10 mR/hr was within the desired range. Summarizing, the lithium covered zinc sulfide detectors seems to be a very promising alternative solution for delayed neutron detection. Tests of such a detector will be performed in the C-BORD project within the frame of a Horizon 2020 Program (accepted by EU Commission by 06.2015).

2.1.3 Prompt γ-rays

Detection of prompt γ-rays is the most demanding method of special nuclear material detection, especially via photofission with the use of a LINAC working in pulse mode. Measurements of prompt γ-rays must be done in the field of interrogation radiation, and even if the inspection system is based on a pulsed mode neutron generator, the originated prompt γ-rays must be distinguished from the γ-rays emitted by the activated background, materials inside the cargo content and the detector itself. The inelastic scattering and neutron capture process yield γ-rays, which overlap with the prompt photons emitted from nuclear materials. Thus, in all cases the contribution of background to the γ energy spectrum must be taken into account.

One of the methods possible to apply for nuclear material detection is the tagged neutron time-of-flight (TOF) with associated particle method [53, 54]. Obviously, the velocity of neutrons with energy below 14 MeV differs radically from the velocity of γ-rays. The velocity of 1 MeV and 14 MeV neutrons is 1.4 cm/ns and 5.2 cm/ns, respectively, whereas the velocity of γ-rays is 30 cm/ns. When a neutron generator can be operated with a very short neutron emission time (range of nanoseconds), the significant difference in the flight time allows the detection of the γ-rays induced by neutrons interrogation in the cargo. When the nuclear material would be present in the inspected

cargo, prompt γ-rays from fission would be emitted in the range of femtoseconds and, in principle, can be separated from background γ-rays induced by neutrons due to their different registration times.

Prompt γ-rays are the strongest signatures of fission [17], per one event about 7 photons are emitted. Their average energy is about 1 MeV, however, about 3 % of them exceed 3 MeV, which gives their count rate around 0.21 photon/fission, see Table 2.3. However, due to the high complexity and the fact that the penetration of such prompt γ-rays through the cargo container and potential nuclear material shielding is comparable with the delayed γ-rays, this detection method is not common and measurements in this matter will be omitted in the dissertation.

Table 2.3: Number of prompt γ-rays emitted due to fission of various nuclear materials, according to [17].

Material	Total photons per fission	Photons per fission $E_\gamma > 3$ MeV
^{235}U	6.7	0.21
^{238}U	7.2	0.21
^{239}Pu	7.2	0.23

2.1.4 Prompt neutrons

Particular attention should be paid to the energy and intensity of the prompt neutrons from fission and photofission due to their much higher intensity and energy in comparison with delayed neutrons. In the 60's of the previous century measurements of the fast neutrons from spontaneous fission (SF) of ^{252}Cf were performed and reported in [55, 56]. In the Ref. [56], the average prompt neutron energy was estimated to be 2.348 MeV for SF of ^{252}Cf. Thermal fission and photofission can be used in order to measure the prompt neutron energy from nuclear materials. The TOF technique was applied in order to reject the γ-rays and neutrons emitted from LINAC or neutron generators. Energy of prompt neutrons emitted from thermal neutron induced fission varies slightly between various nuclear materials, as shown in [57].

In the early 1960's significant effort was also put into measuring the prompt photofission neutrons by means of TOF technique. In 1965 Sargent et al. [58] reported the angular distribution and velocity of the photofission induced prompt neutrons from ^{232}Th. During this measurement 7.75 MeV Bremsstrahlung photons from a LINAC were used to irradiate the sample. The energy distribution of the prompt neutrons from ^{232}Th is shown in Figure 2.9.

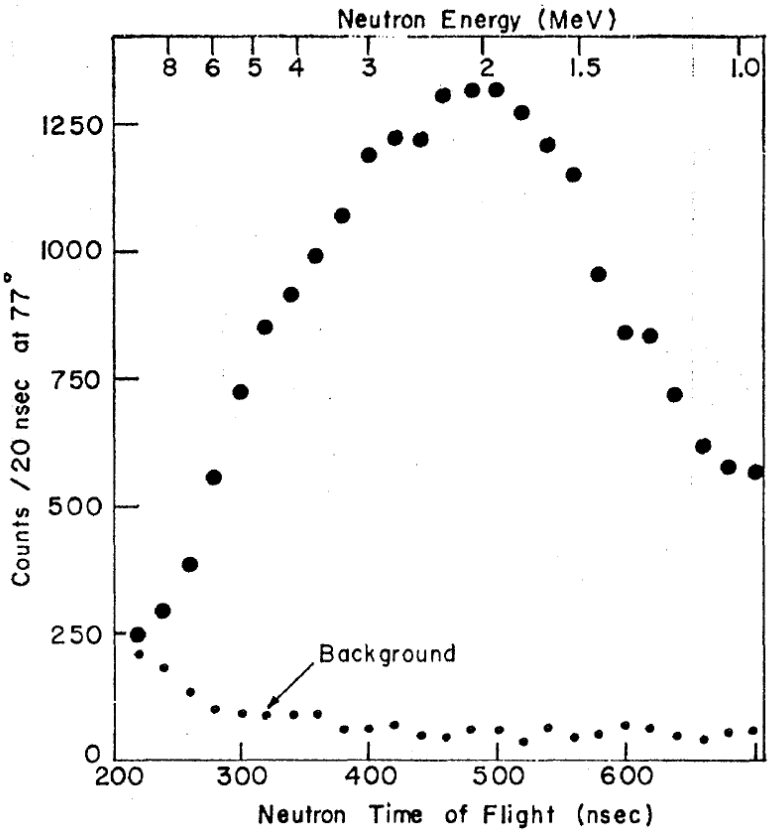

Figure 2.9: Energy profile of the photofission induced prompt neutrons emitted from ^{232}Th [58].

The energy distribution and the intensity of the prompt neutrons vary slightly between nuclear materials, according to [59]. The prompt neutrons mean energy and intensity is presented in Table 2.4. The E_e is the energy of electrons emitted by a LINAC, converted into Bremsstrahlung radiation, ν_n stands for the number of prompt neutrons per fission. It can be seen that the number of neutrons per fission varies be-

tween nuclear materials and the endpoint of Bremsstrahlung photons energy and was estimated to be between 1.963 and 3.43.

Table 2.4: Number of prompt neutrons per photofission for various nuclear materials and electron energy converted into Bremsstrahlung, according to [59].

E_e(MeV)	$\nu_n(^{232}\mathrm{Th})$	$\nu_n(^{235}\mathrm{U})$	$\nu_n(^{238}\mathrm{U})$	$\nu_n(^{239}\mathrm{Pu})$
8	1.963 ± 0.108	2.456 ± 0.086	2.457 ± 0.088	————
10	1.891 ± 0.111	2.697 ± 0.081	2.628 ± 0.083	3.32 ± 0.08
10.2	1.891 ± 0.111	2.612 ± 0.079	2.585 ± 0.082	3.17 ± 0.14
12	2.084 ± 0.107	2.963 ± 0.072	2.802 ± 0.078	3.43 ± 0.10

The recent results, presented in [60], showed significant asymmetry of the photofission prompt neutrons intensity measured at various angles of emission. The response was measured simultaneously in parallel and perpendicular directions, with the use of a half-sphere geometry of 18 neutron detectors. The beam of γ-rays of energy between 5.6 and 7.3 MeV from the High Intensity γ-ray Source (HIγS) was ideally polarized, had high intensity (10^7 γ/s) and was nearly monoenergetic. In the case of ^{235}U, the intensity of the prompt neutrons depends rather slightly on the angular distribution, whereas for ^{238}U significant difference was observed.

Recently the detection of prompt neutrons from photo- or neutron induced fission has become the most interesting and efficient method of concealed nuclear material detection. There are three different approaches published so far:

- Threshold Activation Detection (TAD) [61–63],
- Differential Die Away Analysis (DDAA) [26, 64],
- Continuous Wave (CW) 9 MeV LINAC for prompt neutron detection with the use of the neutron/γ pulse shape discrimination (PSD) technique [65].

In this dissertation particular attention will be paid to the TAD technique that utilizes 6 MeV or 9 MeV Bremsstrahlung from a LINAC. Basically, the method relies on the activation of a material by fast prompt neutrons and the recording of the appropriate characteristic signatures, like γ-rays and β^- particles. The characteristic signatures

appear in a finite time period (usually a matter of seconds) after the activation process in order to avoid the measurement of the very intense photons flash from LINAC. It is even better when the activated material is a scintillator itself, because it allows the detection both signatures simultaneously, nevertheless, other materials can be also used as the "activator" surrounding the detector, for example, teflon (contains ^{19}F). A simplified scheme is presented in Figure 2.10.

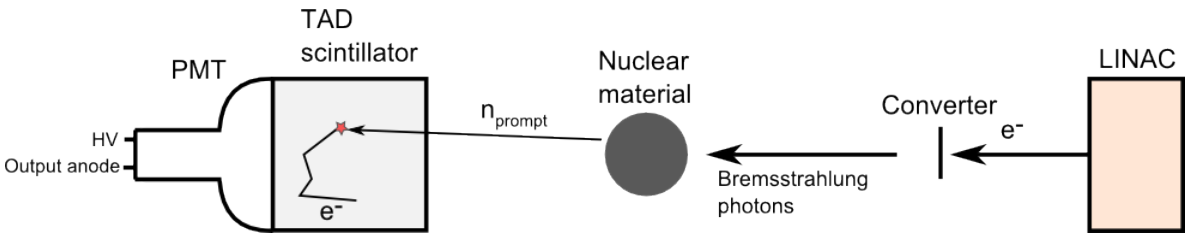

Figure 2.10: Simplified scheme of nuclear material detection by means of TAD technique.

It is required that the chosen nuclei should have an appropriate neutron activation threshold - it should be above 3 MeV to cut-off the photoneutrons generated on the elements of the LINAC electron converter. The main sources of photoneutrons from cargo content and LINAC elements are listed in Table 2.5 and Table 2.6, respectively. Moreover, the activation threshold cannot be too high in order to allow the measurement of prompt neutrons from photofission. Additionally, the excited nuclei should emit easily detectable radiation (β^- particles or γ-rays), with a suitable half-life in the range of seconds allowing their measurements between LINAC beam pulses, and a useful cross section for the neutron activation of about 100 mb, see Figure 2.11. The amount of hydrogen in the scintillator medium should also be as low as possible in order to minimize neutron scattering resulting in energy loss below the activation threshold. According to the [61,62], the best candidates are ^{19}F, ^{23}Na and ^{6}Li. Their half-life, energy of β^- and γ-rays emitted after activation and intensities are shown in Table 2.7.

Particularly, many commercial scintillators contain such isotopes. The inorganic scintillators containing ^{19}F, like BaF_2, CaF_2:Eu, CeF_3 [66,67] as well as inorganic scintillators, like fluorocarbon EJ-313 [68] (or equivalent BC-509) or fluorine-based plastic [15], can be considered for this application. However, the inorganic scintillators are

limited in size and are more expensive than the organic scintillators.

Table 2.5: Photoneutrons production threshold in cargo materials, according to [17].

Isotope	Natural abundance (%)	(γ, n) threshold (MeV)	Where present
^{2}H	0.015	2.225	cargo
^{13}C	1.11	4.947	cargo
^{14}N	99.634	10.559	cargo
^{15}N	0.366	10.838	cargo
^{16}O	99.762	15.672	cargo
^{17}O	0.038	4.144	cargo
^{18}O	0.2	8.046	cargo
^{54}Fe	5.845	13.38	cargo and structural
^{56}Fe	91.754	11.119	cargo and structural
^{57}Fe	2.119	7.647	cargo and structural
^{58}Fe	0.282	10.046	cargo and structural

Table 2.6: Main sources of photoneutrons emitted from elements of LINAC accelerator, according to [17].

Isotope	Natural abundance (%)	(γ, n) threshold (MeV)	Where present
^{181}Ta	100	7.577	x-ray converter
^{180}W	0.12	8.412	x-ray converter
^{182}W	26.5	8.065	x-ray converter
^{183}W	14.31	6.19	x-ray converter
^{184}W	30.64	7.411	x-ray converter
^{186}W	28.43	7.191	x-ray converter
^{197}Au	100	8.072	x-ray converter
^{204}Pb	1.4	8.394	x-ray shielding
^{206}Pb	24.1	8.086	x-ray shielding
^{207}Pb	22.1	6.738	x-ray shielding
^{208}Pb	52.4	7.367	x-ray shielding

Moreover, BaF_2 contains α particle impurities, giving excessive background in the range of 1.5 - 3 MeV. On the one hand, this fact can be an advantage as the α peaks could

Table 2.7: Nuclei that can be considered for TAD technique, according to [62].

Isotope	Reaction	Threshold (MeV)	$T_{1/2}$ (sec)	β^- endpoint energy (MeV)	Intensity (%)	γ energy (MeV)	Intensity (%)
^{6}Li	^{6}Li(n,γ)^{7}Li	Q = 7.2	Stable				
	^{6}Li(n,p)^{6}He	3.18	0.807	3.5	100		
	^{6}Li(n,t)^{4}He	0	Stable				
^{19}F	^{19}F(n,γ)^{20}F	Q = 6.6	11.1	5.39	100	1.63	100
	^{19}F(n,p)^{19}O	4.25	26.9	3.3, 4.6	54.4, 45.4	1.36	50.4
	^{19}F(n,p)^{19}O	1.61	7.1	4.3, 10.4	67, 28	6.1	67
^{23}Na	^{23}Na(n,γ)^{24}Na	Q = 6.96	0.02	6	0.05	0.47	100
			54000	1.39, 4.4	100, 0.06	1.37, 2.75	100, 100
	^{23}Na(n,p)^{23}Ne	3.75	37.2	4.38, 3.95	67, 32	0.44, 1.64	33,
	^{23}Na(n,α)^{20}F	4.04	11.1	5.39	100	1.63	100

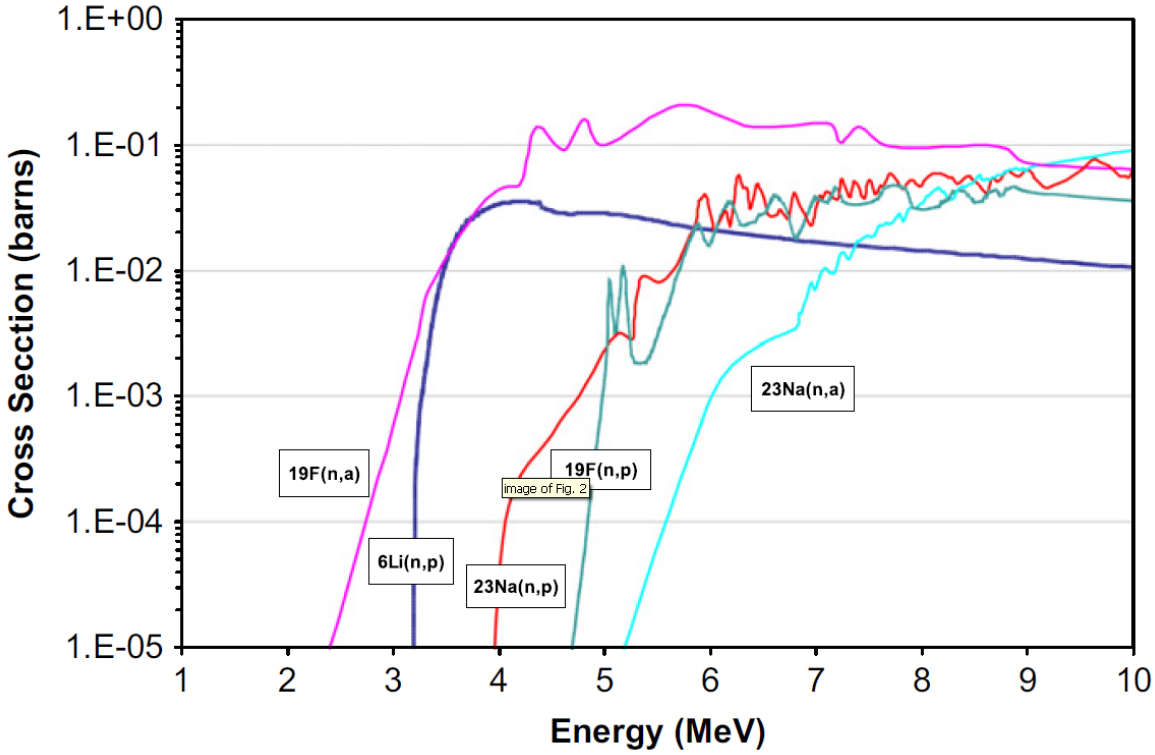

Figure 2.11: Fast neutron cross-sections for threshold activation reactions in some TAD materials, according to [61].

be used for energy self-calibration of the detector. On the other hand, the presence of α contamination reduces the signal-to-background ratio and the sensitivity to prompt neutrons and delayed γ-ray detection in this range of energy. Thanks to the large

stopping power of inorganic scintillators, the mean free path of electrons (β^- particles) is much shorter. Thus, an inorganic scintillator having the same fast neutron detection efficiency as an organic one can have smaller dimensions. The continuous slowing down approximation (CSDA) of the electron range in BaF_2 and EJ-313 is presented in Figure 2.12 and Figure 2.13. The CSDA range is a very close approximation to the average path length traveled by a charged particle as it slows down to rest. The mean free path l is calculated from the Equation 2.2:

$$l = \frac{R}{\rho}, \tag{2.2}$$

where ρ is the scintillator density and R is the particle range obtained from the value of the CSDA range for the defined energy of a particle, expressed in g/cm^2. Calculations for the 10 MeV electron result in a mean free path in the scintillators medium of 13 mm and 30 mm for BaF_2 ($\rho = 4.88\ g/cm^3$) and EJ-313 ($\rho = 1.62\ g/cm^3$), respectively.

The liquid EJ-313 scintillator is based on highly purified hexafluorobenzene (C_6F_6) and is almost free of hydrogen, with a fluorine-to-hydrogen (F/H) ratio of about 308. However, the toxicity of the base material and a low flashpoint of 10℃ can be a serious limitation in commercial applications. The novel fluorine-based plastic, based on pentafluorostyrene ($C_8F_5H_3$), which is known to be polymerizable [70, 71], is a non-flammable organic scintillator possessing F/H ratio of 1.66 and containing an amount of fluorine atoms per cubic centimeter of 3.73 $\times 10^{22}$ [15], similarly to that of EJ-313. The performance of the fluorine-based plastic scintillator will be shown in Section 6.7.

The most popular scintillation material containing ^{23}Na is NaI:Tl, which was discovered in 1949 [72] and precisely characterized in several papers [73, 74]. However, the activation threshold is higher than that for ^{19}F and the energy of emitted β^- particles is lower, and thus, overlaps with delayed γ-rays from the photofission of nuclear materials. Nevertheless, the integration of the total number of counts above 1 MeV could show the presence of a nuclear material, but definitely at a lower sensitivity than in the case of the ^{19}F-based scintillators.

The ^6Li isotope can be present in the Li-based scintillators for neutron detection, such as $LiCaAlF_6$ doped with Ce or Eu (LICAF) [44–46], ^6LiI:Eu [47] and Cs_2LiYCl_6:Ce (CLYC) [48]. Unfortunately, such scintillators are limited in size and expensive, in ad-

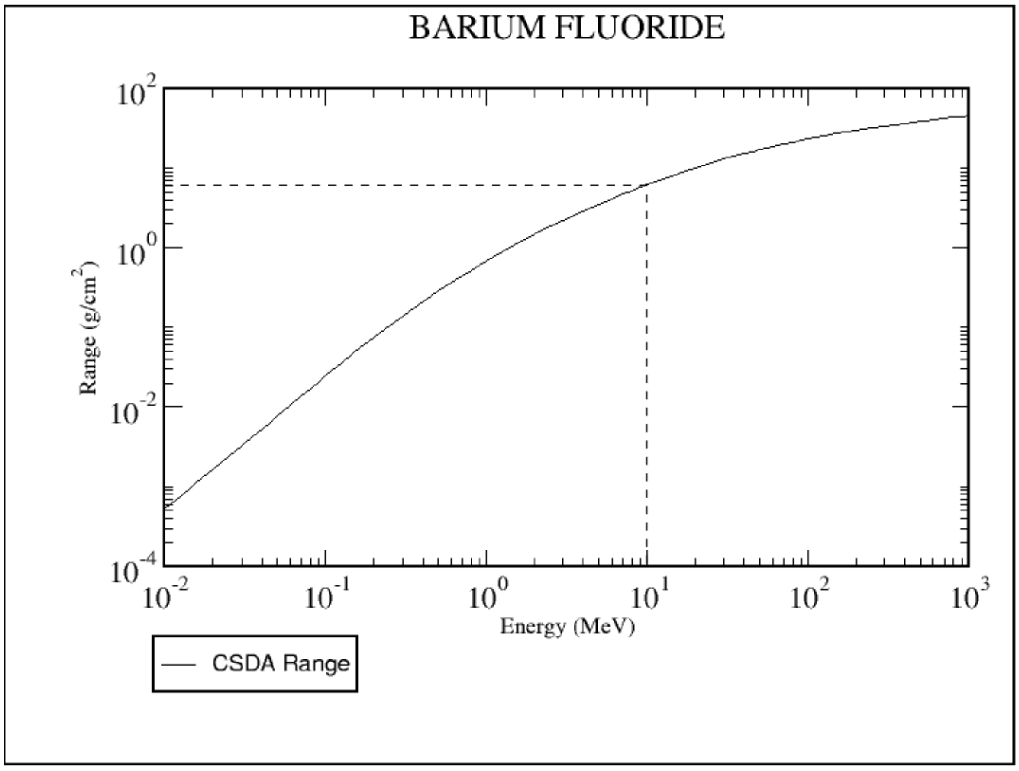

Figure 2.12: CSDA of an electron range for a BaF_2 according to NIST ESTAR database [69]. The CSDA range for a 10 MeV electron energy was indicated with the dashed lines.

dition, the β^- particle deposition energy is rather low. Thus, the response from the β^- particles can be overlaid by high energy γ-rays from the nuclear material and background. Thus, the potential application of such scintillators in the TAD technique is doubtful.

The second method of nuclear material detection, Differential Die-Away Analysis (DDAA) is based on the emission of neutrons from a D+T or D+D generator working in pulse repetition mode in order to activate the SNM inside a cargo container. The primary neutrons are moderated inside the hydrogenous content of a cargo container and can interact with the SNM. Then, emitted neutrons from the nuclear material moderate again in the cargo content and will reach the detector definitely later than prompt γ-rays. The time after the pulse, during which neutrons are registered, is called "die-away time". The die-away time is the characteristic time a neutron will survive before it is

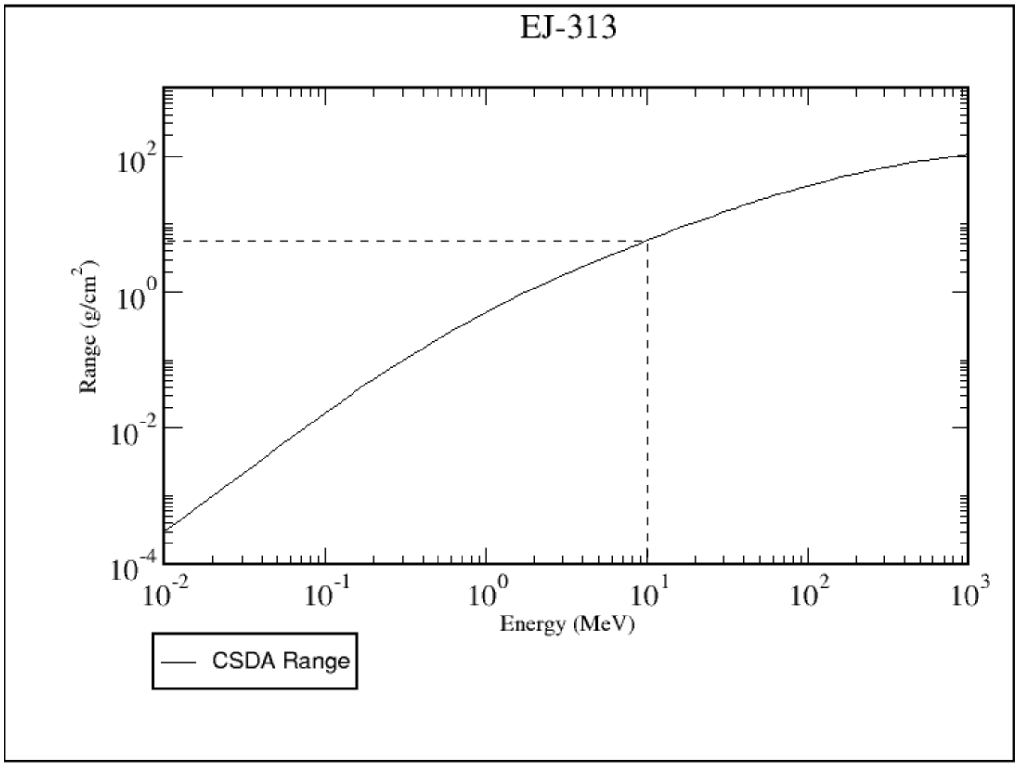

Figure 2.13: CSDA of an electron range for an EJ-313 according to NIST ESTAR database [69]. The CSDA range for a 10 MeV electron energy was indicated with the dashed line.

absorbed in the thermal-neutron detector or escapes from its interior. The neutron die-away normally ranges from 10 to 128 μs depending upon the counter geometry [75]. If the exponentially fitted die away time is longer due to additional registration of neutrons from fission, the presence of nuclear material may be noticed. An example of DDAA plots are showed in Figure 2.14, in accordance with [64]. In the Ref. [64] water was used as a moderator, which can be present in a real cargo container. Measurements were done with and without 347 g of ^{235}U and four ^{3}He detectors were applied to detect the prompt neutrons from the SNM. Additionally, the borax and boric acid was used as a detector poison in order to optimize the efficiency of die-away neutron detection. It was shown that the borax solution decreases the detectors efficiency, but also decreases the decay time of the detector. The shortened decay time allows for better separation of the

detector and fission signal after the neutron beam pulse. The borax-poisoned detector registered smaller amount of neutrons after the beam pulse from neutron generator. Measurements using a borax solution with absorption cross-sections 2, 4, 6, and 12 times that of pure water were performed. The absorption cross section of the borax and boric acid solution, equal to 6 times that of pure water, was shown to be optimum, resulting in the best signal-to-background ratio.

The third method of prompt neutron detection (CW LINAC) inspection system is based on a specially designed LINAC operated at a continuous beam of high energy photons [65]. The prompt neutrons are registered simultaneously with the γ-rays from the LINAC as well as those emitted from the nuclear material. Generally, in this

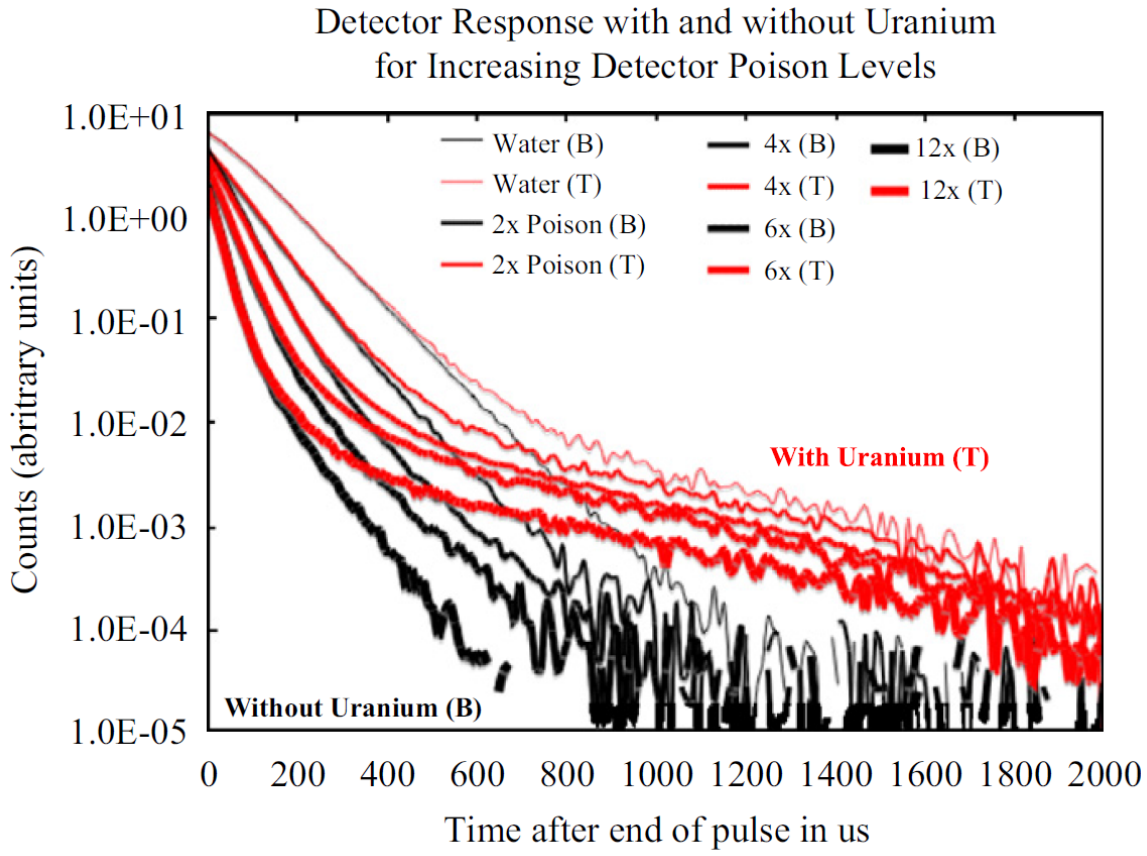

Figure 2.14: Example of DDAA plots showing the die-away time for water and after the addition of borax poison around the ^{3}He detectors. The total signal (red) with Uranium was assigned as T, the background (black) as B. Results taken from [64].

technique all γ pulses are classified as unwanted background, thus, liquid scintillators with pulse-shape discrimination (PSD) capability together with fast acquisition systems are used in order to separate the pulses from the neutrons and γ-rays. In order to analyze huge amount of pile-ups, advanced digital acquisition systems with implemented real-time deconvolution algorithms are applied [65]. Currently, novel digital acquisition system with advanced pile-up rejection algorithms is under development at NCBJ [76]. The method based on the CW LINAC is very promising because the neutron detection with use of liquid or plastic scintillators is efficient and is based on direct registration of recoiled protons after the scattering of the prompt neutrons on hydrogen in the scintillator medium.

Chapter 3

Experimental details

3.1 Acquisition track for delayed γ-rays characterization with the use of a High-Purity Germanium (HPGe) detector

The HPGe detector is the best choice for precise characterization of the delayed γ-rays from photofission thanks to very good energy resolution (about 2 keV at 1333.5 keV γ-rays from ^{60}Co) and the possibility of production in relatively large sizes, for example, $\varnothing$1 inch.

At the beginning, the characterization of a 100 g U sample (passive measurement, U enriched to 93% ^{235}U) was done at the European Array for Gamma Levels Evaluations (EAGLE HPGe) detectors array [12]. Data were collected at two amplification levels allowing for an observation up to 2 and 4 MeV, respectively. Low energy experiment lasted 24 h with about 50 coincidence counts/sec, while higher energy measurement were continued during 48 hours in order to achieve the highest possible statistics. The EAGLE detector array was equipped with 15 anti-Compton shielded (ACS) HPGe detectors with 70 % efficiency with respect to 3" $\times$ 3" NaI:Tl scintillator. The total photo-peak efficiency of the HPGe detectors array at 1.333 MeV was $\epsilon_{ph} \approx 0.5\%$. RadWare software was used for precise analysis of the measured data [77]. In the off-line analysis the sorting procedures were based on program "mult2d" [78]. All coincidences

were checked and compared with that included in Chart of Nuclides database [79].

The acquisition track for delayed γ-ray detection using HPGe is shown in Figure 3.1. The reverse bias voltage of +3000 V from an Ortec 659 HV power supply was sent to a charge sensitive preamplifier embedded into the Ortec GMX-25190-P HPGe detector (n-type, detection efficiency of 25% relative to 3" $\times$ 3" NaI:Tl, energy resolution 2.1 keV at 1333.5 keV). The signal from the preamplifier was transferred to a Spectroscopy Amplifier Ortec 672. The shaping time, which is responsible for the pulse integration time, was set to 6 μs due to the slow response of the HPGe detector to γ radiation. Finally, the Gaussian signals were recorded by a Tukan8k Multi-Channel Analyzer (MCA) with a USB 2.0 communication interface. For the purpose of photofission measurements the Tukan8K MCA was working in acquisition series mode. The uranium sample after irradiation with Bremsstrahlung photons from a LINAC was cooled for 30

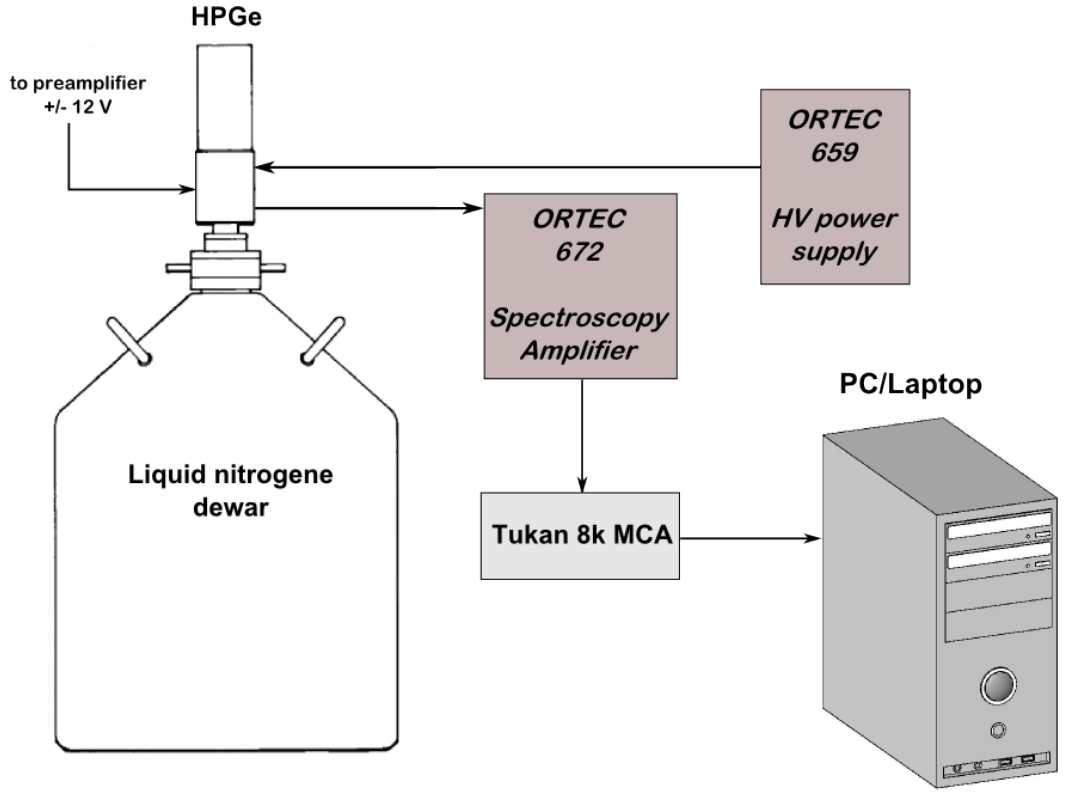

Figure 3.1: Acquisition track based on HPGe for the study of characteristic delayed γ-rays after the irradiation of a nuclear material with Bremsstrahlung photons.

minutes, then was placed in front window of the HPGe detector. The 100 measurement series were acquired, each lasting 10 minutes. Such measurements allow the estimation of the energy and decay time of the most intense γ-lines originated from photofission products.

3.2 Acquisition track for delayed γ-rays characterization with the use of plastic scintillators

In order to detect the delayed γ-rays with appropriate efficiency, scintillation materials used for this application should have a large volume and reasonable price. This goal can be achieved with the use of standard organic plastic scintillators, e.g. the PVT based EJ-200 or the equivalent BC-408. In a few papers inorganic scintillators are also taken into account, like the BGO [80], which is one of the densest scintillator commercially available (7.13 g/cm^3) and can be produced with the size of $\varnothing$3" $\times$ 3". Unfortunately, its price is significantly higher than that of the plastic scintillators of the same volume. Thus, the detection of delayed γ-rays from photofission was performed with the use of $\varnothing$5" $\times$ 3" BC-408 and $\varnothing$3" $\times$ 2" EJ-200.

The acquisition track for delayed γ-rays detection from photofission can be set for out-of-beam and beam-off measurements, see Figure 3.2. The former technique relies on radiation detection after the nuclear material irradiation, the latter is based on detection between LINAC beam pulses. Typically PMTs have an electron gain multiplicity of 10^5-10^6 and the signal from the anode is sufficiently strong to use it without a preamplifier, which can be easily saturated during the intense pulse from the LINAC. It is of high importance during operation with the beam-off technique, where the LINAC works with a frequency in the range of 25 - 400 Hz. In both cases, the anode signal from the PMT was connected to an Ortec 570 spectroscopy amplifier with as short as 0.5 μs shaping time in order to minimize the dead time of an acquisition system. The gaussian signal was processed by a Tukan8K Multi Channel Analyzer (MCA) with USB 2.0 interface connected to a PC, then the energy histogram was recorded.

In order to perform the beam-off measurements, it is required to provide a veto signal, which blocks the acquisition during the beam pulse from a LINAC. To do that,

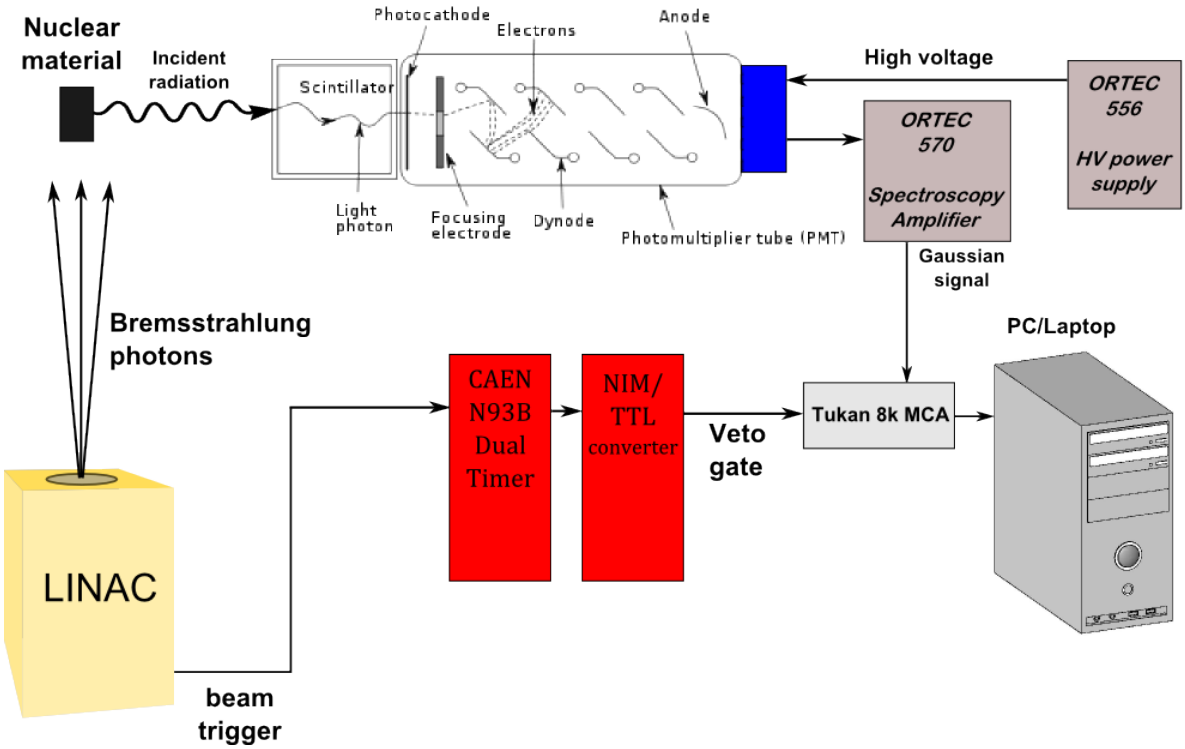

Figure 3.2: Acquisition track for detection of characteristic radiation from photofission with scintillation detector for the beam-off technique. Identical acquisition track is used for prompt neutrons detection.

the logic trigger from a LINAC must be properly shaped to cover the time region of the LINAC beam emission. It was done with the use of a CAEN N93B dual timer which can provide wide logic gate within a long period of time. For the measurements of delayed γ-rays from photofission during operation at 50 Hz, the TTL veto gate was set to 4 ms and then the acquisition window for a subsequent 16 ms. In the case of the Tukan8k USB analyzer, it is not required to set the logic acquisition window for each pulse separately. The logic veto signals are transferred to the "gate" input in the Tukan8k, which then works in the anticoincidence mode.

The measurements of the delayed γ-rays from photofission were performed with the application of the beam-off technique with two LINACs at NCBJ, as described below:

1. Siemens Mevatron KD-2 - a medical LINAC with klystron radio frequency of 2.9985 GHz and Bremsstrahlung energies of 6 and 15 MeV, see Figure 3.3. The

LINAC can be operated in two frequency modes: 50 Hz and 300 Hz, providing dose of 40 cGy/(min ×m) and 200 cGy/(min ×m) at the isocentre, respectively. The isocentre is a common geometry point of the beam axis and the medical LINAC axis of rotation. The pulse duration is 4-7 μs, and the logic trigger signal is +3 V. Delayed γ-ray measurements at the LINAC site were performed with ⌀5" × 3" BC-408 plastic scintillator coupled to an ET9390KB PMT with standard voltage divider and the following beam-off logic signals settings: 4 ms veto and 16 ms acquisition window.

2. Neptun 10P - a modified medical LINAC, designed for characterization of acceleration structures performance, see Figure 3.4. For the photofission study at NCBJ, the LINAC provided Bremsstrahlung photons with the endpoint at 10 MeV and frequency of 50 Hz. The dose rate could be set smoothly from 1 cGy to about 300cGy/(min ×m) at isocentre. Delayed γ-ray measurements at the LINAC site were performed with a ⌀3" × 2" EJ-200 plastic scintillator coupled to a ⌀3" Photonis XP5312 PMT. The time regime was identical to that for the Siemens KD-2 LINAC.

The results of the delayed γ-rays measurements with the HPGe detector and plastic scintillators will be described in Section 4.

3.3 Acquisition track for delayed neutrons detection

The delayed neutrons are the most unique signatures of fission. The acquisition track is very similar to that used for delayed γ-rays detection. Only the detector consisting of the scintillator and the PMT, was replaced with the ^{3}He gaseous counter coupled to an NCBJ Fast Preamplifier. The signal was shaped by the spectroscopy amplifier working at 3 μs shaping time and was finally recorded by the Tukan8k MCA connected to a PC. Photofission of nuclear materials was induced with the Siemens Mevatron KD-2 LINAC (see Figure 3.3) emitting Bremsstrahlung photons with an endpoint at 6 MeV, which is sufficient for fundamental research, and 10 MeV Neptun 10P (Figure 3.4) An additional advantage of 6 MeV energy is that the photons do not generate photoneutrons from

Figure 3.3: The Siemens Mevatron KD-2 LINAC.

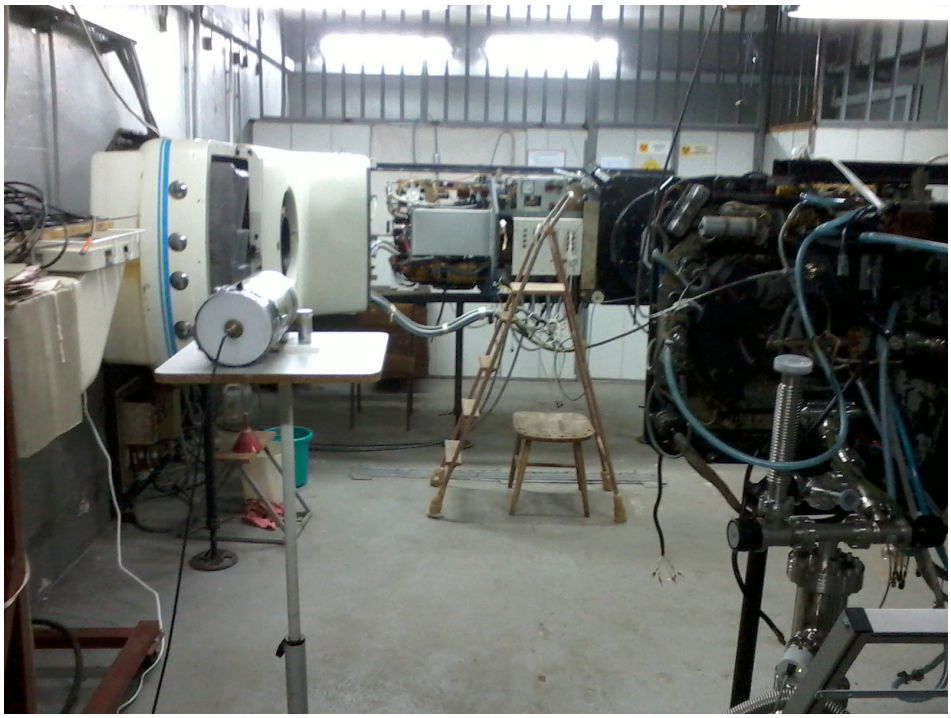

Figure 3.4: The measurement site with the Neptun 10P LINAC.

the LINAC construction elements, resulting in degradation of the signal-to-background ratio during beam-off measurements. The LINAC was working with the frequency of 65 Hz for 6 MeV, 45 Hz for 15 MeV and 4-7 μs beam pulse duration.

Measurements of delayed neutrons from photofission were performed in the Siemens Mevatron KD-2 LINAC facility at NCBJ. A 4.7 kg block of depleted uranium (DU) was situated 1 meter above the basement level. Photofission of the DU block was induced by the Bremsstrahlung photons with endpoint at 6 MeV and 15 MeV. In contrast to 15 MeV, advantage of the measurements with 6 MeV endpoint energy is that the photons does not generate photoneutrons from the LINAC construction elements, resulting in the degradation of signal-to-background ratio during the beam-off measurements. The measurements were performed with use of the beam-off technique, providing the veto gate during the beam for 3.5 ms and opening the acquisition for 12 ms for 6 MeV Bremsstrahlung. For the 15 MeV, the measurement was closed for 5.5 ms and opened for 16.5 ms. The high pressure ^{3}He gas detector was placed at different distances from the nuclear material, from 20 cm up to 300 cm. A special design preamplifier (NCBJ Fast Preamplifier) with a short relaxation constant (RC constant) developed in NCBJ was applied for the delayed photofission neutrons measurements. Such a preamplifier was applied because during an intense beam pulse from the LINAC standard preamplifiers (RC constant of 50 μs) reaching amplitude saturation and pulses from delayed neutrons cannot be recorded. The averaged waveforms presenting the relaxation times for the NCBJ Fast Preamplifier and commercially available Cremat CR-110 are shown in Figure 3.5.

The delayed neutrons were registered with a ^{3}He gaseous detector manufactured by LND, type 252184. In this study, measurements of the delayed neutrons from photofission were conducted with a ^{3}He cylindrical detector manufactured by LND Inc. The main parameters of the detector are listed below:

- Dimensions: $\varnothing$1.5" $\times$ 11.34".
- Active area: $\varnothing$1.43" $\times$ 9.60".
- Construction material: Stainless steel.
- Effective volume: 263 cm^3.

- Sensitivity: 300 cps/nv, according to the datasheet provided by the manufacturer.
- Pressure: 7600 torr (10 atm). In fact, the detector contains 7524 torr ^{3}He and 76 torr CO_2.

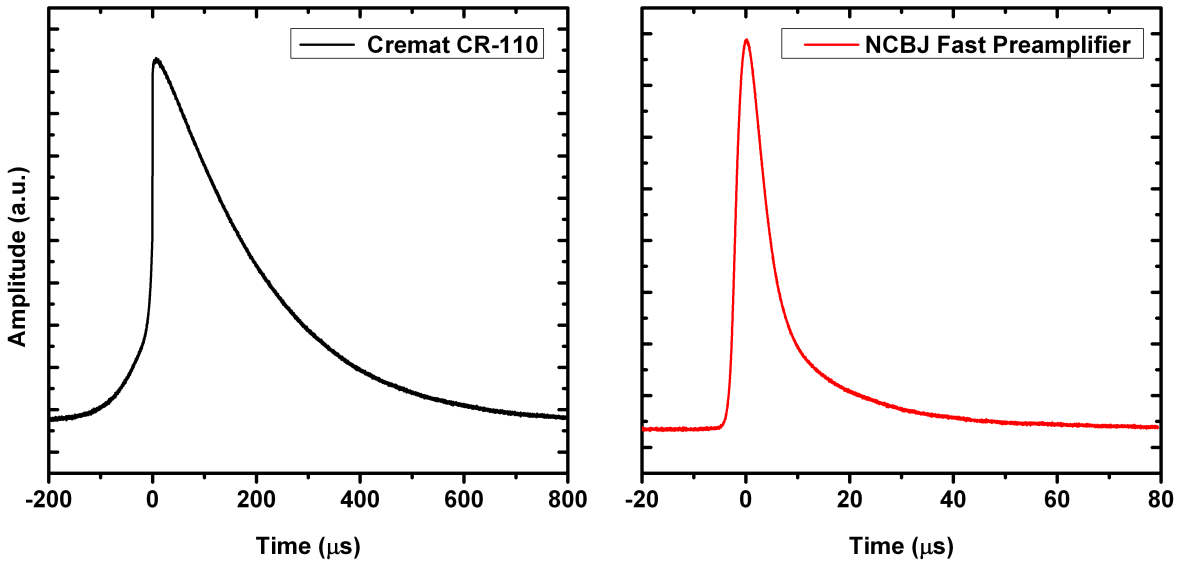

Figure 3.5: Comparison of the relaxation times of the commercial CR-110 and Fast Preamplifier developed in NCBJ. These waveforms were recorded by Tektronix TDS5054B Digital Oscilloscope and averaged over 10000 events.

The high cross section of 5530 b for the ^{3}He $+n_{therm}$ reaction, very low sensitivity to γ-rays and good signal-to-background ratio are undoubtedly the most important parameters for a delayed neutrons detector. The low energy neutrons are registered by the ^{3}He detector by means of ^{3}He(n, p)T reaction, with Q value of 764 keV, that corresponds to the maximum energy that can be deposited by the proton and tritium (T) in the detector at the same time. However, it is possible that the reaction products reach the wall, resulting in partial deposition of the carried energy. This phenomenon is known as a wall effect. The amplitude of the direct signal from the ^{3}He detector is very low, thus, it is required to use a charge sensitive preamplifier in order to integrate the charge and increase the signal amplitude. Moreover, if the detector would work in the beam-off mode, it is also required that the preamplifier RC constant should be as low as possible in order to prevent signal saturation. Measurements in the beam-off mode

and with higher Bremsstrahlung endpoint energy, e. g. 9 MeV, result in photoneutrons emission. Thus, the ^{3}He detectors are covered by 1 mm Cd foil in order to absorb thermalized photofission neutrons emitted from the LINAC construction materials. For the efficient detection of delayed neutrons, the MCNPX simulation of cylindrical shaped polyethylene (PE) moderator thickness was performed. The PE moderator covered the ^{3}He detector, and the thickness was calculated to be 5.5 cm. A simplified scheme is presented in Figure 3.6. The above mentioned ^{3}He detector was exposed to neutrons from the calibrated ^{252}Cf source on order to compare the detector neutron detection efficiency with the results obtained with MCNPX simulations. Results are presented in Section 5.2. The ^{252}Cf source emitted 55000 neutrons per second on the day of measurements, see Figure 3.7. The neutron source was placed 56.5 cm from the geometrical center of the detector, both the detector and source were placed 1 meter above the basement level. The detector was placed in side-on orientation relative to the neutrons source in order to obtain better detection efficiency - the solid angle for that geometry is significantly greater than that for the front orientation. Measurement lasted 2 h.

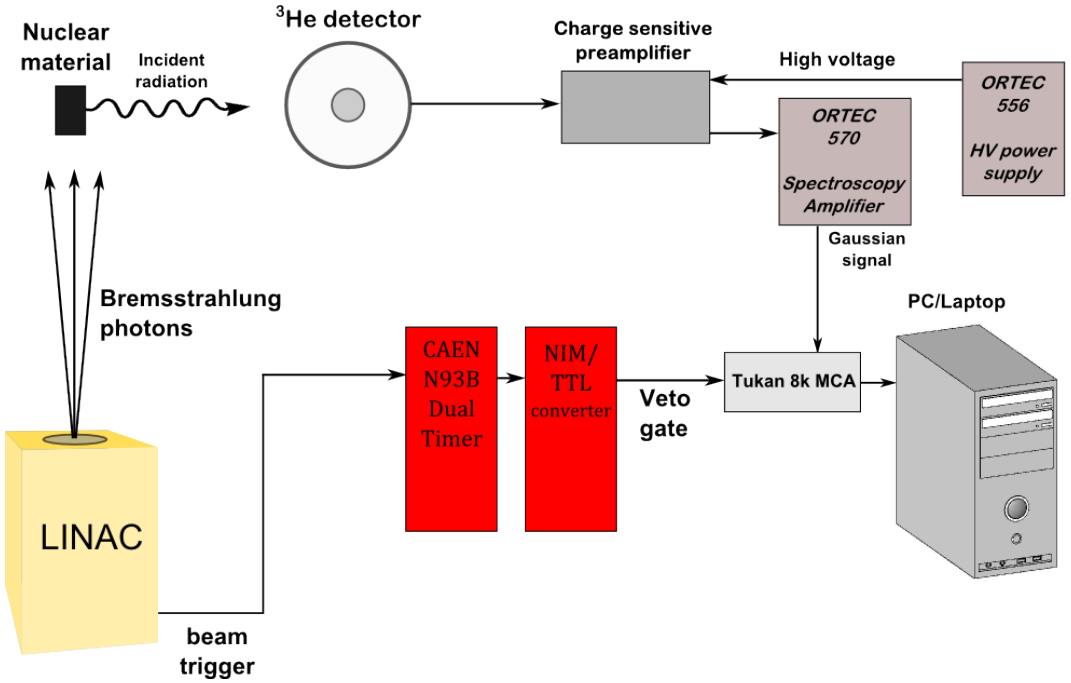

Figure 3.6: The block scheme showing the ^{3}He counter coupled to the acquisition system dedicated to delayed photofission neutrons detection.

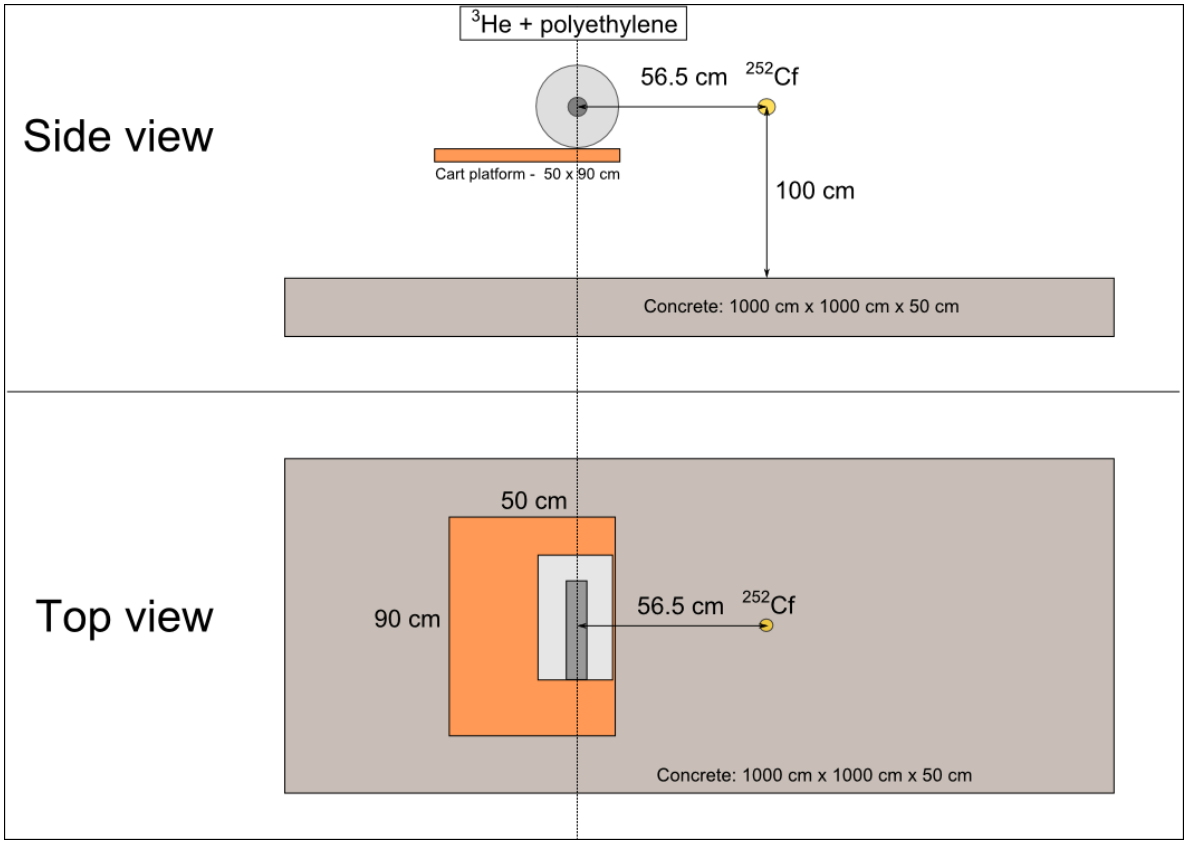

Figure 3.7: The geometry set for neutrons detection from the ^{252}Cf source with use of the ^{3}He detector. The geometry was then applied in the MCNPX simulation.

3.4 Acquisition track for prompt neutrons detection with the use of fluorine-based scintillators

The measurements of prompt fission neutrons detection were based on Threshold Activation Detection (TAD), described in detail in the Introduction. Basically, fast neutrons from photofission activate an atomic nucleus of the material (e.g. scintillator) having an activation threshold above 2.5 MeV and short half-lives of the activation products. Particularly, scintillators containing ^{19}F are the best solution for this technique due to the high energy endpoint of the β^- particle of approximately 10.4 MeV, exceeding the region of the contribution of delayed γ-rays and the optimal activation threshold as well as the half-lives of the activation products. Low amounts of hydrogen

in a scintillator medium are mandatory in order to prevent neutrons slowing down via the scattering process. Scintillators based on the ^{19}F that can be applied to the TAD technique are:

1. Liquid organic scintillators based on highly purified hexafluorobenzene (C_6F_6) and with a low content of hydrogen ($10^{20}/cm^3$), such as EJ-313 or BC-509. Currently the scintillators were produced in the form of a box with dimensions 40 × 40 × 40 cm^3.

2. Inorganic scintillators, such as BaF_2, CaF_2 or CeF_3 [66,67]. BaF_2 and CaF_2 scintillators are available commercially in size ⌀3" × 3", both in reasonable prices, however, the CaF_2 is slightly cheaper than the former. CeF_3 is the densest scintillator and contains the highest amount of F atoms per volume, however, large sizes are commercially unavailable.

3. Organic plastic scintillator based on pentafluorostyrene, containing a high amount of fluorine (3.73×10^{22} g/cm^3). This material was developed in collaboration between NCBJ and CEA Saclay, France. However, the scintillator contains hydrogen, and the F/H value, driven only by the pentalfuorostyrene, is 1.66. This material is under further investigation.

The neutron detection efficiency of the ^{19}F based scintillators by means of activation with a ^{252}Cf source emitting 57000 n/s at the day of measurements was roughly estimated. The acquisition track for continuous measurement (without the beam-off logic designed for measurements between beam pulses) is presented in Figure 3.8.

The amplitude of the signal from the PMT is sufficiently high, thus, use of the preamplifier is not required. The anode signal was shaped by the Ortec 570 spectroscopy amplifier, which was finally recorded by the Tukan 8K USB MCA. The same acquisition track was used for estimation of the fast neutrons relative efficiency of the TAD detectors with use of the Sodern Genie 16GT D+T neutron generator. The neutron generator provides the neutrons from d(T,n)^{4}He reaction with energy of 14.1 MeV. The scintillators were placed at the distance of 50 cm from the deuterium target and 1 meter above the basement level. The acceleration voltage of the deuterium ions was set to 80 kV, and the beam current to 20 μA, providing the neutron flux of 0.3×10^8 n/s

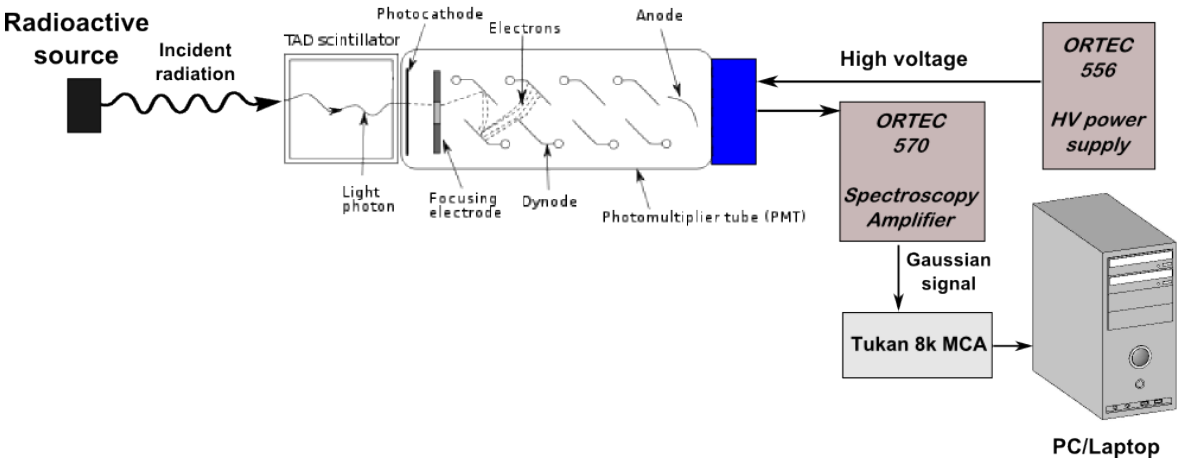

Figure 3.8: The block scheme of the acquisition track based on the TAD scintillator without the beam-off logic.

in 4π. Scintillators were exposed to the 14.1 MeV neutrons for 120 s, then the beam was stopped and the spectrum was measured through 60 s.

The beam-off technique was applied when the activation of ^{19}F nuclei in the BaF_2 scintillator with neutrons from the D+T neutron generator was measured with the HPGe GMX 60-P4-83-CW detector. During this measurement, the logic signals were provided by the D+T generator. The veto logic was set to 5 ms, then, the data was measured through 25 ms.

Measurements of prompt photofission neutrons with the $\varnothing$ 2" $\times$ 3" BaF_2 scintillator were conducted at the SAPHIR facility, CEA LIST, Saclay site, France. In order to induce photofission in nuclear material, a Varian LINATRON M9 LINAC emitting Bremsstrahlung photons with an endpoint energy of approximately 9 MeV was used. A 1.2 kg sample of depleted uranium (DU) was placed 1 meter from the conversion target and exposed to high energy photons. The detector and DU were placed 1 meter above the basement level. The distance between the detector and the DU was also 1 m. The simplified scheme of the measurement site is presented in Figure 3.9.

The acquisition track is actually identical with that for the delayed γ-rays measurements with plastic scintillators. Instead of the plastic, the $\varnothing$2" $\times$ 3" BaF_2 (TAD detector) was used for prompt photofission neutron detection from the DU using the TAD technique. The LINAC beam frequency was set to be 33 Hz for beam-off mode

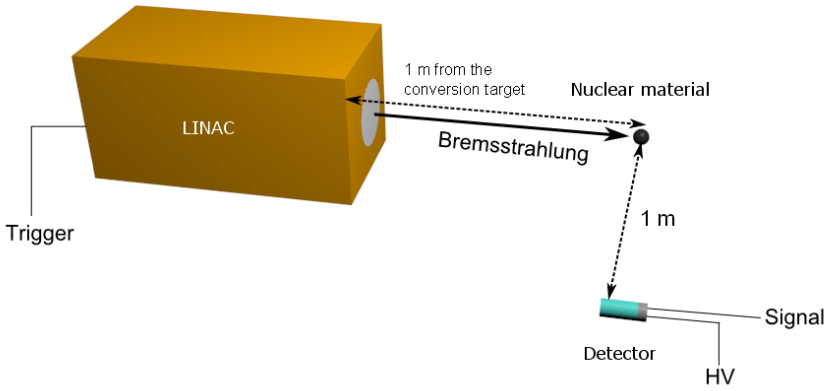

Figure 3.9: The geometry setup during the measurements performed at the SAPHIR facility.

and 385 Hz for after beam measurement. The veto logic signal lasted 21 ms and the acquisition was opened for 9 ms in order to avoid saturation of the detector and possible environmental activation by photoneutrons. Results will be discussed in Chapter 6.

Two methods were evaluated in order to detect prompt photofission neutrons by means of the TAD technique. The first one is based on data acquisition after irradiation of the nuclear material at a frequency of 385 Hz and an intense dose of 30 Gy during 60 s without data recording between pulses, the spectrum was recorded within 60 s after beam turn-off. This approach is introduced as the "out-of-beam" method.

The second method is based on enabling the acquisition between the LINAC beam pulses and was introduced as the "beam-off" inspection technique, see Figure 3.10. In the latter, the trigger from the LINAC was converted into the wide TTL veto logic gate, set at 21 milliseconds (ms), with the logic gate opening the acquisition for 9 ms. In this case, the beam frequency was set to 33 Hz and inspection lasted 120 s. The 21 ms veto time break after irradiation was introduced in order to let the detector recover after saturation caused by the intense photon beam from the LINAC and the possible registration of high energy γ-rays emitted in the ms time range and related to the neutron scattering on Ba and F nuclei. In this study, the scintillators were not shielded from the scattered radiation in order to observe the contributions both from nuclear

material and background, thus, the investigation can be considered as a ground work for further study.

In the paper [14], the term of "active background" was also introduced, which stands for the number of events registered during beam-off measurement. The data acquisition is opened for 9 ms, without nuclear material on the irradiation site. This active background is mainly composed of γ-rays from the scintillator and structural materials activated by photoneutrons from the LINAC, natural and cosmic radiation (protons, muons), and also possibly from scattered Bremsstrahlung photons and pile-up contribution at the high-energy range.

The measurements of the pentafluorostyrene-based plastic scintillator's (F-plastic) response to γ-rays and neutrons from ^{252}Cf and PuBe sources was performed. The emission spectrum, light output by means of the single photoelectron method and decay time was also measured.

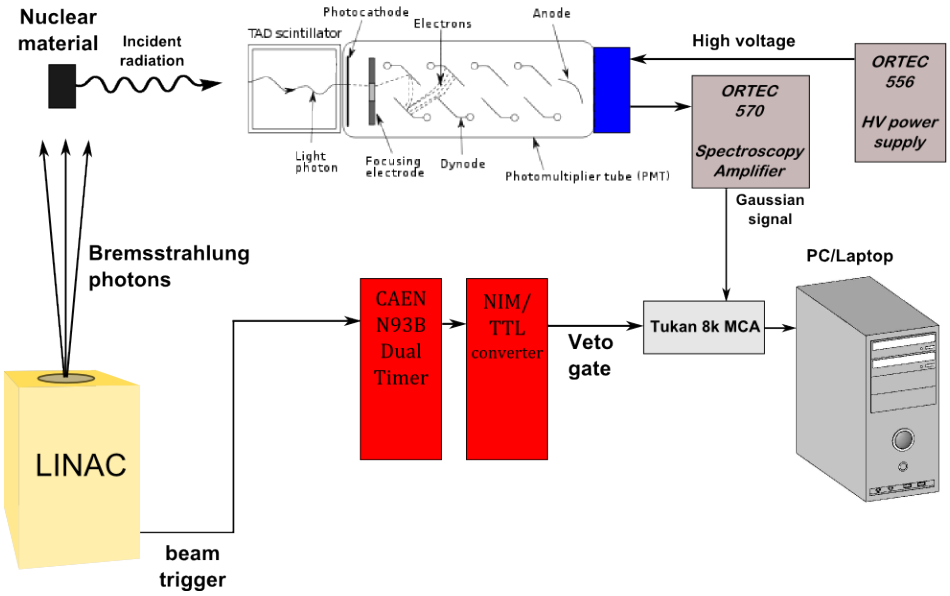

Figure 3.10: The block scheme of the acquisition track based on the TAD scintillator with the beam-off logic. The acquisition track is the same for the LINAC and D+T neutron generator used as a radiation source.

Radioluminescence and fluorescence spectra were recorded using a Horiba Jobin Yvon Fluoromax 4P spectrofluorometer. Light excitation was performed at 300 nm for the fluorescence experiment. To access the radioluminescence spectrum, light excitation

was shutdown, and a 24 MBq Sr/Y source was used to irradiate the scintillator.

For the study of scintillation decay time, the scintillators were coupled in separate measurements to the Hamamatsu R2059 fast timing PMT with a transit time spread (TTS) of 550 ps [81]. A Tektronix TDS5054B digital oscilloscope was used for the measurement of scintillation decay time. The result was based on averaged 10000 waveforms.

In order to characterize the detectors in term of scintillation yield, the number of photoelectrons $N_{phe/MeV}$ was measured using a single photoelectron method. The technique, which was proposed by Bertollacini et al. [82] and used in later studies [83], relies on the comparison of the 661.7 keV full absorption peak centroid or 477.3 keV Compton edge (CE) position P_{ctr} measured for the ^{137}Cs source with the position of the peak originated due to thermionic emission of single electrons from a PMT photocathode P_{1phe}. The full energy peak was used in the case of BaF_2, the CE for organic scintillator, in which full γ-ray deposition in the higher energy range is not observed due to the low Z of the scintillator. The centroid position is corrected by the signal gain ratio G_{ratio} of the spectroscopy amplifier (e.g. Ortec 672) and expressed per one MeV energy unit. Usually, the photoelectron yield is measured with a ^{137}Cs source. Photoelectron number per 1 MeV is calculated from Equation 3.1:

$$N_{phe/MeV} = \frac{\frac{P_{ctr}}{P_{1phe}} \times G_{ratio}}{E(MeV)}. \tag{3.1}$$

The 1phe and ^{137}Cs spectra are shown in Figure 3.11. Concerning the CE position (L_{CE}), one needs to emphasize that the Compton maximum L_{max} is not the true position of the CE due to the finite energy resolution of the scintillator. Using the Wide Angle Compton Coincidence technique [84], it was possible to precisely extract the position of the CE. It turned out that it can vary depending on the energy of incident γ-ray, type of scintillator and its size. Basing on this paper, the ^{137}Cs CE position of 477.3 keV was taken to be 80% of the L_{max} height.

Light output, in terms of photons per MeV (ph/MeV), was determined for F-plastic coupled to a Photonis XP5212 PMT characterized by a high blue sensitivity of 12.2 mA/lm Corning blue. The choice is supported by the fact that the production of exces-

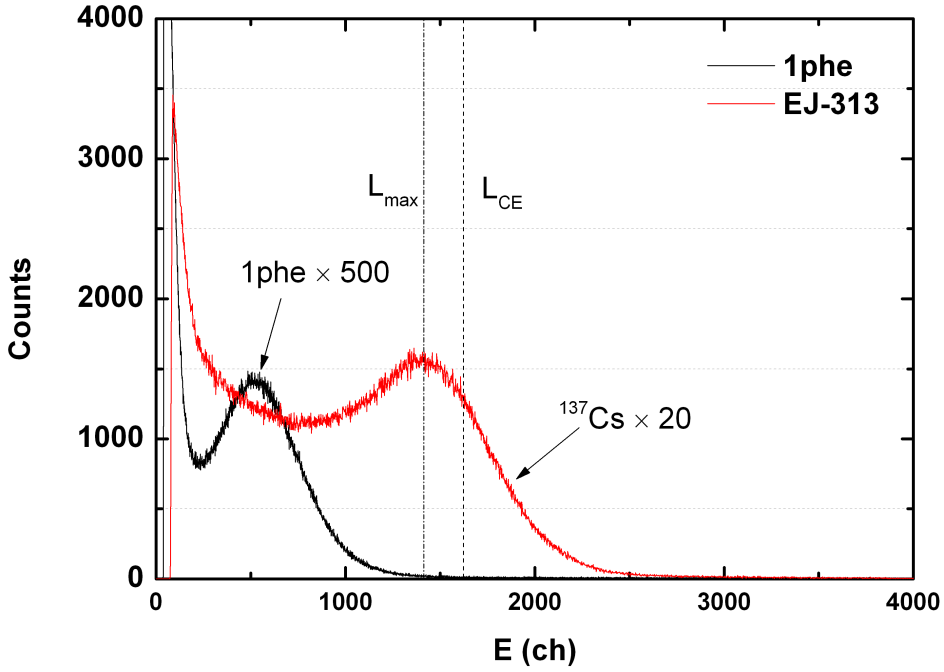

Figure 3.11: The spectra of single photoelectron and ^{137}Cs for the ⌀5" × 3" EJ-313 scintillator. L_{max} and L_{CE} stand for position of Compton maximum and position of CE, respectively. The numbers 20 and 500 are the gain set on spectroscopy amplifier for measurement of ^{137Cs} spectrum and 1phe, respectively.

sive space charge in dynode structure for that PMT can be neglected [85], which in turn increases the precision of the obtained value of absolute light output. According to the datasheet delivered together with the PMT, the quantum efficiency (QE) at 400 nm for the XP5212 PMT is 30 ± 3%. The anode signal from the XP5212 PMT was sent to an Ortec 113 preamplifier, and then shaped by an Ortec 672 spectroscopy amplifier with the shaping time set to 0.5 μs. The Gaussian signals were recorded with a Tukan8k Multi-Channel Analyzer (MCA) with USB 2.0 interface. [86].

Chapter 4

Detection of delayed γ-rays emitted from Special Nuclear Material

In this Chapter, passive measurements of γ-rays emitted from enriched uranium sample with EAGLE array were conducted. Moreover, after-beam measurements of highly enriched uranium (HEU) with Ortec GMX series HPGe with 25% efficiency (relative to 3"$\times$ 3" NaI:Tl) were also performed [13]. Moreover, active photofission measurements of 4.7 kg depleted uranium (DU) block with 3" $\times$ 2" EJ-200 and 5" $\times$3" BC-408 plastic scintillators were also conducted with use of 6 MeV and 10 MeV LINACs.

4.1 Fundamental γ-ray spectroscopy of highly enriched Uranium (HEU)

In order to gain a better knowledge of the energy spectra of nuclear materials, precise γ-ray spectroscopy (passive measurements) were performed. These measurements were done for a 100 g Uranium rod (enriched to 93%) in order to establish the most prominent γ lines in the natural decay series and photofission reaction. The first experiment included measurements of single γ-ray spectra and γ-γ coincidences before irradiation with the use of the European Array for Gamma Levels Evaluations (EAGLE) consisting of 15 High Purity Germanium (HPGe) detectors located at Heavy Ion Laboratory (HIL),

University of Warsaw [12]. In the second experiment, the 100 g U sample was irradiated with 15 MeV photons (Bremsstrahlung radiation) from a Siemens Mevatron KD-2 linear accelerator located in the National Centre for Nuclear Research (NCBJ), Otwock. The single γ-ray and γ-time spectra after 10 min irradiation time were carried out with a large volume HPGe detector. The information obtained from such spectra are crucial for the detection of smuggled nuclear material by high-resolution systems designed for border monitoring or for nuclear waste content characterization.

4.2 Measurement of γ - γ coincidences with the EAGLE HPGe array

The γ-γ coincidence measurements for a 100 g U sample (ϕ = 0.8 cm in diameter and 10 cm length, enriched to about 93% ^{235}U - according to formal specification) intended to learn more about radioactive natural decay chains in heavy nuclei were performed with the EAGLE detector array [12]. Data was collected at an amplification level allowing for an observation of γ-rays with energy up to 4 MeV. Results of the passive measurements at EAGLE are presented in Table 4.1 and Figure 4.1. The 4n, 4n+1, 4n+2 and 4n+3 stands for Thorium, Neptunium, Uranium and Actinium decay chain, respectively.

Table 4.1: The γ-γ coincidence data of a 100 g U sample (before irradiation with 15 MeV photons). For each γ line its relative intensity, the list of the most prominent γ-rays observed in coincidence as well as its origin are given.

$E_\gamma^{a)}$(keV)	$I_\gamma^{rel\ b)}$	Coincidence$^{c)}$ (keV)	Origin of E_γ	Decay series
115.2	27	123.5, 176.6, 300.1	^{212}Pb$\rightarrow^{212}$Bi	4n
143.8	48	202.1, 266.5	^{235}U$\rightarrow^{231}$Th	4n+3
163.4	28	246.8	^{231}Th$\rightarrow^{231}$Pa ^{235}U$\rightarrow$ ^{231}Th	4n+3

Table 4.1: Continued

185.7	327	202.1, 266.5 186.2	^{235}U→ ^{231}Th, ^{226}Ra	4n+3 4n+2
202.1	14	143.8, 185.7	^{235}U→ ^{231}Th	4n+3
205.3	34	173.3, 182.6, 246.8	^{235}U→ ^{231}Th	4n+3
215.2	0.6	109.2, 143.8, 163.4, 185.7, 195.0, 205.3	^{235}U→ ^{231}Th	4n+3
238.6	3	176.7	^{212}Pb→ ^{212}Bi	4n
246.8	1	109.2, 163.4, 205.3	^{235}U→ ^{231}Th	4n+3
252.6	0.2	510.7, 583.2, 2614.5	^{208}Tl→ ^{208}Pb	4n
277.4	2	583.2, 2614.5	^{208}Tl→ ^{208}Pb	4n
291.7	0.3	96.09, 143.8	^{235}U→ ^{231}Th	4n+3
300.1	0.6	115.2 115.3	^{212}Pb→ ^{212}Bi ^{233}Pa→ ^{233}U	4n 4n+1
311.1	0.6	weak 143.8 and 163.4	^{233}Pa→ ^{233}U	4n+1
510.7	24	583.2, 2614.5	^{208}Tl→ ^{208}Pb	4n
569.8	0.05	1063.7	^{211}Po→^{207}Pb	4n+2
583.2	46	277.4, 510.7, 722.0, 763.1, 982.7, 1282.8, 2614.5	^{208}Tl→ ^{208}Pb	4n
609.3	1	768.4, 934.1, 1120.3, 1238.1, 1408.0	^{214}Bi→^{214}Po	4n+2
727.3	5	785.37, 893.4, 952.1, 1073.6, 1078.6	^{212}Bi→^{212}Po	4n
763.1	2	583.2, 2614.5	^{208}Tl→^{208}Pb	4n
860.6	10	2614.5	^{208}Tl→ ^{208}Pb	4n
893.4	0.6	727.3	^{212}Bi→^{212}Po	4n
1001.0	0.7	weak 135.3 and 166.5	^{234m}Pa→^{234}U	4n+2
1063.7	0.1	569.7	^{211}Po→^{207}Pb	4n+2
1078.6	1	727.3	^{212}Bi→^{212}Po	4n
1093.9	0.4	2614.5	^{208}Tl→ ^{208}Pb	4n
1120.3	0.8	609.3	^{214}Bi→^{214}Po	4n+2
1238.1	0.4	609.3	^{214}Bi→^{214}Po	4n+2

Table 4.1: Continued

1284.0	0.2	609.3	^{214}Bi$\rightarrow^{214}$Po	4n+2
1764.5	0.7	964.1	^{214}Bi$\rightarrow^{214}$Po	4n+2
2204.1	0.2	weak 581.9	^{214}Bi$\rightarrow^{214}$Po	4n+2
2614.5	100	277.4, 510.7, 583.2, 763.1, 860.6, 927, 983, 1093.9, 1282.8	^{208}Tl$\rightarrow$ ^{208}Pb	4n

[a)] The energies are accurate within 0.3 keV for strong well resolved lines. For other lines the uncertainty may rise up to 0.6 keV.

[b)] Intensity normalized to 100 for the 2614 keV line. Estimated uncertainties are less than 10 % for strong well resolved lines. For other lines they may rise up to 20 %.

[c)] In most of the gates considered, strong coincidences with Pa (region 96-108 keV), U (region 98-110 keV) and Th (region 93-105 keV) $K_{\alpha\beta}$ X-rays are observed.

Inspection of Figure 4.1 (based on the γ-γ coincidences analysis) reveals that one of the most intensive high energy γ-rays in the spectrum is $3^- \rightarrow 0^+$ transition of energy 2614.5 keV appearing due to ^{208}Tl$\rightarrow$ ^{208}Pb decay in ^{232}Th series (4n) (see Table 4.1). It is worth pointing out that the isotope naturally occurs in non-purified uranium samples. It is noteworthy that when measuring the γ-ray spectra of an enriched uranium sample, which was has not been purified off ^{232}Th, this strong γ line will always be observed. Because its energy is sufficient to penetrate cargo walls and thin shielding, observation of this γ line is a good signature indicating the possible presence of ^{235}U in cargo containers, which can be recorded by passive radiation monitors and hand-held devices [87, 88].

4.3 Estimation of HEU enrichment

It is possible to roughly estimate the enrichment of the uranium sample through the analysis of the γ-ray single spectrum by comparing the intensities of 185.7 keV γ line from ^{235}U and 111.0 keV X-rays with 1001.0 keV from ^{238}U [89]. Particularly, this method can be successfully applied to the enrichment estimation of uranium powders due to the neglected self-absorption contribution of X-rays and γ-rays. However, the

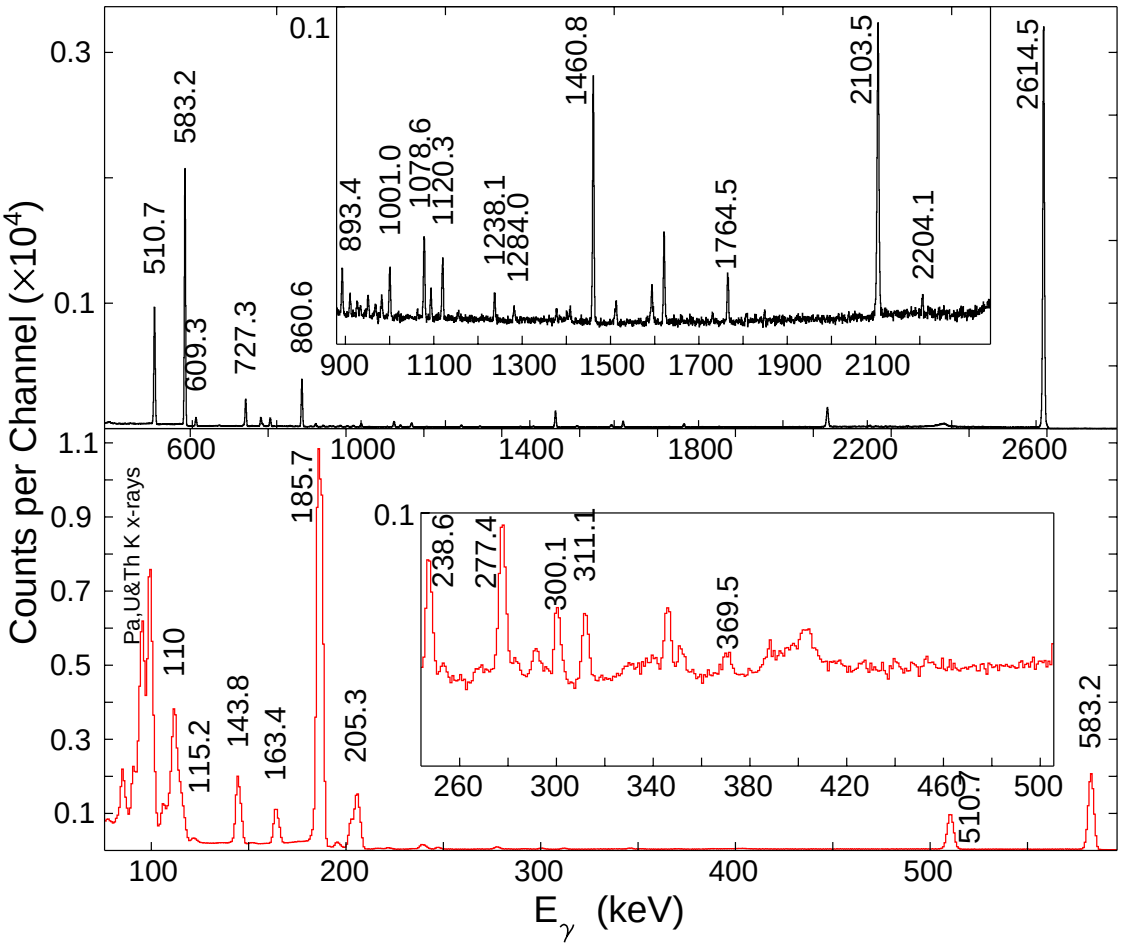

Figure 4.1: Example of efficiency corrected γ-γ coincidence spectrum of 100 g Uranium sample (before irradiation) measured with 15 HPGe Compton suppressed detectors of about 70 % efficiency with respect to 3" × 3" NaI:Tl scintillator.

uranium X-rays are disturbed by other close energy radiations present in the sample, like e.g. ^{232}Th contribution to the uranium X-ray intensity. Also the low intensity of the 1001.0 keV line (appearing in the 1.17 min decay of ^{234m}Pa $\rightarrow$ ^{234}U, being a member of the uranium natural decay series) makes the accuracy of enrichment determination rather uncertain. Moreover, the detector efficiency at 185.7 keV and 1001.0 keV is significantly different and due to the large energy gap between the lines, uncertainties in the efficiency could cause a significant impact on the final enrichment estimation. According to [90] the coincidence summing correction factors should also be taken into account when analyzing the radionuclides belonging to the three natural decay series.

Therefore, the estimation of the relative yields of an actinium (^{235}U) to uranium (^{238}U) series is a rough measure of enrichment.

Summing the relative intensities of all the γ lines corresponding to each decay series (taken from Table 4.1), the yields of the decay series were estimated to be: $(thorium) : (uranium) : (actinium) \simeq (9.9\%) : (0.9\%) : (79.2\%)$, with $\pm$ 5.0% error margin. The presence of a neptunium series was also noticed (by its 300.1 and 311.1 keV γ-rays), however, it was neglected due to its very low intensity. Comparing the intensities of the actinium and uranium chains, the enrichment value was estimated as:

$$En = \frac{I_\gamma(Actinium\_series)}{I_\gamma(Uranium\_series)} = 88 \pm 5\%, \tag{4.1}$$

which is not far from the known 93 % level. It is worth noting that the estimation was done for the 100 g HEU rod $\varnothing$0.8 cm $\times$10 cm, thus, even with the self-absorption contribution, the final level of enrichment is in good agreement with the formal specification.

4.4 Photofission of uranium and characterization of delayed γ-rays with use of HPGe detector

Our previous investigation, described in Section 4.2, included γ-γ coincidence spectroscopy in order to get a proper knowledge of the spontaneous X and γ-ray spectra of the enriched uranium. Observed γ peaks appeared up to 2614.5 keV, the last was ascribed to ^{208}Tl$\rightarrow^{208}$Pb from the Thorium decay chain. Afterward, measurements of delayed γ-rays spectra were carried out in order to show the most intense γ lines with energy up to 4 MeV. The 100 g U sample enriched to 93% was irradiated with high energy Bremsstrahlung photons with an energy endpoint at 15 MeV. For this purpose we used a Siemens KD-2 Linear Accelerator. A dose rate of 40 cGy/(min $\times$m) and a repetition time of 45 Hz was achieved. Acquisition of the γ spectra was started after 10 minutes of sample irradiation and 30 minutes of cooling time to obtain an acceptable counts rate and avoid pile-ups. One hundred series of γ spectra were acquired, each

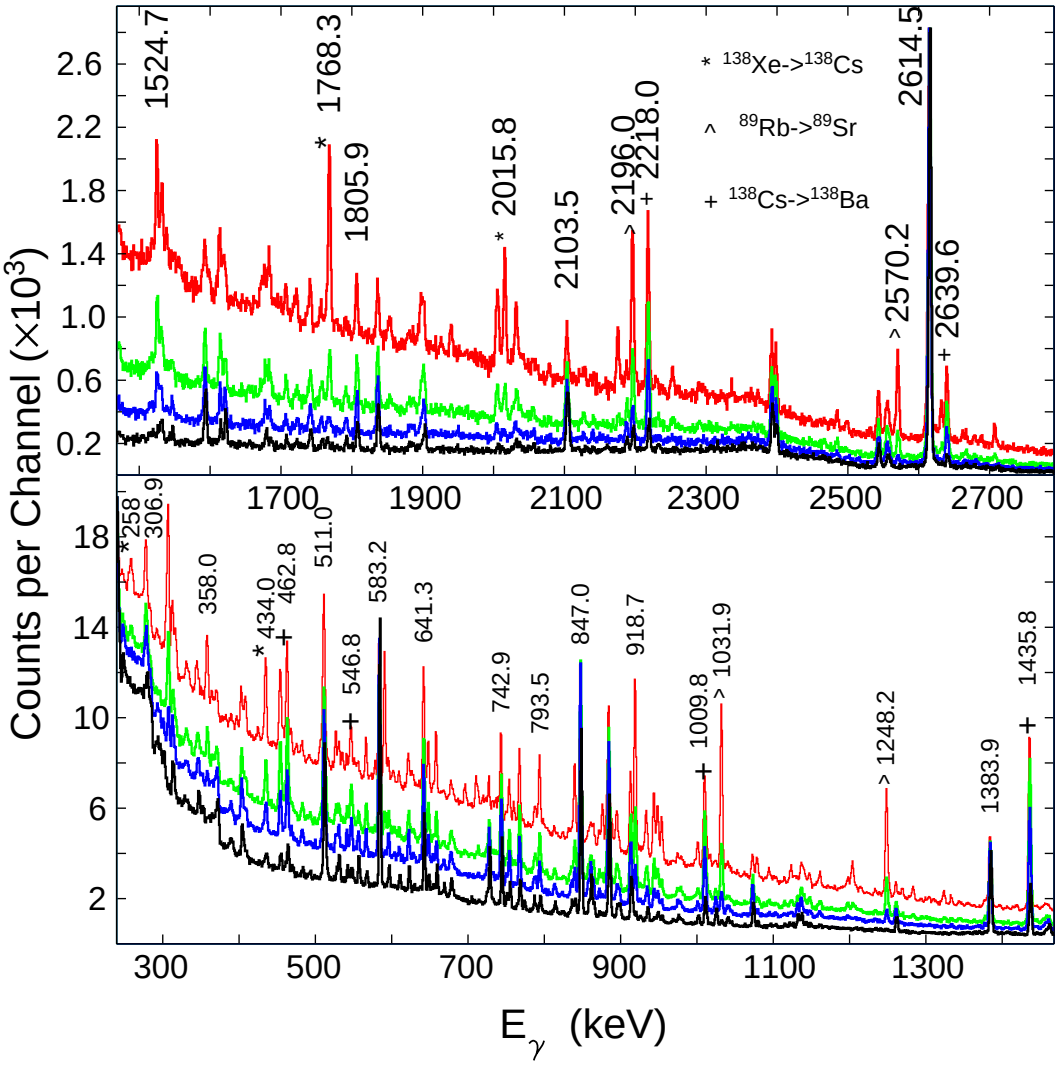

Figure 4.2: Energy spectra plotted for four subsequent measurements using HPGe (25 cm^3) detector after 10 minutes irradiation with 15 MeV photons of 100 g Uranium rod (of ϕ=0.8 cm diameter, and 10 cm length) and after 30 minutes of cooling time. From the top to the bottom, spectra acquired in 0, 30, 50, and 90 minutes after the end of cooling time are plotted.

measurement lasted 10 minutes. The illustration of spectra measured in this way is given in Figure 4.2, where 4 spectra are displayed in a function of time: the first measurement corresponds to time equal to 0 minutes - the next spectra were taken 30, 50, and 90 minutes later. The most prominent decays were presented in Table 4.2.

On the basis of the data presented in Figure 4.2 several values of photofission prod-

Table 4.2: List of the most prominent decays of photofission products appearing after 10 min. irradiation with 15 MeV photons of a 100 g enriched U sample.

Photofission product decays	E_γ(keV)	$T_{1/2}$(min)		
		Present exp.	Average	References
^{95}Y$\rightarrow$ ^{95}Zr	3576.0	11.3 $\pm$0.8		
^{95}Y $\rightarrow$ ^{95}Zr	2632.4	7.7 $\pm$1.8	9.8 $\pm$1.1	10.3 $\pm$0.1 [91]
^{95}Y $\rightarrow$ ^{95}Zr	954.0	10.5 $\pm$0.8		
^{89}Rb $\rightarrow$ ^{89}Sr	2570.2	16.1 $\pm$0.5		
^{89}Rb $\rightarrow$ ^{89}Sr	1248.2	16.7 $\pm$0.5	16.8 $\pm$0.4	15.2 $\pm$0.1 [92]
^{89}Rb $\rightarrow$ ^{89}Sr	1031.9	17.6 $\pm$0.6		
^{138}Xe $\rightarrow$ ^{138}Cs	2015.8	17.7 $\pm$0.2		
^{138}Xe $\rightarrow$ ^{138}Cs	1768.3	16.6 $\pm$0.9	19.8 $\pm$1.0	14.0 $\pm$0.8 [93]
^{138}Cs $\rightarrow$ ^{138}Ba	2639.6	32.5 $\pm$1.2	32.5 $\pm$1.2	33.4 $\pm$0.2 [94]

ucts half-lives were determined. In order to obtain the half-lives of the photofission products, the number of net counts under the considered peak were calculated after each subsequent 10 min of data acquisition. Then, the exponential function was fitted to the calculated number of counts. The half-lives of the most intense observed lines are in the range 10 min $<T_{1/2}<$ 32 min. The plots presenting the half-lives estimation are presented in Figure 4.3. The half-lives of the photofission products estimated during this experiment are in good agreement with the data available in the mentioned databases.

The γ-rays from the irradiated uranium sample together with their relative intensities and parent nuclei are listed in Table 4.3. The Table shows that the most intense γ-rays are in the energy range from 306.9 keV up to 3927.5 keV due to the decay of the photofission products. The peaks assigned with (*) were measured and normalized to 1435 keV from ^{138}Cs after the 10^{th} measurement session due to a half-life greater than 5 h and lower radiation background. In the case of multiple unresolved peaks, the total intensity is shown and the energies of the mixed peaks are averaged. The low energy threshold of 306.9 keV was selected in order to cut-off from the Pa, U and Th KX-rays and low energy γ-rays appearing due to the presence of ^{235}U nuclei. Particularly important are the high energy lines 3576.0 keV, 3927.5 keV, 2570.2 keV, 2639.6 keV and 2252.3 keV, identified as belonging to ^{95}Y, ^{84}Br, ^{89}Rb, ^{138}Cs and ^{138}Xe, respectively.

Such high energy γ-rays can indicate the presence and origin of special nuclear material in suspected cargo and bulky nuclear waste. The spectrum presenting the high energy region of induced γ-rays is shown in Figure 4.4. According to [95], more than 43% of γ-rays with energy of 4 MeV pass through a 1 cm thick lead shielding. Moreover, the contribution from natural background is very slight above energy levels of 2.5 MeV. Thus, the γ-ray signatures at energy range above 2.5 MeV are very important from the point of view of shielded nuclear material detection at border crossings.

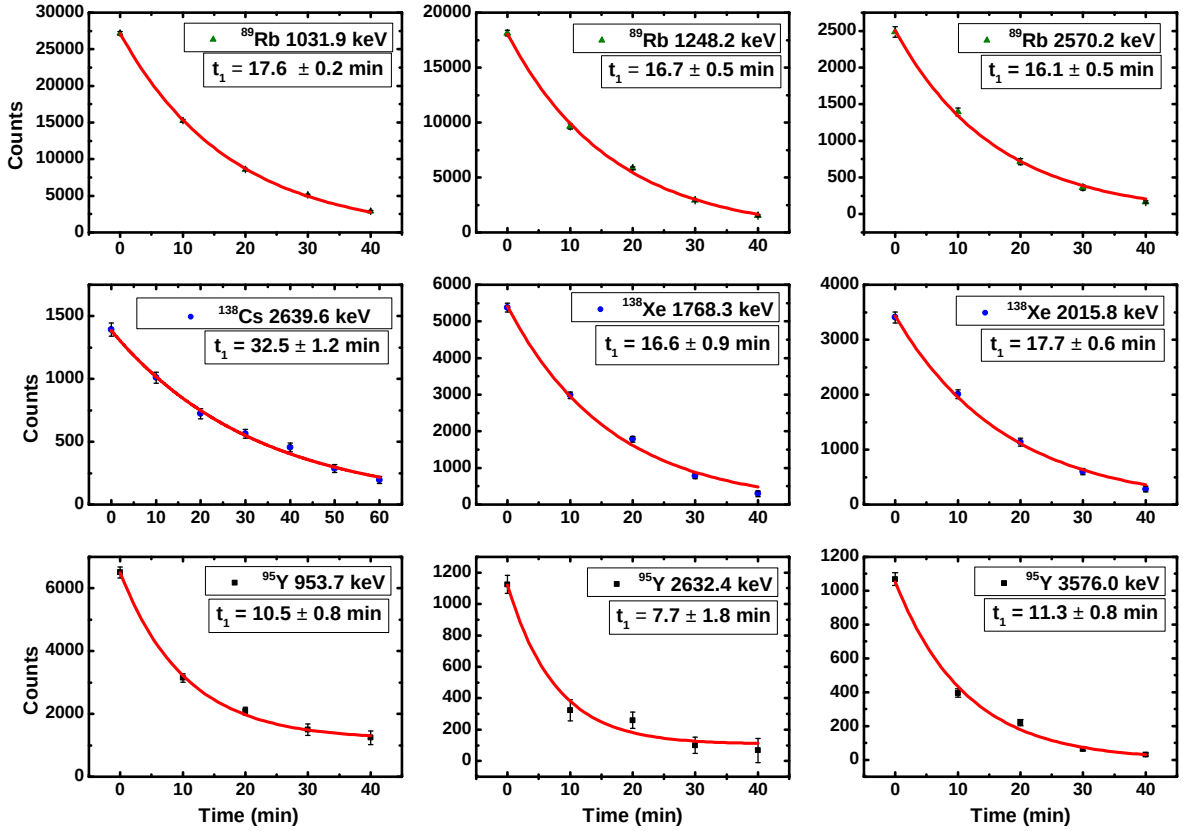

Figure 4.3: Estimated half-lives of the delayed γ-rays belonging to ^{89}Rb, ^{95}Y, ^{138}Xe and ^{138}Cs photofission products.

Table 4.3: List of γ transitions in energy range between 306.9 and 3927.5 keV originated from the photofission products. The data presented in [96] were used to assign the parent nucleus to each γ line. The efficiency corrected intensities are relative to the 1435.8 keV line ascribed to the ^{138}Cs decay.

E_γ (keV)	Photofission product	I_γ^{rel}	E_γ (keV)	Photofission product	I_γ^{rel}
306.9	^{101}Tc	22.0 ± 1.8	1383.9	^{92}Sr	40.3 ± 1.5
313.1	^{133}Te/^{128m}Sb	9.2 ± 1.7	1435.8	^{138}Cs	100.0 ± 1.6
316.0	^{146}Ce	8.8 ± 1.7	1456.4	^{135}I/^{134}I	10.6 ± 1.3
343.7	^{141}Ba	15.4 ± 1.8	1524.7	^{146}Pr	11.3 ± 1.2
358.0	^{104}Tc	12.2 ± 1.5	1531.1	^{88}Kr/^{101}Mo	8.4 ± 1.1
404.0	^{134}I/^{87}Kr	7.8 ± 1.4	1612.8	^{134}I/^{104}Tc	6.0 ± 1.1
408.3	^{138}Cs/^{133}Te	9.1 ± 1.5	1683.2	^{133m}Te	5.9 ± 1.0
434.0	^{138}Xe/^{134}I	16.9 ± 1.6	1704.4	^{133m}Te	2.6 ± 0.9
453.9	^{146}Pr	17.3 ± 1.6	1720.0	^{131}Sb	2.5 ± 0.9
462.8	^{138}Cs	22.1 ± 1.7	1741.1	^{87}Kr/^{84}Br/^{134}I	3.7 ± 1.0
529.9	^{133}I	5.6 ± 1.7	1768.3	^{138}Xe	19.6 ± 1.3
546.8	^{138}Cs/^{135}I	9.1 ± 1.4	1805.9	^{134}I	5.7 ± 1.0
567.0	^{134}Te	5.8 ± 1.4	1836.0	^{88}Rb	5.7 ± 1.0
590.2	^{93}Sr/^{101}Mo	26.3 ± 1.6	1854.4	^{131}Sb	2.6 ± 0.9
641.3	^{142}La	29.2 ± 1.7	1876.8	^{84}Br	< 1
647.5	^{133m}Te	11.6 ± 1.5	1897.8	^{84}Br	4.8 ± 1.1
657.8	^{89}Rb/^{131}Sb	14.8 ± 1.6	1940.3	^{95}Y	3.0 ± 1.0
742.9	^{134}Te/^{128m}Sb	20.0 ± 1.6	2005.0	^{138}Xe/^{133m}Te	9.8 ± 1.0
753.8	^{128m}Sb	8.9 ± 1.1	2015.8	^{138}Xe	13.8 ± 1.1
760.8	^{129m}Sn	3.6 ± 1.3	2029.7	^{84}Br/^{88}Kr	8.5 ± 1.0
767.0	^{134}I/^{134}Te	18.5 ± 1.5	2079.2	^{138}Xe	0.6 ± 0.3
793.5	^{130}Sb	19.5 ± 1.5	2102.5	escape [a]	
840.1	^{130}Sb	22.5 ± 1.5	2175.6	^{95}Y	7.1 ± 1.0
847.0	^{134}I/^{133}Te/^{87}Kr	54.6 ± 1.9	2187.2	^{142}La	1.9 ± 0.8
875.7	^{93}Sr	11.0 ± 1.4	2196.0	^{89}Rb	20.6 ± 1.5
881.6	^{84}Br	49.1 ± 1.8	2218.0	^{138}Cs	21.1 ± 1.1
884.2	^{134}I/^{104}Tc	47.8 ± 1.8	2252.2	^{138}Xe/^{146}Pr	4.4 ± 0.8
894.4	^{142}La/^{142}Ba/^{104}Tc	11.3 ± 1.4	2392.1	^{88}Kr	9.5 ± 0.9
912.7	^{133m}Te	25.5 ± 1.6	2397.8	^{142}La	8.3 ± 0.9
918.7	^{94}Y	57.9 ± 1.9	2484.1	^{84}Br	2.6 ± 0.7

Table 4.3: Continued

934.1	^{131}Sb/^{130}Sb/^{101}Mo	15.2 ± 1.4	2496.6	^{131}Sb	1.3 ± 0.6
943.4	^{131}Sb	22.4 ± 1.5	2542.7	^{142}La	6.2 ± 0.7
948.2	^{89}Rb/^{142}Ba/^{134}I	16.3 ± 1.5	2554.8	^{87}Kr	5.5 ± 0.7
953.7	^{95}Y/^{92}Sr	14.6 ± 1.4	2570.2	^{89}Rb	12.1 ± 0.8
1009.8	^{138}Cs	38.2 ± 1.7	2632.4	^{95}Y	5.9 ± 0.7
1024.3	^{91}Sr	9.0 ± 1.4*	2639.6	^{138}Cs	11.1 ± 0.8
1031.9	^{89}Rb	63.5 ± 1.9	2707.3	^{89}Rb	2.7 ± 0.6
1072.6	^{134}I	8.0 ± 1.3	2971.0	^{142}La	2.1 ± 0.5
1078.7	^{142}Ba	7.5 ± 1.2	2996.7	escape [b]	
1094.1	^{142}Ba/^{93}Sr	3.5 ± 1.2	3045.4	^{84}Br	1.0 ± 0.4
1131.5	^{135}I	8.9 ± 1.3*	3063.2	escape [c]	
1137.5	^{134}I/^{94}Y	8.9 ± 1.4	3235.3	^{84}Br	0.6 ± 0.3
1160.6	^{142}La/^{101}Mo/^{141}Ba	5.6 ± 1.2	3249.0	^{95}Y	1.1 ± 0.4
1197.3	^{141}Ba	5.1 ± 1.2	3313.8	^{142}La	1.2 ± 0.2
1204.3	^{142}Ba	13.1 ± 1.3	3365.8	^{84}Br	1.5 ± 0.4
1233.5	^{131}Sb/^{142}La	1.8 ± 1.0	3415.5	escape [d]	
1248.2	^{89}Rb	51.8 ± 1.9	3451.4	^{95}Y	0.8 ± 0.3
1260.4	^{135}I	12.0 ± 1.3*	3508.7	^{89}Rb	1.4 ± 0.3
1267.0	^{131}Sb/^{93}Sr	4.5 ± 1.1	3576.0	^{95}Y	7.1 ± 0.5
1283.2	^{139}Cs	5.7 ± 1.1	3612.1	^{142}La	0.3 ± 0.2
1324.0	^{95}Y/^{93}Sr	5.3 ± 1.0	3632.7	^{142}La	0.5 ± 0.2
1333.2	^{133}Te	2.7 ± 1.5	3927.5	^{84}Br	3.3 ± 0.3

[a] Single escape peak from 2614.5 keV line. [b] Single escape peak from 3508.7 keV line.

[c] Single escape peak from 3576.0 keV line. [d] Single escape peak from 3927.5 keV line.

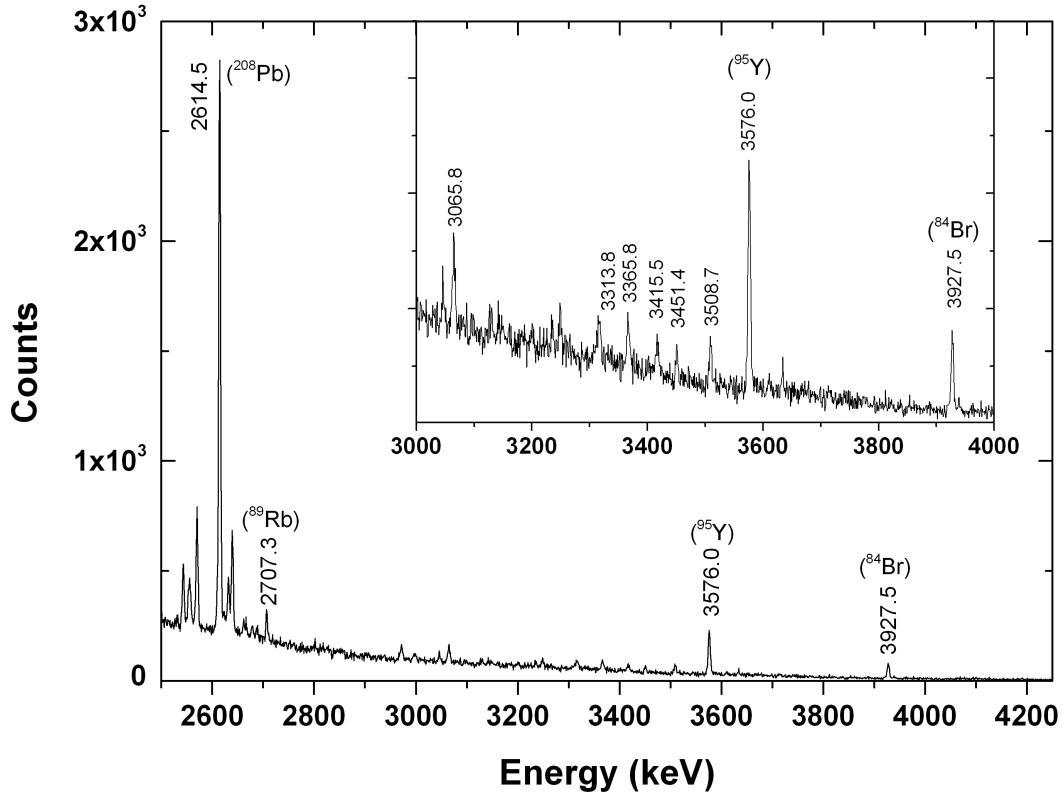

Figure 4.4: High energy region of the HPGe spectrum measured after 10 minutes irradiation of a 100 g Uranium rod by 15 MeV photons. The γ-rays belonging to photofission products ^{89}Rb, ^{95}Y and ^{138}Cs and also to ^{208}Pb nucleus are marked.

4.5 Using a plastic scintillator for detection of delayed γ-rays from photofission

In general, organic plastic scintillators, due to their low cost and possibility of production in large sizes, have a large potential role to play in the detection of delayed γ-rays from photofission. The comparison of the number of counts from background and from nuclear materials were investigated with 5" $\times$ 3" BC-408 and 3" $\times$2" EJ-200 plastic scintillators in various geometries, depending on accessibility at LINAC facilities. Measurements were conducted with the Siemens KD-2 and modified Neptun 10P LINACs.

4.5.1 Measurements at Siemens KD-2 LINAC site

During tests the Siemens KD-2 LINAC was working at 50 Hz of beam frequency and emitted Bremsstrahlung with an endpoint of 6 MeV. Despite of the fact that such energy is only slightly above the photofission threshold of depleted uranium (DU), the delayed γ-rays from photofission were successfully registered. The provided dose rate was about 40 cGy/(min $\times$ m). 4.7 kg of DU was used for the investigation of the delayed γ-rays. The acquisition track was described in detail in Chapter 3. During measurements the $\varnothing$5" $\times$ 3" BC-408 scintillator was placed 25 cm from the nuclear material, which was positioned 70 cm from the conversion target of the LINAC. The measurement was performed in the beam-off mode, which allows recording the delayed

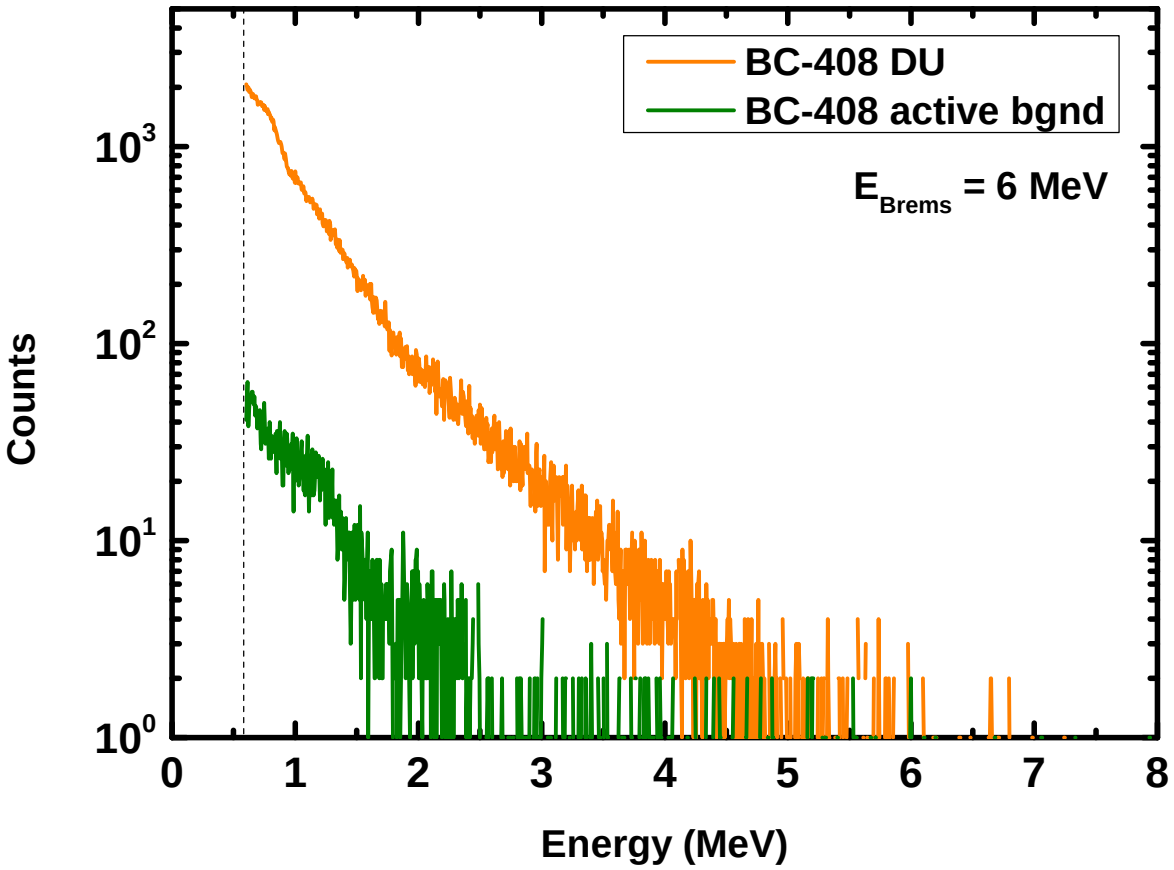

Figure 4.5: The delayed γ-rays spectrum measured for 4.7 kg of DU together with the measured active background, registered with the 5" $\times$ 3" BC-408 plastic PVT scintillator.

radiation between LINAC beam pulses. The plots presenting the delayed γ-rays from the DU and the contribution of the active background are shown in Figure 4.5. For such geometry, the total number of counts originated from delayed γ-rays emitted by the DU was around 29 times greater than that from the active background, which is mainly due to the registration of 1460.8 keV and 2614.5 keV γ-rays from ^{40}K and ^{208}Pb, respectively. These background-nature γ-rays are emitted from the walls at the LINAC facility. Moreover, the contribution of the active background to the passive background is very low, as shown in Table 4.4.

Table 4.4: Number of counts in the energy range between 0.5 - 8 MeV acquired with ⌀5" BC-408 at Siemens LINAC site.

Radiation source	Mode	Number of counts
4.7 kg DU	active	143100 ± 380
background	active	4900 ± 70
background	passive	4200 ± 65

This measurement confirms that the registration of the delayed γ-rays from nuclear materials is a powerful solution for application at country border inspection systems. Large quantities of unshielded DU - those exceeding the mass of 25 kg DU, according to the documentation of the Nuclear Regulatory Commission - could be detected even with compact low-energy accelerators. However, the photofission threshold for some nuclear materials is higher than the Bremsstrahlung with an endpoint of 6 MeV from the Siemens LINAC, thus, for the efficient detection of all kinds of nuclear materials the use of a LINAC providing maximum photons energy of 10 MeV is required. This fact was a motivation for further investigation with accelerators emitting high energy photons with an endpoint at 10 MeV, which will be presented in the next Subsection 4.5.2. However, the higher energy of Bremsstrahlung photons, greater than the 10 MeV, are undesirable in active inspection systems at borders due to safety reasons - such photons are highly penetrative and can generate additional background as well as photoneutrons from the LINAC construction materials.

4.5.2 Measurements at the Neptun 10P bunker

As mentioned in the previous Subsection, photons with an energy endpoint at 6 MeV can be insufficient to induce photofission in an efficient way. The amount of such photons is very low and the photofission cross section of nuclear materials is close to the threshold value, thus, measurements with the 10 MeV Neptun 10P LINAC were performed. During this measurement ⌀3" × 2" EJ-200 plastic scintillator (equivalent of BC-408) coupled to a ⌀3" Photonis PMT was used. During these measurements, only 100 g of U (93% enrichment - HEU) was exposed to high energy photons, the same as which was used in measurements presented at the beginning of this Chapter. This material was placed very close to the front of the EJ-200 scintillator. The detector was

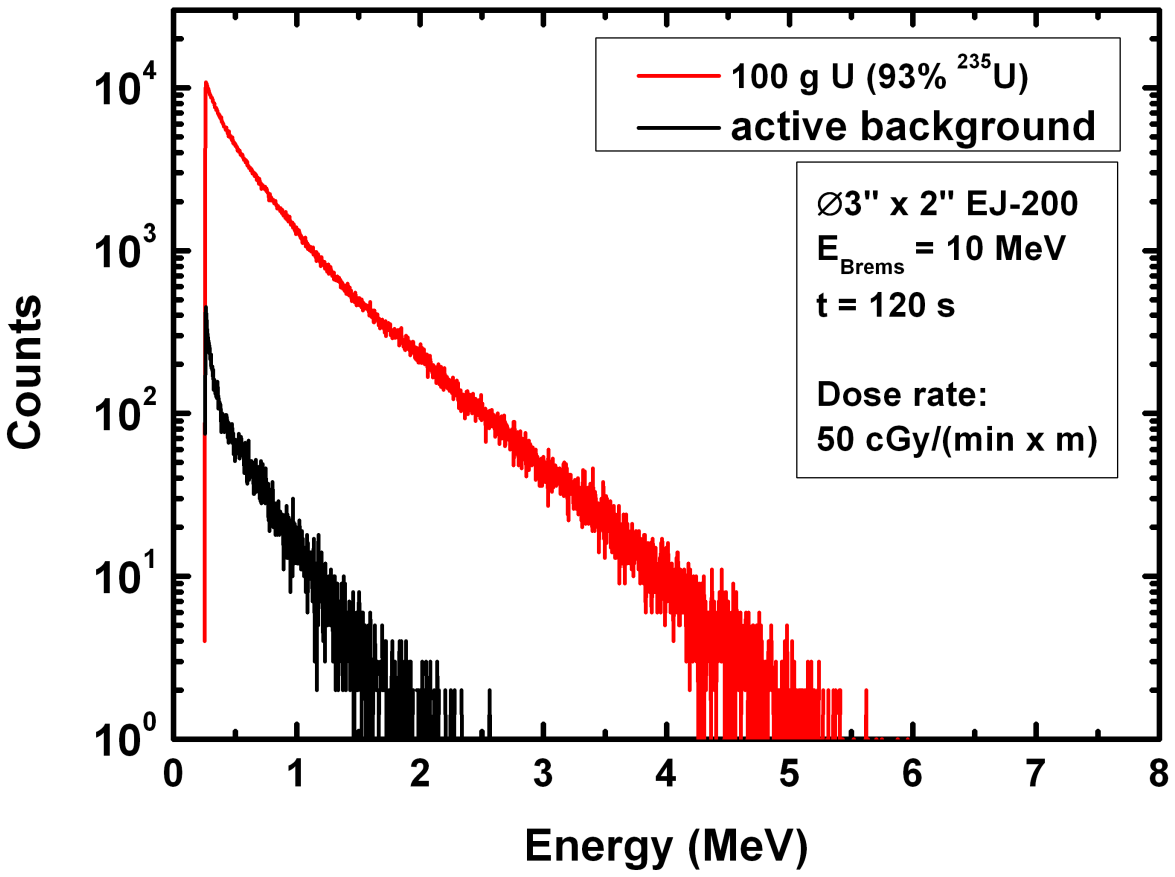

Figure 4.6: The delayed γ-rays measured after photofission the 100 g HEU together with the recorded active background and γ-rays related with natural series decay chains from of the HEU sample.

placed 100 cm from the conversion target of the LINAC. The LINAC was working with a frequency regime of 50 Hz and the beam-off technique was applied, with a 4 ms gate of blocking veto signal and 16 ms for acquisition window. Acquisition time lasted 120 s. The plots from the irradiated HEU sample and the measured active background were shown in Figure 4.6. The Figure presents the spectrum of delayed γ-rays of energy up to 6 MeV registered with the $\varnothing$3" $\times$ 2" EJ-200 plastic scintillator during the 120 s of beam-off measurement (4 ms logic veto, 16 ms acquisition window). For the same beam-off settings and system geometry, the active background was also measured. Details are depicted in the Table 4.5. From Table 4.5 it can be seen that the contribution of delayed γ-rays from the photofission of the HEU is significant, over 86 times larger than that of the active background in the energy range between 0.5 - 8 MeV. In contrast to the passive measurements with the HPGe detector, the active technique of nuclear material detection via photofission results in high energy delayed γ-rays emission, which can potentially pass through the cargo walls and potential shieldings.

4.6 Summary

The study presented in this Chapter shows the techniques of delayed γ-rays detection. For the application in border monitoring, i.e. scanning cargo containers, the large volume scintillators seems to be the best solution because of their high total detection efficiency. After the photofission of nuclear materials a large amount of γ-rays are emitted, often of similar energy values. Thus, the method that will be applied to resolve γ-rays with scintillator of low energy resolution would fail even when an expensive $LaBr_3$ scintillation detector is used. In the [97] measurements of delayed γ-rays in the range of 0.1 - 9 MeV with a $\varnothing$3" $\times$ 2" $LaBr_3$:Ce scintillator were performed, however, the full energey peaks structure was not shown. It is highly probable that the energy

Table 4.5: Number of counts in the energy range between 0.5 - 8 MeV acquired in the Neptun 10P bunker.

Radiation source	Mode	Number of counts
100 g HEU	active	715000 $\pm$ 900
background	active	8300 $\pm$ 90

resolution of the $LaBr_3$:Ce is still insufficient for precise analysis of the delayed γ lines. It seems that the best solution is to use the large volume plastic scintillators, allowing the efficient detection of scattered γ-rays (Compton scattering). Based on the total number of counts registered during cargo inspection and comparing with that from the active background, it is possible to determine the presence of radioactive or nuclear material.

The best solution for precise identification of nuclear material composition is an HPGe detector possessing excellent energy resolution, significantly better than that offered by scintillation materials. However, due to the requirement of cooling to the LN_2 temperature, limited volume, high price and sensitivity to radiation damage from neutrons, resulting in degradation of the energy resolution over time, their potential use in cargo scanning systems is doubtful.

Chapter 5

Detection of delayed neutrons from photofission

Delayed neutrons are the most unique signatures of fission. Actually, with a few exceptions, such as the ^{17}O(n,p)^{17}N reaction when the energy of the incident neutron is above 10.4 MeV, or ^{18}O(γ,p)^{17}N with a half-life of 4 s and the γ energy above 15 MeV, only disintegration of a very heavy nucleus is related with the emission of delayed neutrons [17]. As the energy of delayed neutrons is divided into six groups between 0.25 and 0.63 MeV [31], being significantly lower than that of prompt neutrons, the probability of their interaction in a low-Z environment is definitely higher [98]. Thus, the delayed neutron detectors should not be used as a sole solution. Moreover, LINACs providing high energy Bremsstrahlung photons generate large amounts of photoneutrons emitted from a conversion target and construction elements, which can be mixed with the delayed neutrons. In this Chapter results on the delayed neutrons measurements from photofission of various types of nuclear materials detected with the an ^{3}He detector will be discussed.

Many benefits of the ^{3}He detector, such as the high cross section for thermal neutrons detection, low sensitivity to γ-rays and good signal-to-background ratio, favor this type of gas detector in delayed neutron detection. The thermal neutron capture cross section for the reaction with ^{3}He is 5530 barns and is higher than that for ^{10}B (3848 $\pm$38 b [99]) and ^{6}Li (940 b). Due to the fact that the energy of the delayed neutrons is mainly in

the range of 0.25-0.63 MeV [31], a cylindrical polyethylene (PE) moderator was used in order to slow down the neutrons and improve the ^{3}He detector efficiency.

5.1 Delayed neutrons detection using the ^{3}He proportional counter

Measurements of delayed neutrons from photofission were performed in the Siemens Mevatron KD-2 LINAC facility at NCBJ. Experimental details are in Section 3.3. The LINAC was working in two modes; the Bremsstrahlung endpoint energy was set to 6 MeV and 15 MeV in separate measurements. The attenuating jaws of the LINAC were shaped into a rectangle (20 cm $\times$10 cm). After the measurements conducted with the the nuclear material, consecutive measurements of the active background were performed. An example of registered signals for the irradiated 4.7 kg DU and background with the ^{3}He detector are shown in Figure 5.1. The LINAC was emitting Bremsstrahlung photons with an endpoint energy at 6 MeV. The region of interest is between 190 and 850 keV, where the energy of the reaction products is deposited. The number of registered counts as a function of distance between detector and DU for 6 MeV and 15 MeV endpoint photons is shown in Figure 5.2. The measurement points were fitted with the use of power function (Belehradek model), which is shown in Equation 5.1:

$$y = a(x - b)^c. \tag{5.1}$$

The significant increase of the counts from the background is noticeable during the operation with 15 MeV endpoint photons. It is due to the fact that the photons generated by 15 MeV electrons on a tungsten (W) target can give rise to photoneutrons from γ+W reaction. According to [100], for the peak current of 100 mA, the number of photoneutrons generated on a tungsten target can reach 2.72×10^{10} n/s and 7.69×10^{10} n/s for 14 MeV and 17 MeV electrons emitted by a LINAC, respectively. It is worth to emphasize that these values are greater than that for many compact D+D or D+T neutron generators. For example, a Sodern Genie 16 series D+T neutron generator

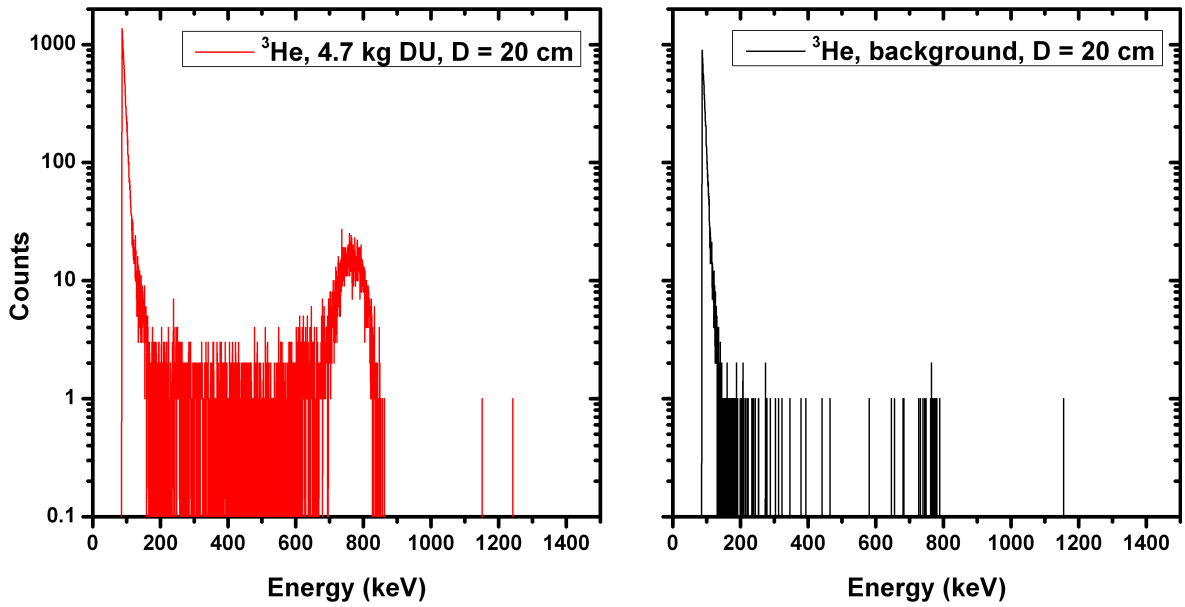

Figure 5.1: Signals recorded with the ^{3}He during measurement of 4.7 kg of DU placed 20 cm from the detector (left picture) and background between a LINAC pulse (right picture). The uranium block was situated in the beam isocentre.

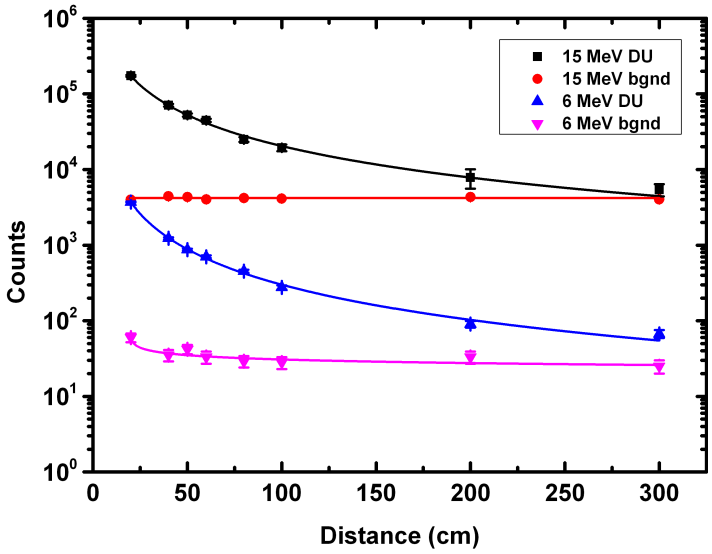

Figure 5.2: Number of counts recorded for DU and active background registered by the ^{3}He detector as a function of distance from the DU. Two modes of LINAC work were chosen: Bremsstrahlung photons with an endpoint at 6 MeV and 15 MeV. In most cases error bars are within the size of the points.

emits approximately 2×10^8 n/s. Particularly, photoneutrons can be a serious problem in border monitoring because of penetrability, higher dose equivalent compared to γ-rays and neutron deactivation γ-rays after the irradiation. However, photoneutrons can induce additional fission reactions in nuclear materials. Thus, in some cases, can be useful for Homeland Security applications, for example, for scanning bulky nuclear waste packages and detection of the delayed neutrons after strong irradiation. As a consequence of photoneutron emission, the signal-to-background ratio for the beam-off technique is worse for the LINAC emitting endpoint photons of 15 MeV, as shown in Figure 5.3. On the other hand, it is important to emphasize that the number of 6 MeV photons able to induce photofission is definitely lower than that when using the LINAC working at 15 MeV.

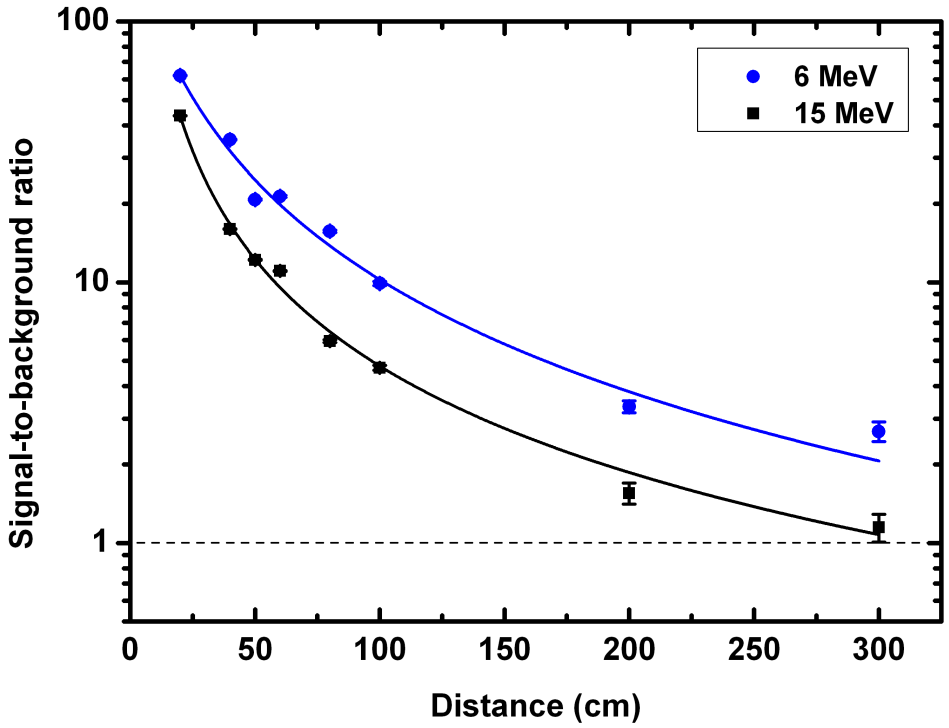

Figure 5.3: The signal-to-background ratio for the measurements with the 4.7 kg DU with 6 MeV and 15 MeV endpoint photons as a function of the nuclear material - detector distance.

5.2 Experimental results and an MCNPX simulations of the ^{3}He response to neutrons

In general, the comparison of simulations with experimental results provides good basis for the further development of more complex systems, allowing for the minimization of potential mistakes, reduction of costs and simplification of the efficiency estimation for larger detection systems. At the beginning, in order to detect the delayed neutrons with good efficiency, the calculation of polyethylene shielding must be calculated. Using the MCNPX code, the optimal thickness of the PE was calculated to be 5.5 cm. In order to absorb the thermalized neutrons from the environment, the PE moderator was covered with 1 mm Cd foil.

The motivation of the presented study is to simulate the ^{3}He response to neutrons from ^{252}Cf and compare the results with the experiment with the best possible accuracy. The experimental result and the simulated response of the ^{3}He detector to the ^{252}Cf neutron source are presented in Figure 5.4 [101]. The simulated response is in

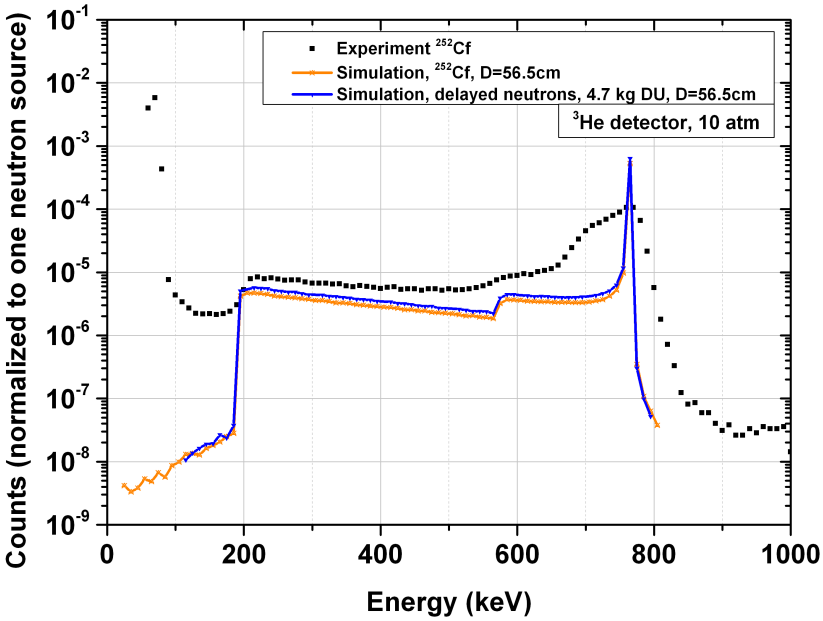

Figure 5.4: Simulated and experimental response of the ^{3}He detector to neutrons from the ^{252}Cf source. Both spectra are normalized to one neutron source [101]. The efficiency to delayed neutrons for the 4.7 kg of DU was also calculated.

a raw form, meaning that the spectrum was not broadened by the contribution of the electronic noise. Additionally, efficiency of delayed neutron detection from the 4.7 kg DU was also simulated, showing slightly better efficiency compared to that obtained for ^{252}Cf. This is due to optimization of the PE cover of the detector, which is dedicated to the delayed neutron detection. Within the ^{3}He(n,p)T reaction, the tritium T and proton can fully deposit their energies in the detector, then, the peak at 764 keV is noticeable. In some cases, the p or T (or both particles) can reach the detector walls and decrease the amount of deposited energy into the signal amplitude - this phenomenon is known as a "wall effect". The performed simulations showed that the detection efficiency in the integrated energy gate for the full deposition peak, between 710 and 800 keV, is identical to that from the experiment. The total efficiency in the whole energy range is lower and was calculated to be about 35% of that from the experiment. It is supposed that the wall effect is not well simulated in the MCNPX code or there are other effects on the ^{3}He detector, which were not included in the simulation. This phenomenon should be investigated in the future.

5.3 Summary

As presented in this Chapter, the ^{3}He is a very efficient medium for photofission delayed neutrons detection. It was possible to measure the delayed neutrons from 4.7 kg of DU with use such a low endpoint energy as 6 MeV and dose rate of 40 (cGy / (min $\times$ m)). The NCBJ Fast Preamplifier allowed to measure the delayed neutrons between LINAC beam pulses, with the duty factor better than 50 %. Despite of the fact that the shortening of the preamplifier relaxation time resulting in electronic noise increase, it was still low enough to discriminate γ-rays and neutrons before the beginning of the 191 keV triton wall effect. It was also showed that the signal-to-background ratio for a LINAC working at 6 MeV mode is better than that for 15 MeV due to significant contribution of photoneutrons from the LINAC target and construction materials. However, 9 MeV LINAC seems to be the best solution for the detection of delayed neutron after photofission of nuclear materials. This is due to the larger amount of photons covering the photofission cross section.

Chapter 6

Detection of prompt neutrons emitted from nuclear materials

Due to the two order of magnitudes yield ratio of the emission of the photofission prompt neutrons and that of the delayed neutrons, the detection of the prompt neutrons emitted in the reaction of photofission seems to be more efficient and a promising solution for SNM detection. Due to higher mean prompt neutrons energy, the method could be well-suited for detection of shielded SNM inside cargo containers. Over the last few years, detection of fast neutrons by means of ^{19}F activation in the scintillator medium triggered considerable interest in the field of Homeland Security. In this dissertation, the fast neutron detection technique will be based on TAD, which was proposed in order to detect prompt neutrons emitted due to photofission of Special Nuclear Materials (SNMs) [61, 63]. The performance of this technique for EJ-313 and BaF_2 scintillators was verified in [14]. Due to an ^{19}F(n,α)^{16}N or ^{19}F(n,p)^{19}O reaction with an effective neutron energy threshold of 2.5 MeV [62], it is possible to determine the presence of nuclear material via registering β particles from ^{16}N and ^{19}O decay with a half-life of 7.1 s and 26.9 s, respectively [96]. In this PhD dissertation $\varnothing$5" $\times$ 3" EJ-313 liquid fluorocarbon, as well as $\varnothing$2" $\times$ 3" BaF_2 scintillators were exposed to neutrons from both a ^{252}Cf source and a Sodern Genie 16 GT DT neutron generator in order to compare the number of counts originated by β^- particles carrying maximum energy of 10.4 MeV.

An EJ-313 scintillator is based on highly purified hexafluorobenzene, so the amount of hydrogen in the scintillator content is very low (1.02×10^{20} per cm^3, according to the datasheet [68]). The fluorine/hydrogen (F/H) ratio is about 308, thus, the probability of neutron scattering of hydrogen, resulting in neutron energy decrease below the activation threshold, is significantly limited. After background subtraction of the ^{252}Cf energy spectra and integrating the counts in the energy range between 6.0 and 10.5 MeV, detection efficiency of fast neutrons by means of ^{19}F activation and characteristic β^- particle emission for the mentioned scintillators can be estimated.
The research for another solution for prompt neutron detection is motivated by the potential application of inorganic scintillators, i.e. BaF_2, and novel organic materials, i.e. fluorine-based plastic scintillator. These detectors can be also supportive for detection of delayed γ-rays. Additionally, in the case of a BaF_2, the presence of α impurities in the BaF_2 medium can be exploited for energy self-calibration of the detector. The energy of the peaks from α emission in BaF_2 scintillators were described in [102], the 7.7 MeV peak was ascribed to emission from ^{214}Po. However, due to the interaction with a scintillator, part of the α particle energy is transferred to non-radiative processes and only a fraction of the light from ionization is emitted. This effect is known as scintillation quenching [103]. Thus, the observed centroid position of the α-peak is shifted towards lower energies.

6.1 Estimation of the photoelectron yield

The set of used scintillators for prompt neutron detection is showed in Table 6.1. The Table also contains the number of photoelectrons per one MeV of γ-ray energy, measured by means of single photoelectron method introduced by Bertollacini et al. [82] and described in detail in Section 3.4.

According to the data presented in Table 6.1, it can be seen that EJ-313 generates about 8.7 times lower amount of photoelectrons per one MeV in comparison with BC-408 of the same size coupled to the same PMT. The estimated number of photoelectrons per MeV (phe/MeV) of ⌀ 5" EJ-313 coupled to the Electron Tubes 9390KB (ET9390KB) was 190 ± 20 phe/MeV. The smaller ⌀ 2" EJ-313 coupled to the Hama-

matsu R6233 PMT yielded the number of photoelectrons 230 ± 20 phe/MeV and is slightly greater due to better quantum efficiency (QE) of the Hamamatsu PMT than that of ET9390KB. The similar values of $N_{phe/MeV}$ of these two EJ-313 samples confirm the low light attenuation in the scintillator medium and reasonable uniformity of the ET9390KB PMT photocathode. The Hamamatsu R6233 PMT offered better QE, it means that it converts photons into photoelectron more efficiently than the ET9390KB. Despite the lower photoelectron yield, it is still possible to detect γ radiation with energy as low as 300 keV, still above the electronic noise. From the point of view of high energy β^- particles detection, carrying energy up to 10.4 MeV, the photoelectron yield is pretty enough for application in prompt neutron detection by means of an n + ^{19}F reaction. The photoelectron yield of smaller BC-408 coupled to Photonis XP5500B PMT having high QE was measured by Swiderski et al. [104], whereas the photoeletron yield of BaF_2 scintillators were already reported in the early 1980's. Measurements of BaF_2 scintillators were performed with a standard PMT with a bialkali photocathode and a borosilicate entrance window [105] as well as a PMT with Vacuum Ultraviolet (VUV) transparent windows, such as quartz [106] and MgF_2 (sapphire) [107]. Due to the fact that the BaF_2 scintillator partially emits light in the VUV range, the measured photoelectron yield is greater when the PMT with quartz or sapphire entrance window is used. However, the wavelength of maximum emission intensity of BaF_2 is situated at 310 nm. It is related to the slow decay component, in which 80 % of the total light yield from the BaF_2 scintillator is emitted. The performance of the BaF_2 coupled to a standard PMT is appropriate for recording the β^- continuum and delayed γ-rays for the application in the TAD technique.

Table 6.1: Scintillators and photodetectors used in the prompt neutron detection experiments.

Scintillator	Size	Used PMT	N_{phe}/MeV
EJ-313	⌀5" × 3"	⌀130 mm ET9390KB	190 ±20
EJ-313	⌀2" × 2"	⌀3" Hamamatsu R6233	230 ±20
BaF_2	⌀2" × 3"	⌀2" EMI with borosilicate glass	700 ±70
BC-408	⌀5" × 3"	⌀130 mm ET9390KB	1650 ±160

6.2 Response to ^{252}Cf neutron source and observation of β^- decay events from the n+^{19}F reaction in EJ-313 and BaF_2 scintillators

A calibrated ^{252}Cf source, emitting 57000 n/s on the day of measurement, was used to estimate the neutron detection efficiency by means of TAD technique. The ^{252}Cf source were placed 15 cm from the detector and data were taken with and without 5 cm thick Pb shielding. During measurements BaF_2 was positioned in side-on and front-on orientation with respect to the ^{252}Cf source, whereas EJ-313 was placed only in the front-on position. The ^{252}Cf source can be considered as a good simulator of prompt fission neutrons [62], with an average neutron energy of 2.348 MeV [56]. The energy spectra acquired within 12 h for EJ-313, BaF_2 and BC-408 (without ^{19}F) are shown in Figure 6.1. The continuum structures originating from β^- decays with endpoint of 10.4 MeV are clearly visible in $\varnothing$ 5" $\times$ 3" EJ-313 and the BaF_2 spectra. The spectrum from the β^- with endpoint of 4.3 MeV is also visible for the EJ-313 scintillator.

Figure 6.2 (top) shows an excess of counts in the energy range of 6.0 - 10.5 MeV measured with the EJ-313 and BaF_2 due to the reaction of neutrons with ^{19}F. The spectrum obtained using $\varnothing$5" $\times$ 3" BC-408 was also included as a reference, showing the contribution of pulses in the range between 6.0 and 10.5 MeV apart from the events based on the ^{19}F threshold of neutron activation. Figure 6.2 (bottom) shows the benefit of counts for the side-on oriented BaF_2 instead of the front-on orientation, which suggests that efficiency of TAD detector is strongly dependent on the geometrical solid angle. Correcting the obtained spectra by background subtraction resulted in an almost pure contribution of β^- particles between 6.0 and 10.5 MeV. However, use of a continuously emitting radioactive source can bias the results with a contribution of high energy γ-rays from the neutron capture and scattering of Ba, C and F nuclei present in the scintillators. The high energy γ-rays from ^{252}Cf are prompt and delayed γ-rays as well as those coming from α decay of impurities inside the scintillator. Details will

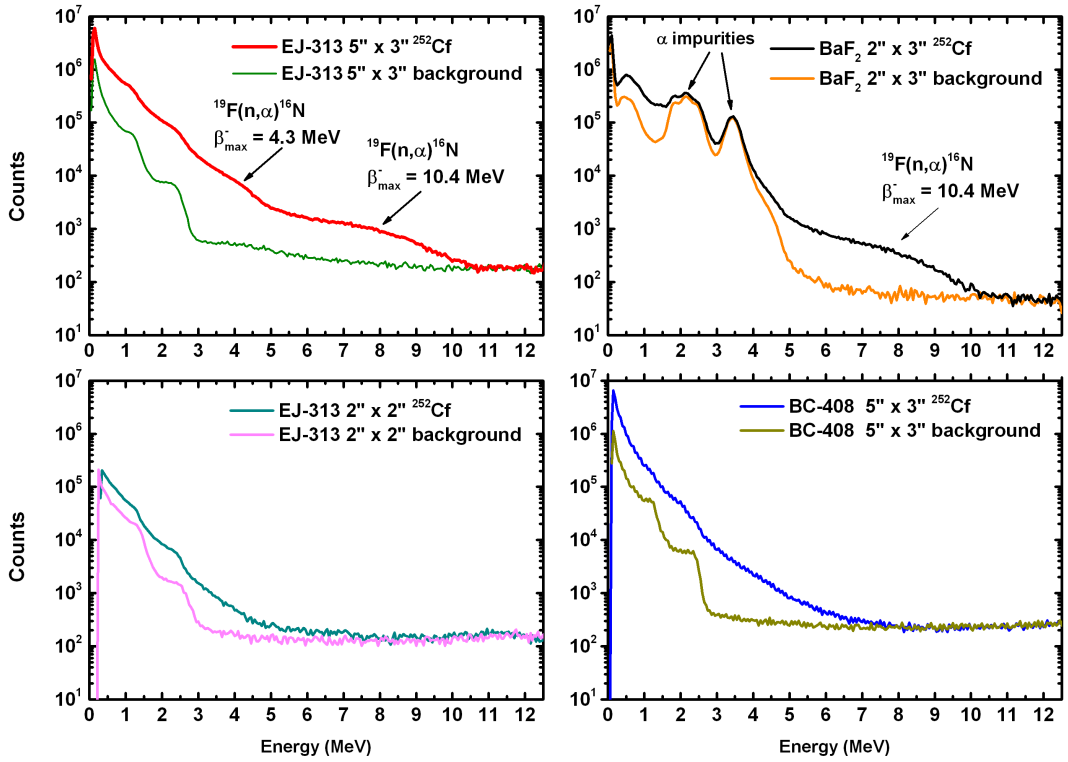

Figure 6.1: Energy spectra of 5 cm lead shielded ^{252}Cf source acquired with EJ-313 and BaF_2 scintillators together with recorded background. The spectra of BC-408 were included as a reference.

be presented in Sections 6.4 and 6.5 dedicated to the measurements of the neutrons response of the BaF_2 and EJ-313 scintillators with the use of the D+T neutron generator. It allows to reduce the contribution of activation background from the scintillators and structural materials.

Particularly, using the calibrated ^{252}Cf source, it is possible to roughly estimate the neutron detection efficiency for the investigated scintillators in the energy range between 6.0 and 10.5 MeV. In general, the detection efficiency can be described as shown in Equation 6.1:

$$\epsilon = \frac{S}{\Omega \times A \times t \times B}, \tag{6.1}$$

where S stands for the net number of counts in the energy range of 6.0-10.5 MeV, Ω is a solid angle, A is the total number of neutrons emitted from the ^{252}Cf in 4π, t is

the time of measurement and B is the branching ratio of the given reaction. For the ^{19}F(n,α)^{16}N reaction, the intensity of the branch that results in pure β^- emission with a maximum energy of 10.4 MeV is 28%. The calculations were performed for the geometry mentioned above, results are presented in Table 6.2. The estimated uncertainties were obtained from standard deviations of the average value of counts, taking solid angle and energy calibration into account.

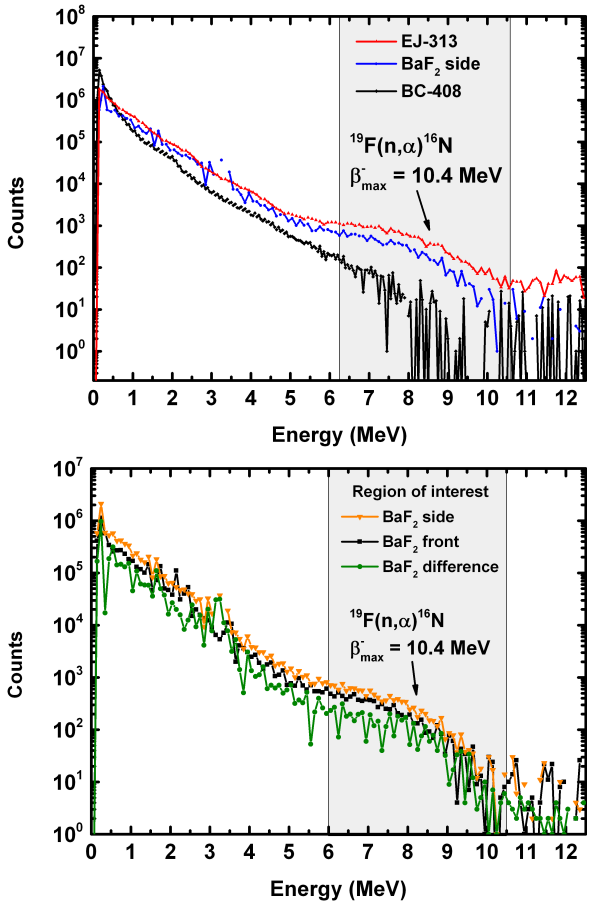

Figure 6.2: Energy spectra of 5 cm lead shielded ^{252}Cf source acquired with EJ-313 and BaF_2 scintillators after background subtraction (top). The gray-colored energy window indicates the region of spectra integration between 6 and 10.5 MeV, related to ^{19}F activation. The spectrum of ⌀5" × 3" BC-408 plastic was included as a reference. On the bottom, the benefit (difference) of the counts from the ^{252}Cf source (without Pb shielding) recorded with the side-on oriented BaF_2 after subtraction by the front-on orientation is shown.

The BaF_2 scintillator exhibited significantly better incident-to-registered (intrinsic) neutron detection efficiency than the EJ-313 in the range between 6.0 and 10.5 MeV. This is due to the absence of hydrogen atoms in the crystal lattice and the much shorter range of electrons from ^{16}N and ^{19}O β^- decays in BaF_2 medium, which are the signatures of interaction with fast neutrons of energy above 2.5 MeV. According to the CSDA range calculation [69], the range of 10 MeV electrons in the EJ-313 medium is about 30 mm. Thus, the probability of such an electron reaching the detector wall is higher than in the case of the BaF_2, so the pulse-height distribution in EJ-313 should favor lower energy events than in BaF_2, as Figure 6.1 indeed shows. In the case of smaller ⌀2" × 2" EJ-313 it was hardly possible to observe the excess of counts above the background during measurements with the ^{252}Cf source, thus, for comparing efficiencies, only the larger EJ-313 was taken into account. Furthermore, the number of registered β^- particles significantly increases when the BaF_2 is placed in the side position instead of the front. Overall, due to the lower volume of the BaF_2 (compared to the EJ-313), the number of registered β^- particles is at least 50% lower.

Neutron detection efficiency obtained from the experiment with Pb shielding showed a decrease of the events in the energy region of 6.0 - 10.5 MeV by a factor of 2, see Table 6.2. This is due to the fact that the Pb strongly scatters the neutrons due to high Z-value and attenuates potential γ-rays from the fission of ^{252}Cf. The number of

Table 6.2: Neutron detection efficiency of the investigated detectors, measured with ^{252}Cf in a gated energy region from 6.0 to 10.5 MeV. The ^{252}Cf source was placed 15 cm from the detectors. The signal above the background for ⌀ 2" × 2" EJ-313 was barely visible and was thus not included in the table.

Detector	Ω (%)	Counts with 5 cm Pb	Efficiency(%) (with Pb)	Counts without Pb	Efficiency(%) (without Pb)
⌀ 5" EJ-313	4.5	24000 ± 1200	0.08±0.01	52000±2400	0.18±0.01
⌀ 5" BC-408	4.5	2900±300	–	6200±310	–
BaF_2 (side-on)	1.4	11400±600	0.13±0.01	23200±1200	0.26±0.02
BaF_2 (front-on)	0.7	7700±400	0.17±0.01	12400±700	0.27±0.02

counts, defined as I_{BaF_2} / $I_{EJ-313-5"}$, is 32.0% ± 2.3% and 44.6% ± 3.4% for a front-on and side-on oriented BaF_2, respectively. Using an MCNPX simulation, it will be shown in the next Section that in the front-on geometry the contribution of γ-rays to the β^- events is approximately 10.3% for the BaF_2 crystal.

6.3 Simulations of the BaF_2 response to neutrons from ^{252}Cf source

The computer simulations of the front-oriented BaF_2 to neutrons from a lead shielded ^{252}Cf source were performed using an MCNPX code by CEA LIST, Saclay, France. The geometry for the measurements described in Section 6.2 with ^{252}Cf was reconstructed. The values of neutron energy for the ^{252}Cf source, divided into group strength, were taken from the ISO 8529-1:2001 specification [108]. The calculated efficiency for the 5.5-10.5 MeV β^- particles is 89.1% ± 0.0004%; such a good efficiency is due to the quite high density of the BaF_2, resulting in a short range of high energy electrons.

Table 6.3: Comparison of the number of neutrons from ^{252}Cf registered with the BaF_2 in the experiment and in simulation. Integration was performed for the energy range of 6.0-10.5 MeV.

Detector	Number of counts	
	Experiment	Simulation
BaF_2 front with Pb	7700 ± 400	4900 β^- + 380 γ
BaF_2 front without Pb	12400 ± 700	7300 β^- + 750 γ

The contribution of γ-rays above 6 MeV was estimated as well, and the γ / β^- ratio between 6.0 and 10.5 MeV is 7.7 % and 10.3 % for measurements with and without Pb shielding, respectively. A comparison of the results from the experiment and the simulation is presented in Table 6.3, together with the contribution of high energy γ-rays. The values obtained from the MCNPX simulation follow the experimental data, however, the number of counts obtained from the simulation is about 35 % lower

in comparison with the experiment. This could be due to the fact that during the experiment the γ-rays emitted from the scintillator and structural materials can give an additional contribution in the high energy region, as it will be presented in Section 6.4.

6.4 Activation of BaF_2 and EJ-313 with a D+T neutron generator

As mentioned in Section 6.2, the experimental results obtained with the use of the ^{252}Cf source contain unrequired events due to the registration of the high energy γ-rays. The high energy γ-rays are emitted from the products of ^{252}Cf spontaneous fission as well as from the scintillators due to neutron scattering and capture reactions. Thus, in order to minimize the contribution of high energy γ-rays from the induced background and reduce the acquisition time, the out-of-beam measurements using a Sodern Genie 16GT deuterium+tritium (D+T) neutron generator were performed. The neutron flux was set to about 0.3 $\times$ 10^8 n/s in 4π. The $\varnothing$2" $\times$ 3" BaF_2 and $\varnothing$5" $\times$ 3" EJ-313

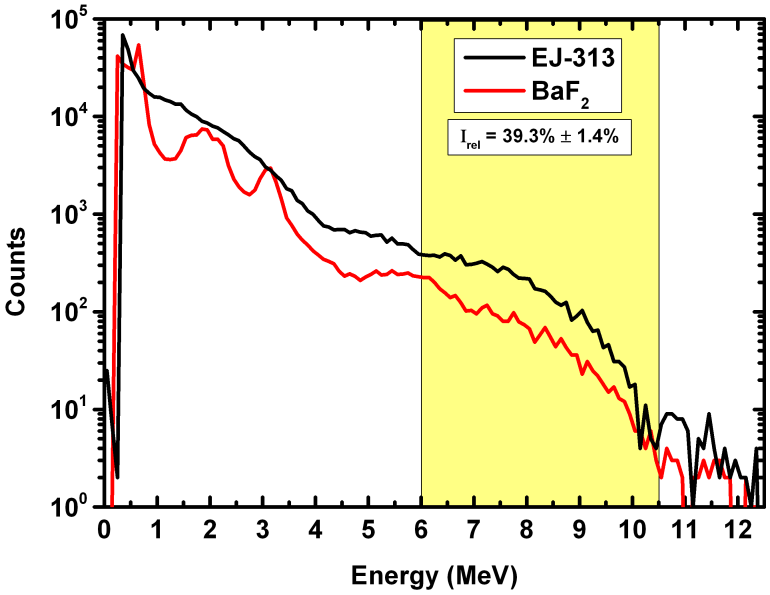

Figure 6.3: The TAD spectra of BaF_2 and EJ-313 recorded with the D+T neutron generator.

scintillators, placed at the distance of 50 cm from the deuterium target, were exposed to 14.1 MeV neutrons during 120 s. Then, the data was recorded for 60 s and the signatures emitted from ^{16}N and ^{19}O were measured. The TAD spectra obtained after neutron activation of ⌀2" × 3" BaF_2 and ⌀5" × 3" EJ-313 scintillators were shown in Figure 6.3. Six consecutive spectra were summed in order to obtain better statistics and minimize the uncertainties. Spectra were binned in order to show statistics per each 100 keV bin. When the TAD measurements with the D+T neutron generator were finalized, six consecutive background spectra were also recorded and summed. The hump in the energy range between 5 and 7 MeV, visible in the BaF_2 spectrum, can be ascribed to registration of γ-rays related with the activation of Ba isotopes. As it will be presented in Section 6.5, the Ba activation need to be further investigated. The background contribution to the total counts between 6.0 and 10.5 MeV is 1.6% and 2.3% for BaF_2 and EJ-313, respectively. According to Equation 6.2, the relative number of counts between 6.0 and 10.5 MeV I_{rel} for these two scintillators was estimated to be:

$$I_{rel} = \frac{I_{BaF2}}{I_{EJ313}} = 39.3\% \pm 1.4\%, \tag{6.2}$$

For the measurements with the D+T neutron generator, the relative number of counts I_{rel} recorded between 6.0 and 10.5 MeV was estimated to be 39.3% with the statistical uncertainty of 1.4 %. The value is about 10% lower than that obtained with ^{252}Cf (see Section 6.2) due to the contribution of high energy γ-rays emitted by the source and continuous work through 12 h, resulting in possible excitation of the Ba and F nuclei by neutrons during measurements. Nevertheless, the results obtained with the D+T neutron generator and ^{252}Cf are in reasonable agreement. A particular advantage of the ^{252}Cf source is that the energy of emitted neutrons is very similar to that from induced fission in nuclear materials. Thus, measurements with a ^{252}Cf source can be applied for rough estimation of the fluorine based scintillators detection efficiency in the energy range between 6.0 and 10.5 MeV. However, the number of emitted neutrons from ^{252}Cf is significantly lower than that emitted by the D+T neutron generator and the neutrons are emitted continuously, resulting in activation the background during data acquisition. Thus, the relative efficiency measured with the D+T neutron generator operated at the pulsed mode is more reliable than that obtained with the ^{252}Cf source.

6.5 Activation background of BaF_2

Neutrons emitted by the source, such as a D+T neutron generator or LINAC (photoneutrons), can be scattered or captured by the scintillator or structural materials, resulting in the emission of high energy γ-rays. Basing on the NNDC Chart of Nuclei online database, it is known that excited Ba nuclei have energy levels up to 9.1 MeV [79]. Some deexcitations of Ba nuclei result in the emission of γ-rays in the region of 4-5 MeV, but for the 9.1 MeV level the deexcitation process in ^{136}Ba is not known. The neutrons scattered of ^{19}F can also excite the nuclei, resulting in the emission of γ-rays with energy up to even 10 MeV.

In order to activate the BaF_2 scintillator, a Sodern GENIE 16GT D+T neutron generator was also used. The neutron generator was working in pulsed mode, with 5 ms beam-on and 25 ms beam-off settings. The γ spectra from the BaF_2 and background were acquired only during the 25 ms beam-off time window with the use of an Ortec

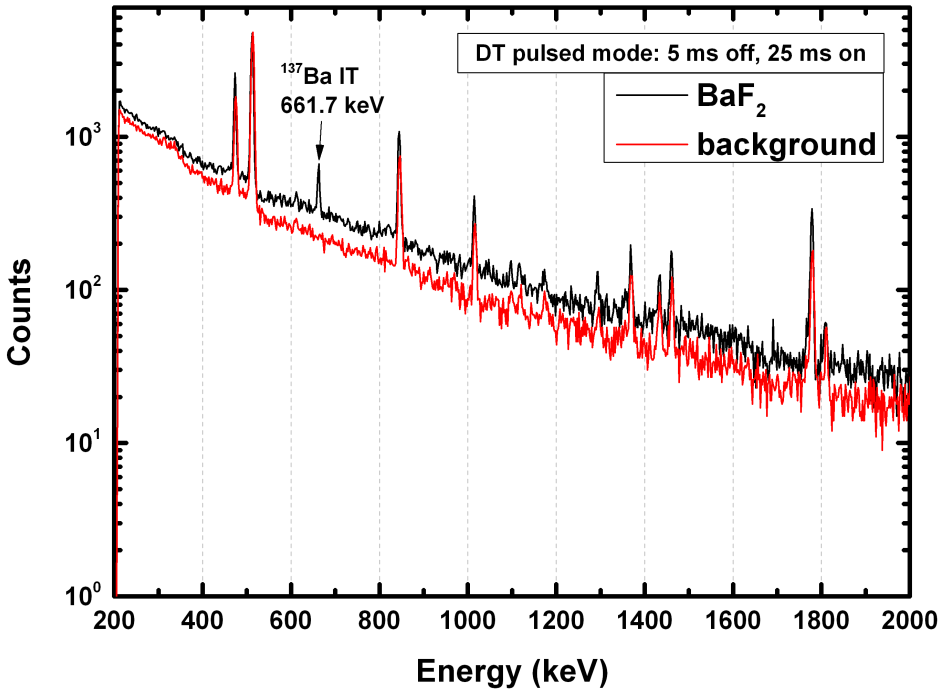

Figure 6.4: γ-ray spectra recorded by the HPGe from the activation of BaF_2 detector and background with the D+T neutron generator. Spectra were showed between 200 and 2000 keV. The 661.7 keV γ line from ^{137m}Ba was observed.

HPGe semiconductor detector model GMX60P4-83-CW (relative efficiency of 60%, energy resolution of 2.3 keV at 1.33 MeV). The BaF_2 scintillator, placed 40 cm from the tritium target, was situated in the vicinity of the HPGe. The γ-ray spectra shapes from BaF_2 and background in the energy range between 200 and 2000 keV, registered for 300 s, are presented in Figure 6.4. The greatest number of counts in the whole energy range was observed when the BaF_2 detector was located on the measurement site. Moreover, the peak at 661.7 keV was clearly visible due to a ^{137}Ba(n, n'γ)^{137m}Ba and ^{137}Ba(γ, γ')^{137m}Ba isomeric transition (IT) reaction. It strongly suggests that the neutrons captured or scattered on the Ba or F can result in additional background signal up to 10 MeV, as shown in Figure 6.5.

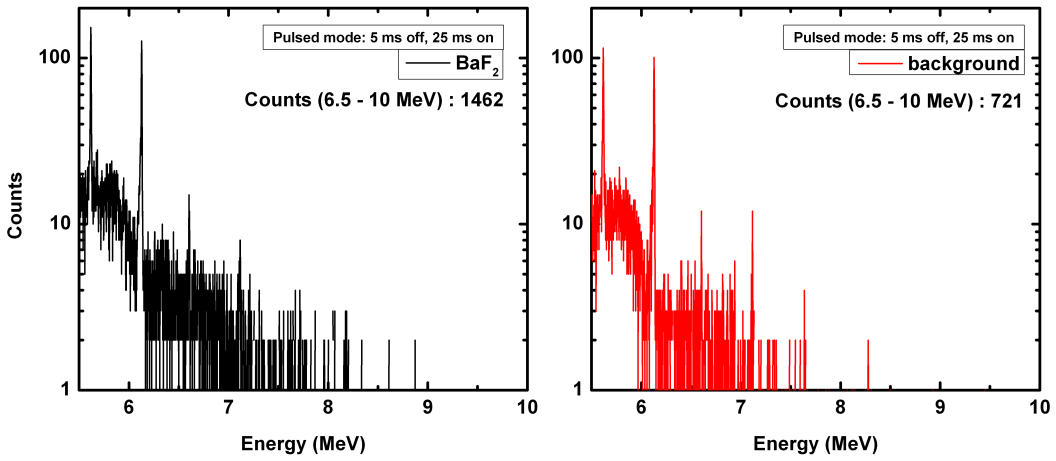

Figure 6.5: Activation spectra recorded by the HPGe from the BaF_2 detector and background between 5.5 and 10 MeV. The number of counts in the range between 6.5 and 10 MeV was also included. Both spectra show γ-rays from ^{16}O levels which can be generated by F activation or $>$ 10.2 MeV neutron activation of ^{16}O.

6.6 Photofission prompt neutrons detection with the use of BaF_2 and 9 MeV LINAC

As stated in Section 6.2 and 6.4, prompt photofission neutrons can be detected in a TAD detector by means of activation of atomic nuclei of a material that emits characteristic β^- particles and γ-rays. It is important to know other contributions to

the photofission prompt neutron spectrum in the range of 6.0 - 10.5 MeV:

1. The fraction of delayed γ-rays above 6 MeV from fission of fissionable materials. During measurements with ^{252}Cf it was estimated that this fraction is around 10%.

2. Photoneutrons emitted from the construction materials and environment during LINAC operation [17].

3. High energy γ-rays emitted by scintillators due to their activation by neutrons slowed down after the beam pulse.

4. Summed pulses originated from consecutive photons or particles that deposit energy in the detector within a very short time interval (so called pile-ups).

5. It was emphasized in [62] that the ^{19}F(n,γ)^{20}F reaction, with no threshold, can occur in the scintillators based on ^{19}F. This reaction results in emission of 5.39 MeV β^- and 1.63 MeV γ-rays in coincidence, which theoretically can create an inherent background up to 7.02 MeV. However, 5.39 MeV is the β^- endpoint energy and the probability of β^- particle emission with energy above 5 MeV significantly decreases. Moreover, 1.63 MeV γ-rays can also deposit only part of their energy via Compton scattering. The average energy of the beta particle from an ^{19}F(n,γ)^{20}F reaction is 2.48 MeV, thus, the deposition of energy above 6 MeV through this reaction is notably limited. As shown in [62], after activation of a large EJ-313 scintillator with a deuterium+deuterium (D+D) neutron generator, the counts above 6 MeV from the ^{19}F(n,γ)^{20}F reaction after summing the 30 consecutive measurements were not observed.

6. Natural background contribution to the measured spectra in the high energy range, such as cosmic rays (protons and muons).

All the photofission measurements included in this Section were performed with a Varian LINATRON M9 LINAC. In Figure 6.6 recorded spectra from the ⌀2" × 3" BaF_2 detector after 60 s irradiation of 1.2 kg DU with high intensity at a beam repetition rate of 385 Hz and high dose rate of 30 Gy/(min ×m) are shown. Spectra

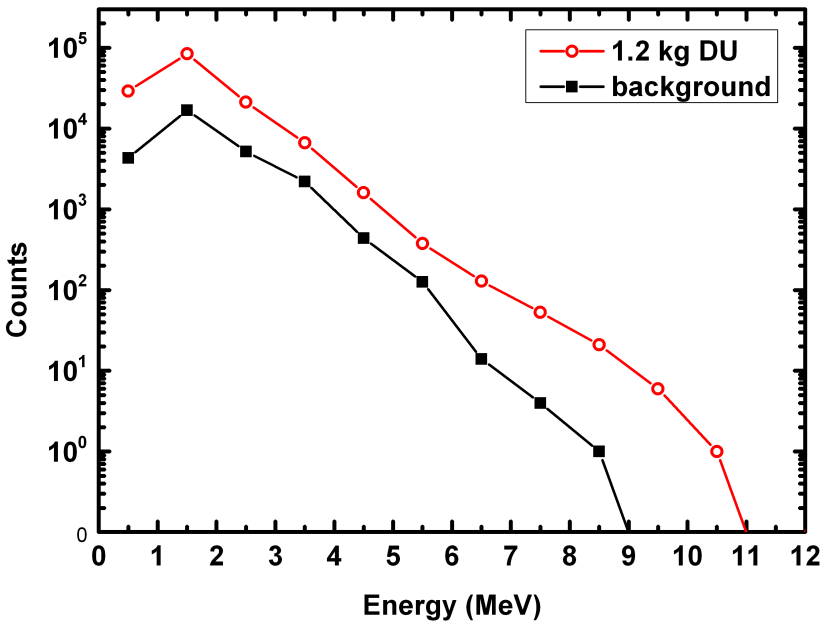

Figure 6.6: Spectra recorded from active background and 1.2 kg of depleted uranium without shielding, recorded after 60 s irradiation with dose rate of 30 Gy/(min × m). ⌀2" × 3" BaF_2 scintillator was used as a detector.

were measured during 60 s after the irradiation stop. In each spectrum, counts were integrated within the energy range between 6.0 and 10.5 MeV and binned in order to show the statistics per each 1 MeV bin. The binning was performed in order to improve the visualization of the counts in the higher energy range. According to the passive measurements with ^{252}Cf, in all measurements the side-on position of the detector was chosen for better detection efficiency. The dose rate was set to 30 Gy per minute at 1 meter. The contribution of prompt neutrons was analyzed in the range between 6.0 and 10.5 MeV, based on an activation of ^{19}F and registering the β^- particles from the consecutive decay of ^{16}N. For this measurement mode, the signal-to-background ratio is about 12. The number of counts after irradiation of the nuclear material was 216 ± 16. When the DU was removed, the number of counts from the active background was 18 ± 4, as showed in Figure 6.7.

In Figures 6.8, 6.9 and 6.10 the responses of 2" × 3" BaF_2 scintillator to photofission-induced 1.2 kg DU in the beam-off mode are presented. In this case, the Varian LINATRON was working in beam-off mode, provided dose rate of 4 Gy/(min × m) and beam

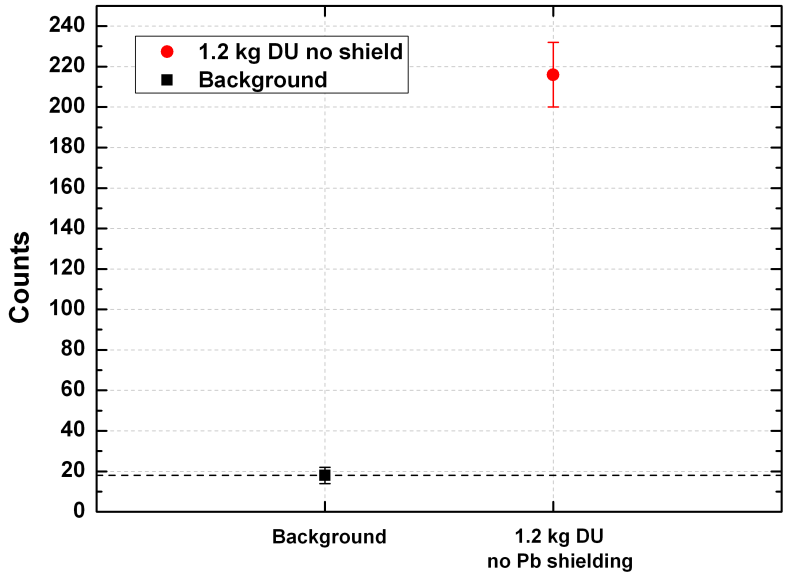

Figure 6.7: Number of counts from background and 1.2 kg of depleted uranium with and without shielding after 60 s of irradiation with a dose rate of 30 Gy/(min × m). Then, the irradiation was stopped and the spectrum was recorded during 60 s. ⌀2" × 3" BaF_2 scintillator was used.

frequency of 33 Hz. Initially, the nuclear material was not shielded (Figure 6.8), then 5 cm of lead was placed in front of the nuclear material (Figure 6.9). In the third irradiation the 5 cm Pb was replaced with 10 cm polyethylene (PE), see Figure 6.10. In each mode the spectra are the sum of three consecutive measurements in order to increase the statistical accuracy. After integrating the energy range between 6.0 and 10.5 MeV, the β^- particles from ^{16}N related to prompt neutron events are obtained together with secondary effects introduced at the beginning of this section. The number of counts between 6.0 and 10.5 MeV for various shielding materials is presented in Figure 6.11. During tests with the unshielded DU the number of counts exceeded the background by a factor of 2.8. It can also be seen that the statistical counts decreased by 21% and 28% (compared to the unshielded case) when lead or PE was used, yielding a signal of 2.2 and 2.0 above the background level, respectively.

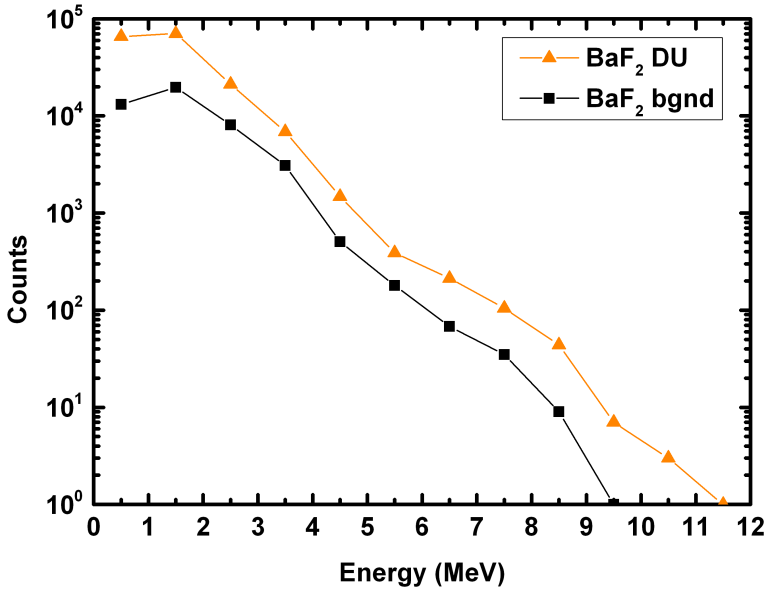

Figure 6.8: Spectra of active background and 1.2 kg of depleted uranium without shielding, recorded during 120 s beam-off inspection and binned in order to show the event statistics in each 1 MeV bin. Three consecutive measurements were summed.

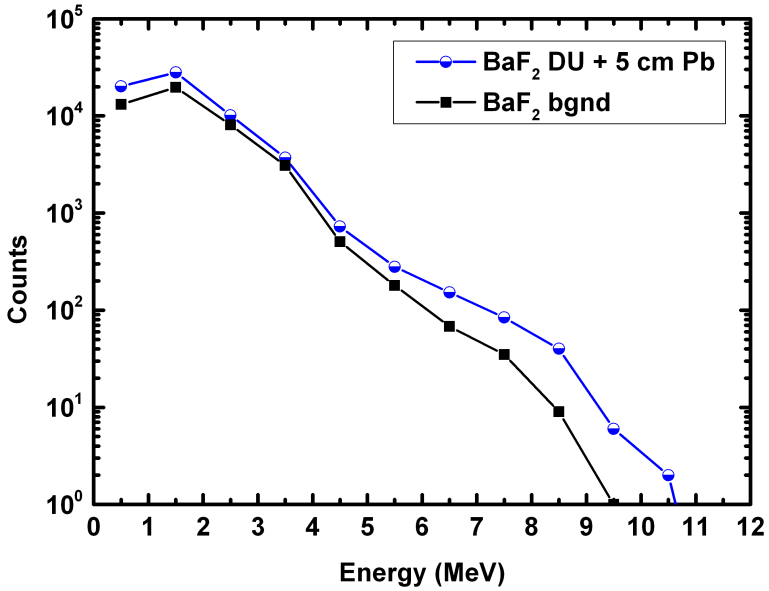

Figure 6.9: Spectra of active background and 1.2 kg of depleted uranium with 5 cm Pb, recorded during 120 s beam-off inspection and binned in order to show the event statistics in each 1 MeV bin. Three consecutive measurements were summed.

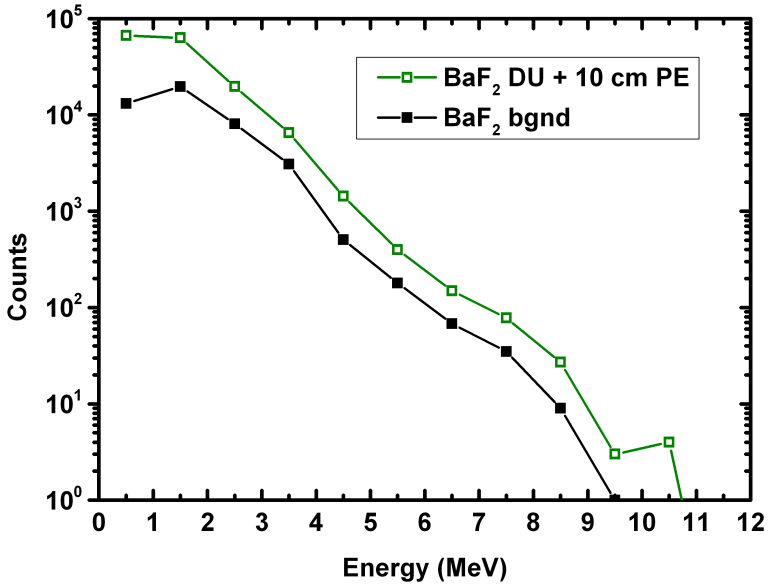

Figure 6.10: Spectra of active background and 1.2 kg of depleted uranium with 10 cm PE, recorded during 120 s beam-off inspection and binned in order to show the event statistics in each 1 MeV bin. Three consecutive measurements were summed.

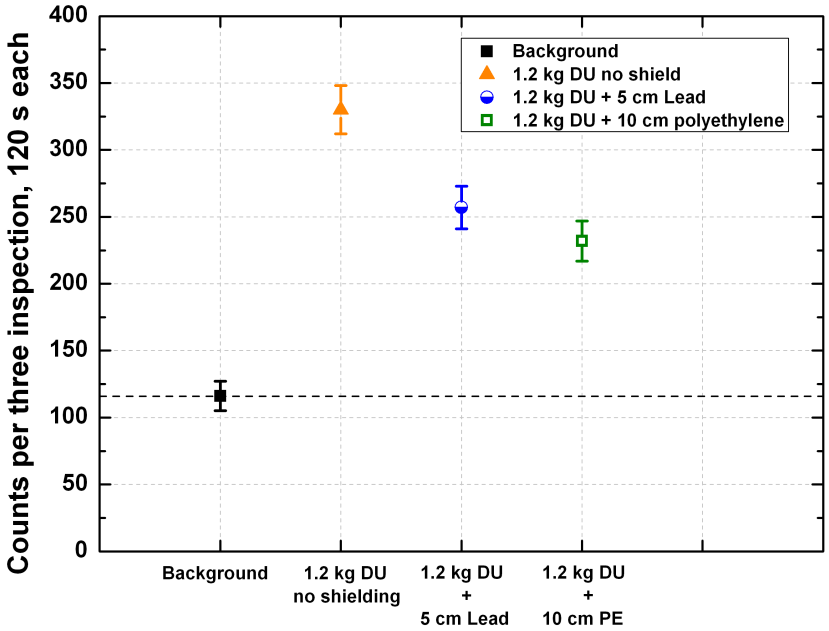

Figure 6.11: Number of counts from background and 1.2 kg of depleted uranium with and without shielding, recorded during 120 s inspection using the beam-off technique for events in the range between 6.0 and 10.5 MeV.

The measurements of prompt neutrons from photofission by means of the TAD technique showed similar tendency with the measurements performed with a ^{252}Cf neutron source. The number of counts, relative to the unshielded case, decreased by 21% after placing the Pb shielding behind the nuclear material. The shielding effect was even greater for the measurements with ^{252}Cf and is due to the scattering of the neutrons on the high Z-value Pb shielding, which was placed close to the detector and ^{252}Cf source. In the geometry set for the present study, better event statistics between 6.0 and 10.5 MeV were acquired via out-of-beam mode. For this method, more intense beams can in principle be applied, resulting in a higher rate of photofission-induced events and lower contribution of active background. In contrary to the out-of-beam mode, the efficiency of the beam-off technique was hampered by the achievable duty factor of the pulse beam sequence (21 ms of recovery time after a beam pulse, followed by a 9 ms data-acquisition window) and the lower dose rate provided by the LINAC. The lower signal-to-background ratio can be related to additional background contributing to the total counts in the energy range between 6.0 and 10.5 MeV. The TAD technique can be very useful for shielded nuclear material detection, as shown in Figure 6.9, where the contribution of the delayed γ-rays to the spectrum was strongly suppressed. However, the TAD technique should be further studied with respect to detection of nuclear materials in the presence of a low-Z environment, where some of the prompt neutrons can be scattered of hydrogen, resulting ub reduced neutron energy below the ^{19}F activation threshold.

6.7 Novel fluorine-based plastic scintillator for fast neutron detection

Recent studies confirmed that large volume EJ-313 and BaF_2 scintillators are good candidates for the TAD technique aiming at the detection of fission prompt neutrons by means of fluorine activation. However, two main drawbacks appear concerning their potential use: toxicity and low flashpoint of the former one and significant increase in the price with detector volume in the latter case. These disadvantages were motivations for searching for a new solution in this domain. The investigation was conducted within

POLONIUM 2013 - 2014 collaboration program between NCBJ and CEA LIST, Saclay, France.

First assumption was to use a plastic scintillator, that usually have a low production price and high volume. The next point was to find a chemical solution containing a significant amount of fluorine which can be easily polymerizable. Mixing these two conceptions a new type of scintillator was prepared - a ⌀32 mm × 4 mm fluorine-based plastic scintillator (F-plastic) [15], containing 3.73×10^{22} F atoms/cm^3, comparable to that of the liquid fluorocarbon scintillators, like EJ-313 or BC-509.

6.7.1 Scintillator preparation

Before preparing the sample one has to choose of the fluorine matrix. The ideal solution seems to be applying the homopolymer of poly(perfluorostyrene). Though this polymer already exists (CAS number 26838-49-3), its preparation is not compatible for scintillation purposes as it requires such harsh conditions as glow discharge or High Pressure and High Temperature (HPHT) conditions, typically 11.500 atm and 155 ℃ in the presence of γ-rays) [109]. Therefore, we turned our attention to a lesser F-content, but polymerizable compound, namely 2,3,4,5,6-pentafluorostyrene (see Figure 6.12), which is known to be able to polymerize by radical initiation [70, 71]. In the case of the pentafluorostyrene, the free radical is CH_3. Radical initiation is a process relying on adding a specific substance which creates radical species under mild conditions (pressure, low heating temperature, illuminating with UV light) and promotes radical reactions. In general, a free radical is such an atom, molecule or ion, which has unpaired valence electrons. These unpaired electrons make free radicals highly chemically reactive towards themselves or other substances. It encourages further polymerization of materials, giving finally, for example, plastic scintillator.

The first produced sample with ⌀ 32 mm and 4 mm height was successfully prepared from the thermal polymerization of pentafluorostyrene containing two dyes suitable for scintillators. Due to a significant loading of fluorine, density of 1.55 g/cm^3 was reached, likely making the F-plastic the densest plastic scintillator ever reported. With the recent heavy plastic scintillators, loads with 10% Pb [110], [111] and 17% Bi [16], and density of 1.12-1.20 g/cm^3 and 1.35-1.39 g/cm^3 were achieved at most, respectively.

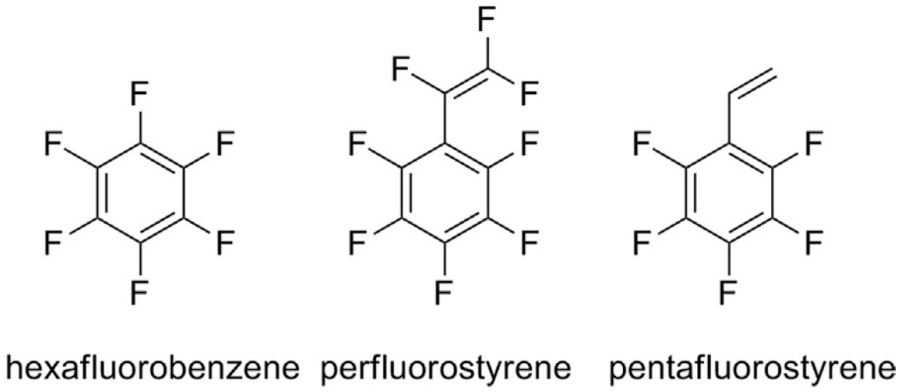

Figure 6.12: Various fluorine containing matrices.

6.7.2 Emission spectrum

Front-face fluorescence spectrum of the F-plastic displays a trident-style emission spectrum with the maximum close to 415 nm (see Figure 6.13). A small shoulder appearing at 360 nm depicts that the Förster energy transfer between the primary and the

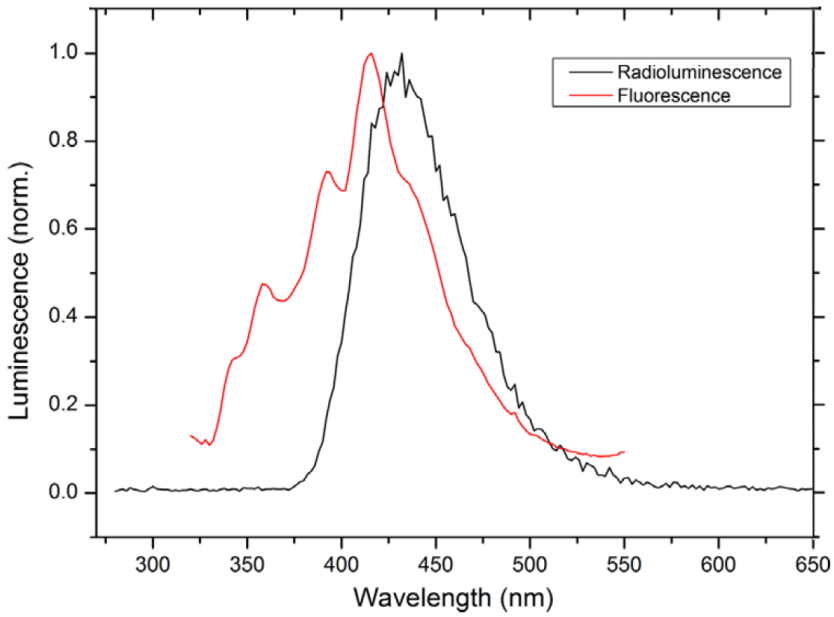

Figure 6.13: Steady-state emission (red) and radioluminescence (black) spectra of F-loaded plastic scintillator (F-plastic).

secondary dye is not complete. However, radioluminescence canceled this assumption as the full spectrum of the secondary fluorophore is clearly visible, and the resulting luminescence is now centered at 425 nm.

6.7.3 Scintillation decay time, light output and non-proportional response of the F-plastic scintillator

A basic study of scintillation performance including light output, scintillation decay time and non-linear response to γ-rays, was performed before further tests with neutrons sources. A same-size EJ-200 PVT plastic scintillator was used as a reference due to its high light output (10000 ph/MeV), fast response (1.9 ns) and the fact that it does not contain fluorine atoms [112].

The decay time of the light pulse for the F-plastic was estimated to be close to 3.0 ns. Under the same measurement conditions, i.e., average recording of 10,000 waveforms obtained from the irradiation of the sample with a ^{54}Mn source and signal recorded with a Tektronix TDS5054B oscilloscope, the EJ-200 displayed a decay time of 1.9 ns, which is consistent with the supplier's datasheet [112].

The estimation of the number of photoelectrons was identical to that performed for EJ-313, BaF_2 and BC-408 scintillators and is based on the technique called the single photoelectron method. For good system geometry, when a scintillator diameter is not larger than a window of the spectroscopy PMT and when the PMT's response as a function of the wavelength is well calibrated, it is possible to derive the absolute light output of the scintillator, expressed in photons per MeV (ph/MeV). The value can be obtained by dividing the number of photoelectrons per 1 MeV ($N_{phe/MeV}$) from Equation 3.1 by averaging the convolution of the PMTs QE and the normalized emission spectrum of the scintillator:

$$N_{ph/MeV} = \frac{N_{phe/MeV}}{\frac{\sum QE_{PMT}(\lambda) \times I_{sc}(\lambda)}{\sum I_{sc}(\lambda)}}, \tag{6.3}$$

The tested plastic F-plastic and EJ-200 scintillators were irradiated by 661.7 keV γ-rays from a ^{137}Cs radioactive source. Then, the number of photoelectrons that are generated in the PMT was estimated by comparing the position of a 477.3 keV Comp-

ton edge at 80% of its height with the position of the single photoelectron peak. After correction by an integral QE, the estimated number of photons for the fluorine-based plastic scintillator is 3100 ± 300 ph/MeV, approximately 30% of what the EJ-200 plastic scintillator can produce.

As already stated by John Birks several decades ago [113], organic scintillators emit less light per unit energy after interaction with γ-rays of lower energy. This so-called non-proportionality of the scintillator response to incoming γ radiation is herein observed [104, 114, 115]. It results in significant light output deviation from 60 to 1536 keV for the both F-plastic and EJ-200 scintillators. Figure 6.14 presents the data recorded in that energy range, where scintillators were exposed to ^{241}Am, ^{22}Na, ^{137}Cs and ^{207}Bi γ sources. Particularly, the non-proportionality curve of the scintillator is normalized to the unity for the value of light output for 661.7 keV γ-ray ^{137}Cs. The shape of the non-proportionality curves is actually identical with that investigated for BC-408 PVT plastic scintillator [114], equivalent to the EJ-200.

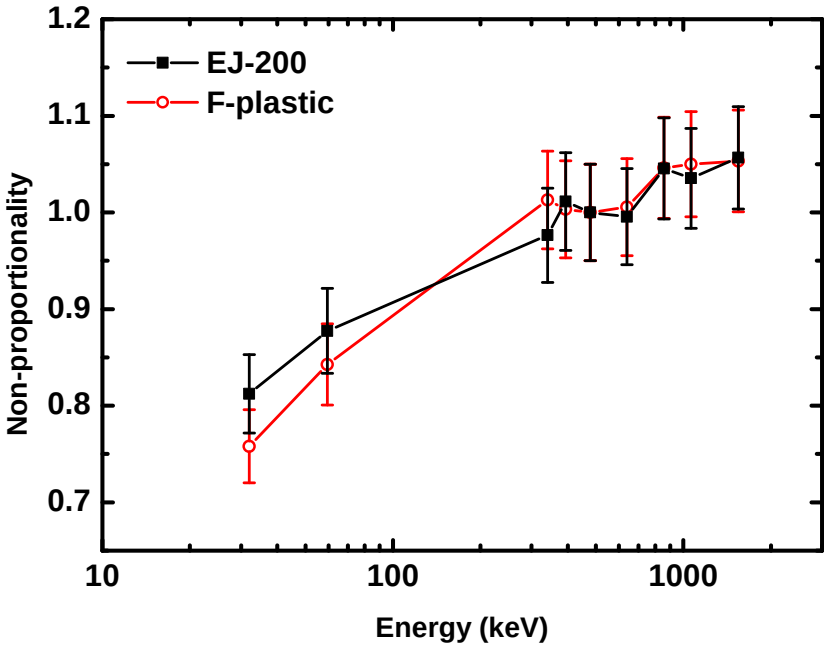

Figure 6.14: Non-proportionality vs. Compton edge energy for F-loaded and EJ-200 plastic scintillators (normalized to a Compton edge at 477.3 keV corresponding to 661.7 keV full energy peak from ^{137}Cs).

6.7.4 Response to neutron sources

The response of the F-plastic and EJ-200 scintillators to fast neutrons was measured with ^{238}PuBe and ^{238}PuC sources, which were shielded by a 5 cm thick lead brick in order to minimize the detection of γ-rays from these sources. Energy calibration was performed using ^{22}Na and ^{137}Cs γ sources with initial activity of a few hundred kBq. The measurement system for spectra analysis was identical to that used for light output estimation. In Figure 6.15, the relative responses of the F-plastic and EJ-200 plastic scintillators to the unshielded ^{238}PuBe source are presented. The difference in spectra shapes for these two scintillators is clearly noticeable, as the F-plastic contains lower amount of hydrogen. It results in lower amount of events related with the neutron scattering on hydrogen and generation of recoiled protons. Moreover, in the case of F-plastic, part of events were observed in the range above 6.5 MeV, suggesting that the deposition of energy by β^- particles after ^{19}F activation occurs.

The background spectra for each scintillator were also measured. The measurement

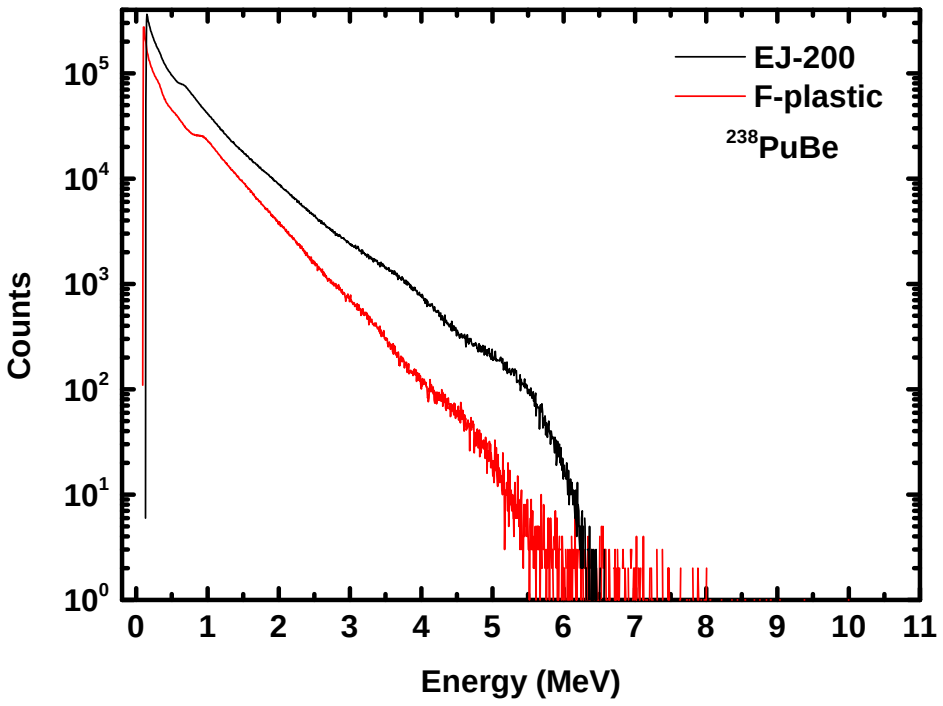

Figure 6.15: Comparison of the ^{238}PuBe spectra recorded with EJ-200 and F-plastic scintillators without Pb shielding.

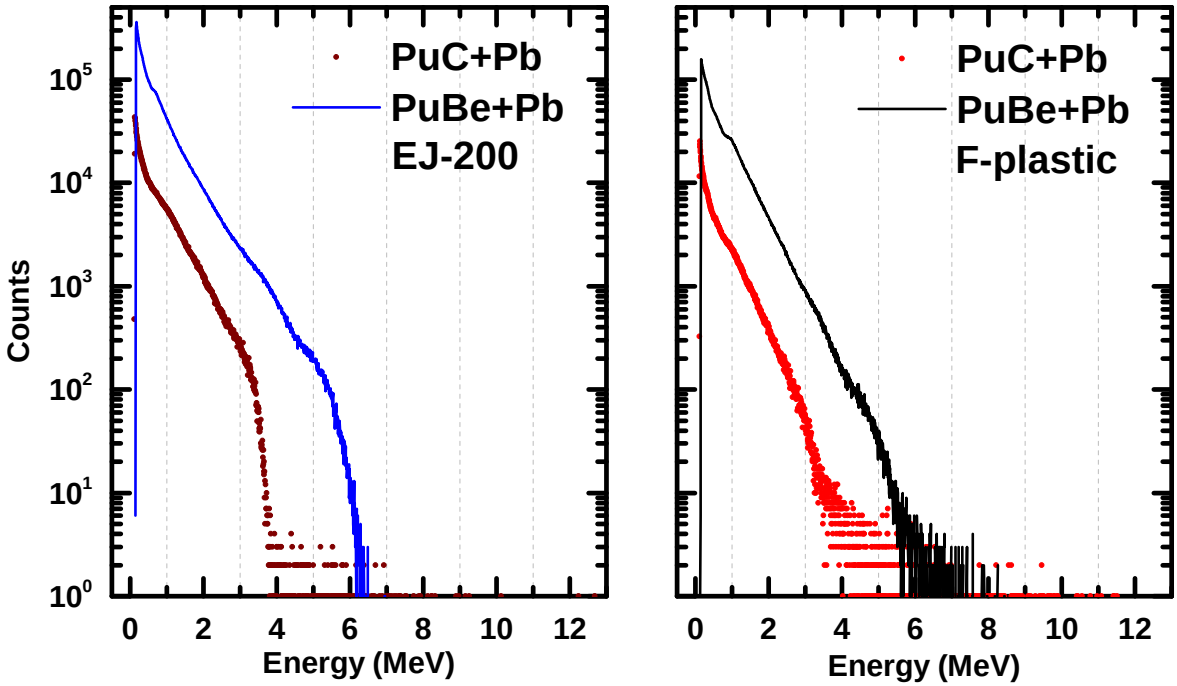

Figure 6.16: Response of EJ-200 and F-plastic scintillators to ^{238}PuBe and ^{238}PuC neutron sources shielded with 5 cm of lead.

time was as long as 12 h. The same measurements were performed with the ^{238}PuC source, emitting neutrons carrying lower energy, in order to compare the spectra shape to that obtained with ^{238}PuBe source. Obtained plots for the neutron sources were summarized in Figure 6.16. The smaller amount of counts in whole energy range for the F-plastic is the result of the much lower hydrogen content.

To compare the number of fast neutrons events registered in reaction with ^{19}F, the data from Figure 6.16 were presented in the higher energy region, as it is depicted in Figure 6.17. The second and third columns of Table 6.4 list the total counts and background in the high energy region (6.5-10.5 MeV) recorded with the ^{238}PuBe neutron source. It shows that the F-plastic registered statistically significant net signal with signal-to-background ratio of about 1.8, contrary to the EJ-200, where true signal and background are on the same level. The total number of counts in the wide energy spectra (i.e. the integral under the curves in Figure 6.15) in whole energy range the F-plastic is substantially lower than that of the EJ-200 plastic scintillator, as indeed Table 6.4 shows.

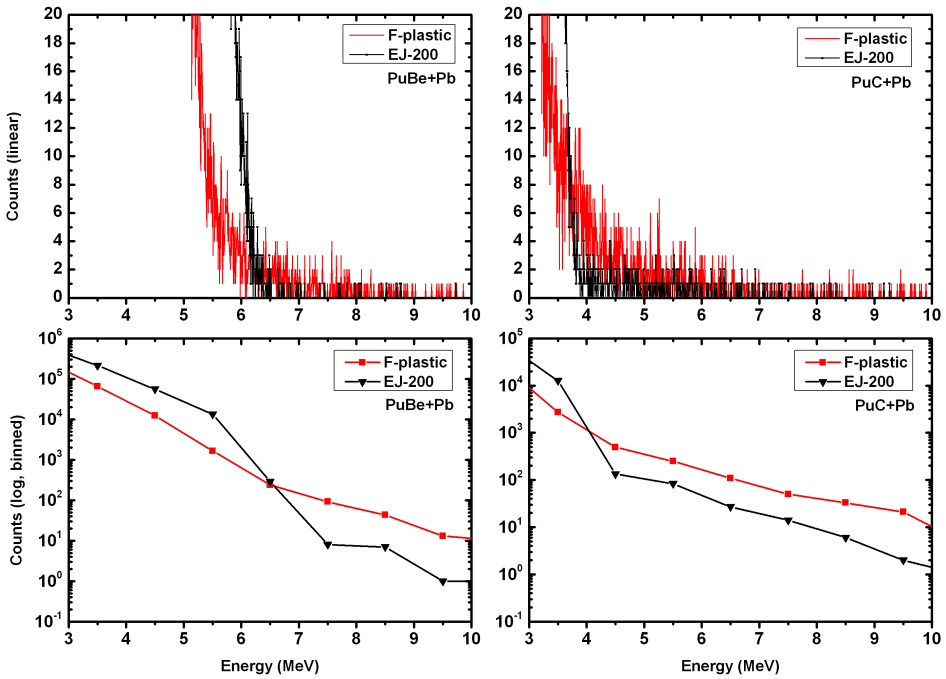

Figure 6.17: ^{238}PuBe and ^{238}PuC spectra recorded with EJ-200 and F-plastic with Pb shielding. The spectra on the bottom were binned with 1 MeV step in order to show the excess of signal. Data are presented in the interesting region of higher energies.

It is plausible that the presence of the higher energy counts in the F-plastic is the result of (n,α) reactions with the fluorine, which generate electrons with a continuous energy spectrum up to 10.4 MeV (β^- particle spectrum). Even though the detector is small (32 mm diameter and 4 mm thickness) and the mean free path of the electrons carrying energy of 10 MeV is about 30 mm, according to the Continuous Slowing Down Approximation (CSDA) range calculations [69], some of the electrons, including those with E $>$ 6.5 MeV, can deposit their energy in the detector in few collisions or even in a single collision. Part of the high energy spectrum of the F-plastic scintillator is probably also due to its poorer energy resolution compared to that of the EJ-200, stretching the spectrum beyond 6 MeV, as presented in Figure 6.17. In order to observe better statistical contribution in this range of energy, future tests with a larger F-plastic scintillator were conducted to assess the various effects. Currently ⌀2" $\times$ 2" F-plastic was prepared in CEA LIST, Saclay, France. Spectra of ^{238}PuBe for the ⌀2" $\times$ 2" F-plastic and same-size EJ-200 were preliminarily measured at the same geometry

Table 6.4: Number of counts registered between 6.5 and 10.5 MeV with the EJ-200 and F-plastic scintillators during 12 h measurement for each sample with the ^{238}PuBe source shielded with a 5 cm of Pb. The last column presents the registered rate in the energy range between 0.15 MeV and 10.5 MeV (both sample have the same size: ⌀32 mm, thickness 4 mm)

Scintillator	Total counts	Background	Total counts/s
EJ-200	44 ± 3	39 ± 3	420
F-plastic	260 ± 20	145 ± 25	224

settings, see Figure 6.18. Although the uniformity of the larger F-plastic scintillator was poor due to low quality of the base material, the excess of counts in the higher energy range was observed. Performance of the ⌀2" × 2" sample of the F-plastic scintillator and the response to the fast neutrons from the ^{252}Cf source will be further performed at NCBJ within the project entitled "the effective Container inspection at BORDer control points" (C-BORD).

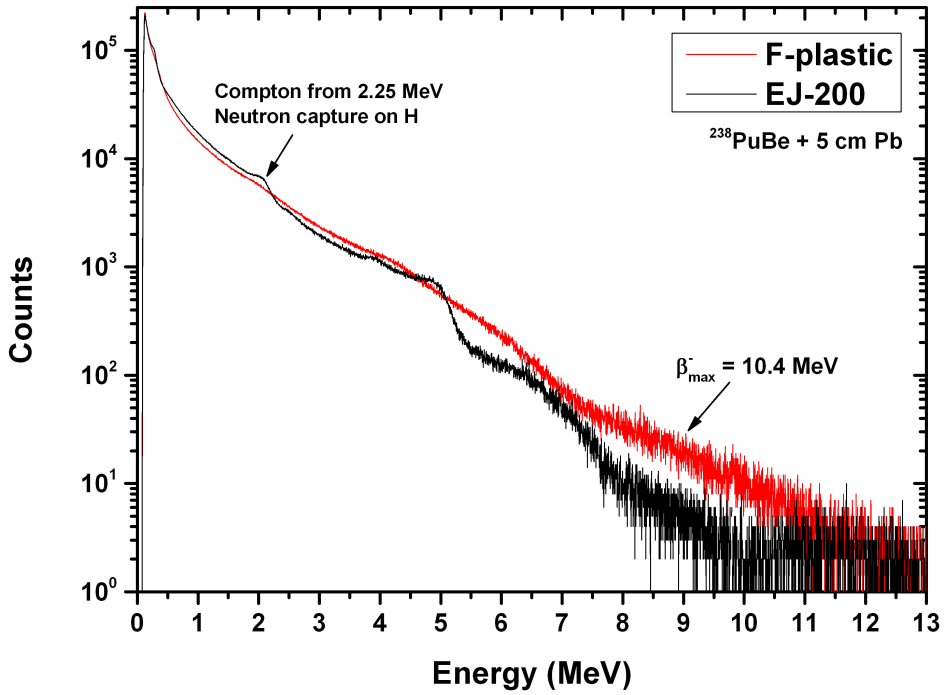

Figure 6.18: ^{238}PuBe and spectra recorded with ⌀2" × 2" F-plastic and EJ-200 shielded with 5 cm Pb.

6.7.5 Pulse shape discrimination (PSD) performance of F-plastic

The relatively low hydrogen content of the F-plastic compared to the standard plastics with PSD possibility (e. g. Eljen EJ-299 series) invites the question whether this scintillator can exhibit pulse shape differences, which can be employed to discriminate between neutron and γ-ray pulses. The neutron pulse shape is determined by the recoil protons. The prompt products of the fast neutron activation of fluorine (alpha and proton) do not contribute to prompt detection of the fast neutrons because of the low interaction cross section (compared with the (n,p) reaction) and the low pulse height generated by the resulting alpha particles. In the matter of the active inspection systems, the PSD method can be applied for filtering the accidental neutrons from background, including photoneutrons emitted from high energy LINACs. Two neutron sources were used to study the potential PSD capabilities: ^{252}Cf spontaneous fission source (average energy of 2.348 MeV [56] and a neutron emission rate of 6.6 $\times 10^4$ n/s/4π) and a higher energetic ^{238}PuBe source (average energy of 4.3 MeV, with a high energy tail reaching 10 MeV and a neutron emission rate of 8.2 $\times 10^5 n$/s/4π). The sources were shielded with 5 cm lead to reduce the γ-rays emitted by the sources. The zero-crossing technique, described in [116], was applied in order to measure the n/γ discrimination capability of F-plastic. Each pulse is digitized and recorded for further offline analysis. The PSD gaussian distribution registered by the Zero Crossing technique (Z/C) [117] and analyzed off-line are shown in Figure 6.19. Three energy cuts with $\pm$ 10% of margin were done in order to increase statistics: low (500 keV), medium (1000 keV) and medium high (1500 keV). The PSD figure of merit (FOM), which is defined as the centroid difference between the Gaussian fitted n and γ peaks (introduced as C_n and C_γ, respectively) divided by the sums of the full width at half maximum (FWHM) of each fitted n and γ gaussian distributions as a function of the pulse height threshold, is shown in Figure 6.20 and can be written as:

$$FOM = \frac{C_n - C_\gamma}{FWHM_n + FWHM_\gamma}. \tag{6.4}$$

F-plastic exhibits modest PSD capability, which may be beneficial for higher energy thresholds. For comparison, EJ-299-33 PSD plastic scintillator presents the FOM value

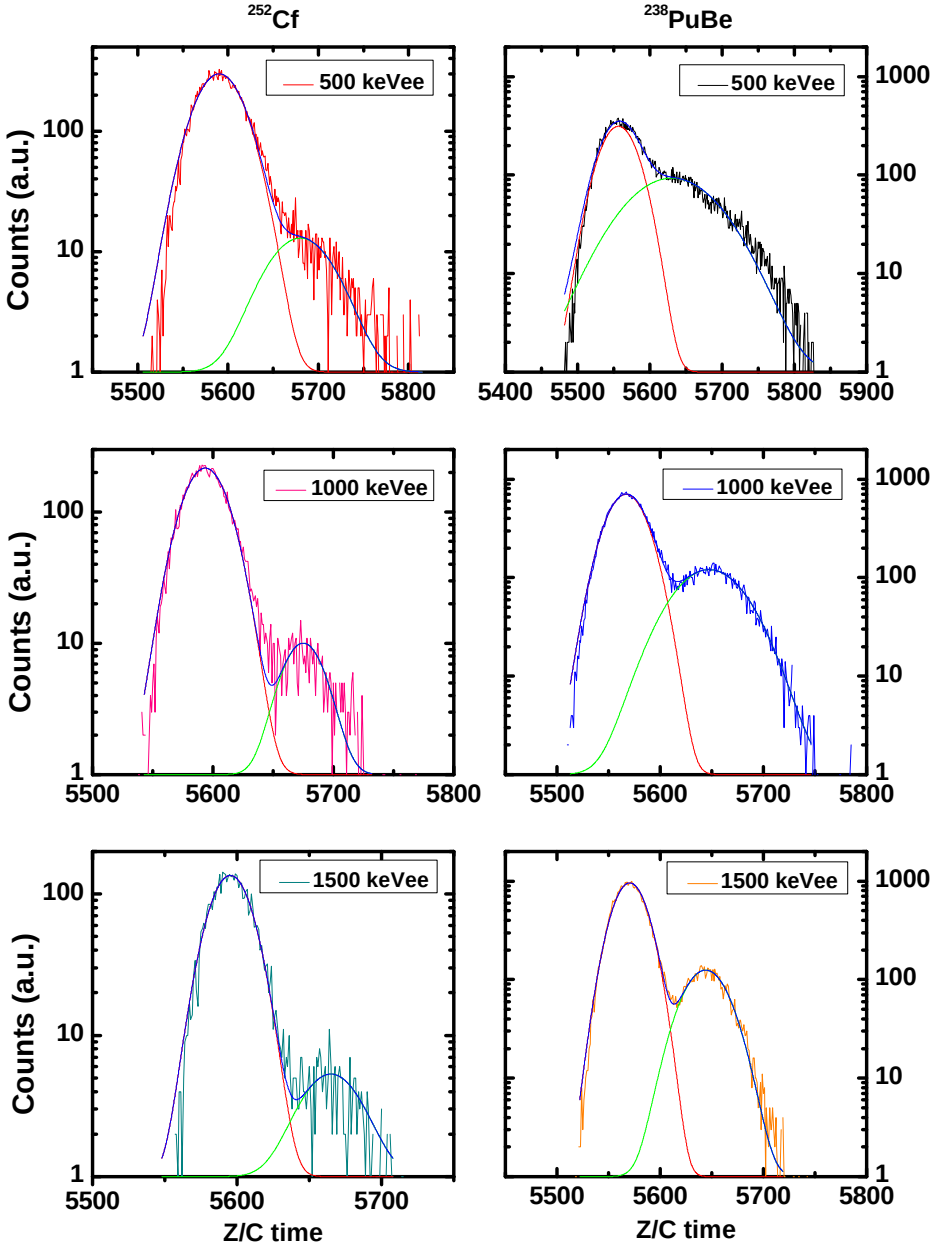

Figure 6.19: Pulse shape discrimination plots for the fluorine loaded plastic scintillator. The scintillator was exposed to neutrons emitted from ^{252}Cf (left column) and ^{238}PuBe (right column). Spectra were cut at 500, 1000 and 1500 keVee.

of 0.9 at 120 keVee [117, 118]. Such a figure of merit value can be achieved for F-plastic only at 3 MeVee.

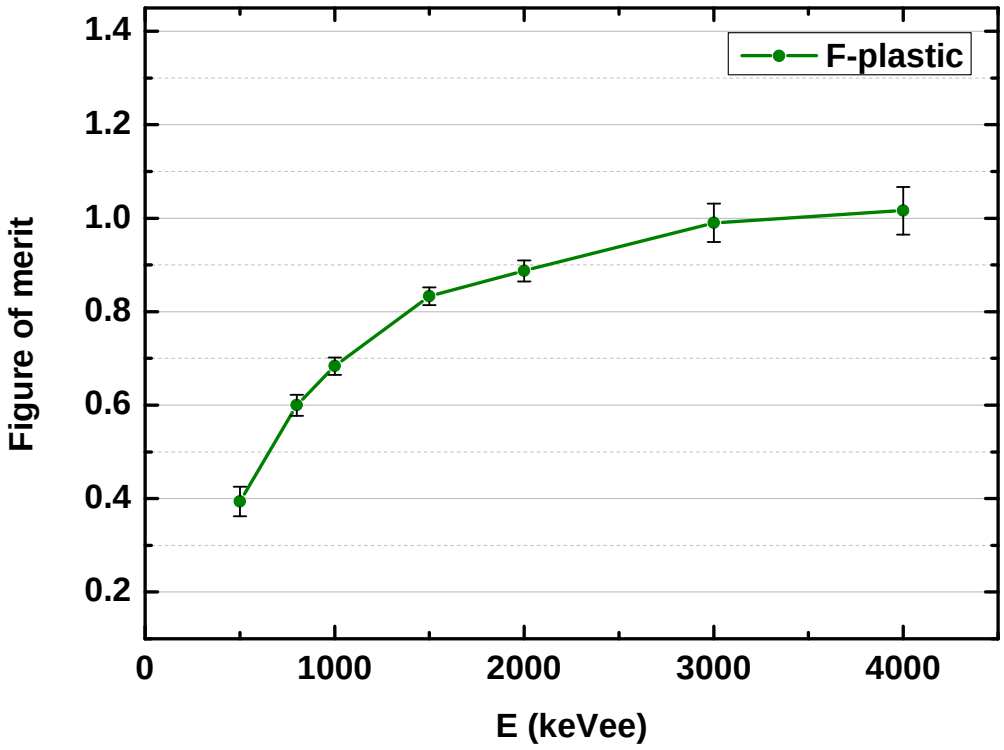

Figure 6.20: FOM of the fluorine loaded plastic scintillator exposed to ^{238}PuBe source.

6.8 Conclusions

The paper [14] presents the response of BaF_2 and EJ-313 to β^- particles emitted due to ^{19}F activation. The response comparison for the BaF_2 and EJ-313 is crucial from the point of view of a detection system designed for active cargo inspection. The performed measurements confirm that EJ-313 is a very attractive scintillator for prompt fission neutron detection. However, with respect to the safety reasons, its low flashpoint of 10°C can be a serious limitation for the use of EJ-313 scintillator in some applications. Thus, BaF_2 seems to be an interesting alternative solution for cargo inspection due to its high density, the short range of high energy β^- particles, absence of hydrogen in the scintillator medium, non-toxicity, non-flammability and the possibility of perform-

ing the energy self-calibration based on α impurities. The self-calibration allows for operation over a broader temperature range and improves the energy calibration stability. The internal radioactive impurities of BaF_2 scintillator give rise to the emission of α particles at energies up to 7.7 MeV (observed at 3.1 MeV due to light quenching). These impurities can decrease the scintillator's usefulness in delayed γ-ray registration, especially with respect to detecting small quantities of nuclear materials. These delayed γ-rays carry energies even of 5 MeV and higher [13, 98], thus, they overlap the energy region of the emitted α particles. Measurements showed that the fast neutron detection efficiency with ^{252}Cf for both scintillators is below 1%. Moreover, the 5 cm Pb shielding in front of ^{252}Cf decreases the number of counts in the energy region between 6.0 and 10.5 MeV by 50 %. The relative number of counts for a front and side oriented BaF_2 measured using the ^{252}Cf source is 32.0% $\pm$ 2.3% and 44.6% $\pm$ 3.4% of that for $\varnothing$5" EJ-313, respectively. For the measurements with the D+T neutron generator, the relative number of counts for side-on oriented BaF_2 was estimated to be 39.3% $\pm$1.4% in comparison with $\varnothing$5" $\times$3" EJ-313. This result is more reliable than that obtained after activation with ^{252}Cf due to lower background contribution between 6.0 and 10.5 MeV. Nevertheless, both results for side-on oriented BaF_2 activated by ^{252}Cf and D+T generator are still in reasonable agreement.

Prompt photofission neutron measurements showed good consistency with the passive experiment based on the ^{252}Cf neutron source. For the out-of-beam measurement, the number of counts from the 1.2 kg DU was about 12 times background level. The beam-off measurements of prompt neutrons from photofission carried out without shielding, then with 5 cm Pb and 10 cm PE also showed that the number of counts from the 1.2 kg DU sample were 2.8, 2.2 and 2.0 times background level, respectively.

The study also showed that the large volume BaF_2 can be a good alternative solution for detection of prompt neutrons with the TAD technique. However, BaF_2 scintillators are limited in size and will not be available in the size possible to obtain with EJ-313. Currently, $\varnothing$3" $\times$ 3" BaF_2 scintillators are commercially available. The price of such 3" $\times$ 3" BaF_2 is also higher than that of $\varnothing$5" $\times$ 3" EJ-313, however, the price difference is not really significant. The next issue is the activation of BaF_2 scintillator by active background. The neutron capture and neutron scattering of Ba nuclei result in emission

of the γ-rays, but mostly below 6 MeV. Many more γ-rays with energy above 6 MeV are emitted from excited ^{19}F, which is present both in BaF_2 and EJ-313 scintillators. Thus, further study will be focused on proper shielding of the scintillator in order to absorb the slow neutrons below the activation threshold of ^{19}F and optimize of the measurement technique.

Additionally, compact systems based on hydrogenous scintillators with pulse shape discrimination (PSD, known also as a n/γ discrimination) for prompt neutron detection from photofission can be considered and will be briefly discussed here. Commercially, a variety of scintillators used for the PSD technique are available: EJ-299 series plastics [117, 119–121], large volume stilbene [122], liquid and composite scintillators [116]. A 9 MeV LINAC working at low dose rate of 4 Gy/(min $\times$m) can be applied for the compact TAD technique, as presented in this Chapter. In the case of the compact PSD system, although the fast neutron detection efficiency is high, the main problem can be related to the photoneutrons generated with a 9 MeV LINAC, resulting in the deterioration of the signal to background ratio. As showed in [100], during work with a LINAC + tungsten converter, emitting Bremsstrahlung photons with an endpoint at 14 MeV, and current of 100 mA, the number of photoneutrons can reach 2.72×10^{10} n/s. The contribution of photoneutrons for such a system can be several decades higher than that from prompt neutrons. Most of photoneutrons are registered at lower energy when compared with the prompt neutrons from photofission, and can, in principle, be discriminated by raising the discriminator level of the liquid (or plastic) hydrogenous proton recoil scintillator. That means a "soft" adjustable threshold - not very sharp because of the large finite pulse height resolution of the scintillator. TAD, on the other hand, has a well-defined threshold, where no neutrons below the energy threshold can be detected.

The activation energy threshold is a great benefit of the TAD technique. A LINAC emitting photons with lower endpoint energy can of course be considered for the PSD-based system, but a lower Bremsstrahlung endpoint implies a lower amount of photons available to induce photofission. In the case of a 9 MeV LINAC workin in beam-off mode, if the current is high, it will incapacitate the detector during the pulse and the prompt fission neutrons will not be detected. In order to validate the usefulness

of the PSD-based system for prompt neutron detection with the use of the pulsed Bremsstrahlung source, further measurements with both TAD and PSD scintillators having large volumes should be performed using the same geometrical setup.

Concerning F-plastic scintillator, for the first time, we were able to prepare a plastic scintillator which polymer matrix is composed of a high percentage of fluorine. The fabricated small scintillator sample when exposed to fast neutrons exhibited a spectrum consisted of a low resolution proton recoil and a high energy tail related with high energy β^- particles from the fast neutron activation of fluorine. The detector also exhibits very modest n/γ pulse shape discrimination capabilities. In the near future, tests of a larger F-plastic scintillator ($\varnothing 2'' \times 2''$) will be performed in order to compare its efficiency at β^- particle detection with that offered by a liquid fluorocarbon scintillator of the same size.

Chapter 7

Summary

The PhD dissertation summarizes the current techniques applicable for measurements of photofission signatures. It is especially focused on prompt neutron detection by means of the TAD technique with the use of fluorine based scintillators due to the fact that the amount of prompt neutrons is two decades greater than that for delayed neutrons (2-3 prompt neutrons/fission vs 0.01 delayed neutrons/fission). Currently, fluorocarbon (such as EJ-313) and BaF_2 scintillators were found to be useful for prompt neutron detection. However, EJ-313 is based on toxic highly purified hexafluorobenzene (C_6F_6) and has a low flash point of 10°C, potentially limiting its application for Homeland Security. Thus, in collaboration with CEA LIST, Saclay, France, an alternative solution based on ^{19}F was introduced - a pentafluorostyrene-based ⌀32 mm × 4 mm plastic scintillator (F-plastic), having the F/H ratio of 1.56, which is non-toxic and non-flammable. For the prompt neutrons detection by means of the TAD technique with ^{19}F-based scintillators, the region of interest between 6.0 and 10.5 MeV was chosen due to the low contribution of radiation to in that energy range to the $beta^-$ spectrum with endpoint at 10.4 MeV. First results showed that the number of counts between 6.0 and 10.5 MeV for F-plastic is greater than that for the standard PVT-based EJ-200 scintillator without fluorine. The first ⌀2" × 2" F-plastic was also successfully manufactured, and, although its uniformity was poor (due to the low quality of the base material from the manufacturer), a β^- particle structure above 6 MeV was observed in the energy spectrum. Currently, a next ⌀2" × 2" F-plastic sample is under develop-

ment utilizing base material from another manufacturer. The TAD method, although it allows the measure of higher-populated prompt neutrons, has a disadvantage related to its low n+^{19}F reaction cross section. The fixed n+^{19}F reaction threshold of 2.5 MeV allows for reducing the photoneutron contribution, but, on the other hand, can reduce the detection efficiency of SNM shielded by a low-Z materials that decrease the neutron energy, even below the activation threshold.

On the basis of the performed study, the usefulness of the techniques for SNM detection presented in this PhD dissertation can be summarized:

- Delayed neutrons - they are a very unique signature of fission, however, they carry low energy and then can be easily attenuated in low-Z environment. Moreover, the amount of emitted neutrons per fission is about 0.01. Such neutrons can be easily detected with an efficient ^{3}He gaseous detector, however, due to the shortage of ^{3}He supplies the price of such detector has drastically increased. Currently companies are working on optimizations of ^{6}LiF/ZnS(Ag) based detectors for delayed neutrons detection and this field seems to be very promising.

- Delayed γ-rays - the best solution for their detection seems to be the high volume scintillators, allowing detection of γ-rays by Compton scattering in the scintillator. Moreover, the plastic scintillators are very cheap. After the photofission of nuclear material, a lot of variable energy γ-rays are emitted, often carrying energies very close to each other. Thus, distinguishing of γ-ray full energy peaks from photofission-induced nuclear materials is possible only with HPGe detectors. The HPGe detectors can be successfully applied for precise characterization of nuclear materials composition, as presented in this dissertation.

- Prompt neutrons - the TAD technique with fluorine-based scintillators can be successfully applied for fast photofission neutron detection, especially when the nuclear material is shielded, with Pb, which has a high density and Z-value, and thus, strongly absorbs delayed γ-rays. However, due to the 2.5 MeV energy threshold, in a low-Z environment (wood, polyethylene) part of the prompt photofission neutrons can fall below the activation threshold.

Summarizing, at the present it is impossible to indicate the best solution for nuclear material detection via photofission. The most efficient border monitoring system should be composed of all the subsystems mentioned above. A complex border monitoring system is currently being developed within the frame of the C-BORD project in the Horizon 2020 (H2020) program. During the research presented in this dissertation many effects were revealed, which require additional studies in the future. At this stage of study the efficiency of delayed versus prompt neutron detection techniques of nuclear materials in a low-Z environment is inconclusive. Moreover, the ^{6}LiF/ZnS(Ag) based detector has not yet been tested for delayed neutron detection. The TAD technique based on ^{19}F seems to be a very promising solution for the detection of shielded nuclear materials, keeping in mind that neutrons are slowed down in low-Z materials present in a cargo container causing the decrease of the prompt neutron detection efficiency. This aspect requires further research. With the TAD detector one can detect delayed γ-rays, which are weakly attenuated in low-Z environment. These all ambiguities will be under study during the upcoming years within the C-BORD project and beyond.

Chapter 8

Glossary

ACS - anti-Compton shield - a set of heavy scintillators (for example, BGO) covering other detector in order to improve the ratio of γ-ray full energy peak to Compton continuum. This solution is often applied to HPGe detectors or $LaBr_3$:Ce scintillators, possessing very good energy resolution.

Active background - the radiation background induced by bremsstrahlung photons and photoneutrons during a LINAC work.

CSDA - continuous slowing down approximation - it is a very close approximation to the average path length traveled by a charged particle as it slows down to rest.

Beam-off - the technique of measurement of characteristic radiation for photofission of nuclear material between the beam pulses from a LINAC.

DDAA - differential die-away analysis - this detection technique is based on emission of neutrons from D+T or D+D generator working on high repetition pulse mode in order to activate the SNM inside cargo container. The neutrons are moderated inside hydrogenous content of cargo container and can interact with the SNM. Then, emitted neutrons from nuclear material moderate again in the cargo content and reach the detector later than prompt γ-rays. The number of registered neutrons distribution in time after the pulse is called "die-away time".

DU - depleted uranium, ^{238}U. It is a fertile material with a lower content of ^{235}U than natural uranium. The DU contains less than 0.3% ^{235}U.

Fertile materials (pol. Materiały rodne) - a materials which cannot undergo nuclear

chain reaction, but can be converted into materials which are fissile by absorption of fast neutrons and subsequent nuclei conversion. Natural fertile materials are ^{232}Th, ^{234}U and ^{238}U.

FOM - figure of merit - the parameter describing the quality of pulse shape discrimination between the peaks from γ-rays and neutrons for a given energy. The parameter is used to characterize the performance of liquid and plastic organic scintillators in neutron detection.

GARRn - Gamma Absolute Rejection Ratio for neutrons - it is defined as the absolute neutron detection efficiency ($\epsilon_{abs\ \gamma n}$) in the presence of both γ and neutron sources, divided by the absolute neutron detection efficiency ($\epsilon_{abs\ n}$) of the neutron detector.

IAEA - International Atomic Energy Agency.

Isocentre - a common geometry point of beam axis and axis of rotation for a medical LINAC. The distance from a conversion target to the isocentre, according to current national standards, is equal to 1 meter. This term is valid only for medical LINACs and is not used in case of industrial LINACs, as the latter do not have the axis of rotation.

LINAC - Linear Accelerator - device, which is used for acceleration of electron (initially using cathode heating and, further, in accelerating structures) to energy range of several MeV. If required, the fast electrons can be converted on tungsten or tantalum target into bremsstrahlung photons.

NII - non-intrusive inspection - the method of inspecting bulk containers without opening it, by means of X-ray imaging, neutron activation and photon interrogation.

Out-of-beam - the technique of characteristic radiation measurement for photofission of nuclear material after irradiation with high energy photons from a LINAC, when the beam was stopped.

PVT - polyvinyltoluene - base material for production of fast low-cost plastic scintillators.

Radical Initiation - radical initiation is a process relying on adding specific substance which creates radical species under mild conditions (pressure, low heating temperature, illuminating with UV light) and promote radical reactions. In general, free radical is such an atom, molecule or ion, which has unpaired valence electrons. These unpaired electrons make free radicals highly chemically reactive towards themselves or other sub-

stances. It lets to further polymerization of materials.

RDD - radiological dispersal device, known also as a dirty bomb - conventional explosives coupled to radioactive or nuclear material.

Significant Quantity - according to IAEA glossary, the approximate amount of nuclear material for which the possibility of manufacturing a nuclear explosive device cannot be excluded. Significant quantities take into account unavoidable losses due to conversion and manufacturing processes and should not be confused with critical masses.

SNM - special nuclear material - isotope of Uranium (233, 235) and Pu (239) which can undergo fission by thermal and fast neutrons. As a result, these materials can undergo nuclear chain reaction.

TAD - threshold activation detection (or detector).

Chapter 9

Acknowledgement

The work conducted within the PhD dissertation was supported by the following projects and programs, which I gratefully acknowledge:

- AiD (Akceleratory i Detektory, eng. Accelerators and Detectors) - program realized between 2008 - 2013. The project was focused on development and construction of demonstration prototypes for medical and homeland security.
- POLONIUM Polish-French staff exchange program, accepted by Polish Ministry of Higher Education and Science (MNiSW) and Campus France during 2013-2014 (shortened name "Photofissium"). The program was realized between two institutes: National Centre for Nuclear Research (NCBJ, Polish program coordinator: Paweł Sibczyński) and Commissariat à l'énergie atomique et aux énergies alternatives (English: Atomic Energy and Alternative Energies Commission, short name CEA, Saclay, France. French program coordinator: Frédérick Carrel).
- Grant for young scientists (Grant dla Młodych) realized within NCBJ support program, entitled "Wytworzenie scyntylatora plastikowego na bazie pentafluorostyrenu o średnicy 2" i wysokości 2" do detekcji prędkich neutronów poprzez aktywację ^{19}F."
- C-BORD EU project - started in 06.2015 - within which the acquired know-how will be applied into development of a system for nuclear materials detection for Border Port.

Bibliography

[1] O. Hahn et al., "Über den Nachweis und das Verhalten der bei der Bestrahlung des Urans mittels Neutronen entstehenden Erdalkalimetalle (On the detection and characteristics of the alkaline earth metals formed by irradiation of uranium with neutrons - Translation in *American Journal of Physics*, Jan. 1964, p. 9-15)", *Die Naturwissenschaften*, vol. 27, pp. 11–15, Jan. 1939.

[2] L. Meinter et al., "Disintegration of uranium by neutrons: a new type of nuclear reaction", *Nature*, vol. 143, pp. 239–240, 1939.

[3] E. Feenberg, "On the shape and stability of heavy nuclei", *Physical Review*, vol. 55, pp. 504–505, Mar. 1939.

[4] N. Bohr et al., "The mechanism of nuclear fission", *Physical Review*, vol. 56, pp. 426–450, Sep. 1939.

[5] R. O. Haxby et al., "Photo-fission of uranium and thorium", *Physical Review*, vol. 59, pp. 57–62, Jan. 1941.

[6] V. Antropov et al., "IREN test facility at JINR", *Proceedings of the International Conference LINAC'96*, 1996.

[7] Y. Kadi et al., "Design of an accelerator-driven system for the destruction of nuclear waste", *Workshop on Hybrid Nuclear Systems for Energy Production, Utilisation of Actinides & Transmutation of Long-Lived Radioactive Waste*, Sep. 2001.

[8] F. Carrel et al., "Measurement of plutonium in large concrete radioactive waste packages by photon activation analysis", *IEEE Transactions on Nuclear Science*, vol. 57, no. 6, pp. 3687–3693, Dec. 2010.

[9] S. F. Mughabghab, "NNDC - Thermal Cross Sections & Resonance Integrals, website: *http://www.nndc.bnl.gov/atlas/atlasvalues.html* (last accessed 29.06.2015)".

[10] J. Borger, "The Mosul Mystery: The missing uranium and where it came from", *The Guardian*, 13 Jul. 2014.

[11] P. Sibczynski et al., "Detection of delayed radiation from highly enriched ^{235}U samples induced by Bremsstrahlung photons", Presented at *Zakopane Conference on Nuclear Physics*, 2014.

[12] J. Mierzejewski et al., "EAGLE - the central European Array for Gamma Levels Evaluation at the Heavy Ion Laboratory of the University of Warsaw", *Nuclear Instruments and Methods in Physics Research Section A: Accelerators, Spectrometers, Detectors and Associated Equipment*, vol. 659, no. 1, pp. 84–90, 2011.

[13] P. Sibczynski et al., "Decay chains and photofission investigation based on nuclear spectroscopy of highly enriched uranium sample", *Applied Radiation and Isotopes*, vol. 82, pp. 170–174, 2013.

[14] P. Sibczynski et al., "Verification of threshold activation detection (TAD) technique in prompt fission neutron detection using scintillators containing ^{19}F", *JINST 10 T09005*, 2015.

[15] M. Hamel, P. Sibczynski, et al., "A fluorocarbon plastic scintillator for neutron detection: Proof of concept", *Nuclear Instruments and Methods in Physics Research Section A: Accelerators, Spectrometers, Detectors and Associated Equipment*, vol. 768, pp. 26–31, 2014.

[16] G. H. V. Bertrand et al., "Influence of bismuth loading in polystyrene-based plastic scintillators for low energy gamma spectroscopy", *Journal of Materials Chemistry C*, vol. 2, pp. 7304–7312, 2014.

[17] T. Gozani, "Fission signatures for nuclear material detection", *IEEE Transactions on Nuclear Science*, vol. 56, no. 3, pp. 736–741, Jun. 2009.

[18] K. Persyn et al., "Influence of the odd neutron on the fragment characteristics in the photofission of ^{235}U", *Nuclear Physics A*, vol. 615, no. 2, pp. 198–206, 1997.

[19] S. Pommé et al., "Fragment characteristics for the photofission of ^{238}U with 6.1 - 13.1 MeV bremsstrahhmg", *Nuclear Physics A*, vol. 572, no. 2, pp. 237–266, 1994.

[20] American Science & Engeenering, "Z-Backscatter Van (ZBV), website: *http://www.as-e.com/products-solutions/cargo-vehicle-inspection/mobile/product/zbv* (last accessed 7.07.2015)".

[21] A. Clarkson et al., "The design and performance of a scintillating-fibre tracker for the cosmic-ray muon tomography of legacy nuclear waste containers", *Nuclear Instruments and Methods in Physics Research Section A: Accelerators, Spectrometers, Detectors and Associated Equipment*, vol. 745, pp. 138–149, 2014.

[22] J. Pruet et al., "Detecting clandestine material with nuclear resonance fluorescence", *Journal of Applied Physics*, vol. 99, no. 12, 2006.

[23] R. Hajima et al., "Detection of radioactive isotopes by using laser compton scattered γ-ray beams", *Nuclear Instruments and Methods in Physics Research Section A: Accelerators, Spectrometers, Detectors and Associated Equipment*, vol. 608, no. 1, Supplement, pp. 57–61, 2009.

[24] T. Hayakawa et al., "Nondestructive assay of plutonium and minor actinide in spent fuel using nuclear resonance fluorescence with laser Compton scattering", *Nuclear Instruments and Methods in Physics Research Section A: Accelerators, Spectrometers, Detectors and Associated Equipment*, vol. 621, no. 1-3, pp. 695–700, 2010.

[25] D.R. Norman et al., "Pulsed photonuclear assessment for the detection of nuclear materials", *IAEA Meeting*, Oct. 2004.

[26] K. A. Jordan et al., "Pulsed neutron differential die away analysis for detection of nuclear materials", *Nuclear Instruments and Methods in Physics Research Section B: Beam Interactions with Materials and Atoms*, vol. 261, no. 1–2, pp. 365–368, 2007.

[27] R. B. Walton et al., "Delayed gamma rays from photofission of U^{238}, U^{235}, and Th^{232}", *Physial Review*, vol. 134, pp. 824–832, May 1964.

[28] E. V. D. van Loef et al., "Scintillation properties of $LaBr_3$:Ce^{3+} crystals: fast, efficient and high-energy-resolution scintillators", *Nuclear Instruments and Methods in Physics Research Section A: Accelerators, Spectrometers, Detectors and Associated Equipment*, vol. 486, no. 1–2, pp. 254–258, 2002.

[29] T. Gozani, *Active nondestructive assay of nuclear materials-principles and applications*, NUREG/CR-0602, 1981.

[30] R. Batchelor et al., "The energy of delayed neutrons from fission", *Journal of Nuclear Energy*, vol. 3, no. 1–2, pp. 7–17, 1956.

[31] D. J. Hughes et al., "Delayed neutrons from fission of ^{235}U", *Physical Review*, vol. 73, pp. 111–124, Jan. 1948.

[32] T. W. Bonner et al., "Energy of the delayed neutrons from the fission of ^{235}U", *Physical Review*, vol. 101, pp. 1514–1515, Mar. 1956.

[33] B. Pfeiffer et al., "Status of delayed-neutron precursor data: Half-lives and neutron emission probabilities", *arXiv:nucl-ex/0106020v1*, 2001.

[34] O. P. Nikotin et al., "Delayed neutrons in the photofission of heavy nuclei", *Soviet Atomic Energy*, vol. 20, no. 3, pp. 300–303, 1966.

[35] P. Peerani et al., "Testing on novel neutron detectors as alternative to ^3He for security applications ", *Nuclear Instruments and Methods in Physics Research Section A: Accelerators, Spectrometers, Detectors and Associated Equipment*, vol. 696, pp. 110–120, 2012.

[36] L. Swiderski et al., "Further study of boron-10 loaded liquid scintillators for detection of fast and thermal neutrons", *IEEE Transactions on Nuclear Science*, vol. 57, no. 1, pp. 375–380, Feb. 2010.

[37] J. L. Lacy et al., "Boron coated straw detectors as a replacement for ^{3}He", in *2009 IEEE Nuclear Science Symposium Conference Record (NSS/MIC)*, Oct. 2009, pp. 119–125.

[38] J. L. Lacy et al., "Boron-coated straw detectors: A novel approach for helium-3 neutron detector replacement", in *2010 IEEE Nuclear Science Symposium Conference Record (NSS/MIC)*, Oct. 2010, pp. 3971–3975.

[39] G. M. Rusch et al., "Inhalation toxicity studies with boron trifluoride", *Toxicology and Applied Pharmacology*, vol. 83, no. 1, pp. 69–78, Mar. 1986.

[40] R. T. Kouzes et al., "BF_3 Neutron Detector Tests", Tech. Rep., Pacific Northwest National Laboratory, Dec. 2009.

[41] General Electrics (GE), "Boron-10 lined proportional counter, website: *https://www.gemeasurement.com/radiation-measurement/homeland-security-detectors/boron-10-lined-proportional-counter* (last accessed 13.07.2015)", 2015.

[42] F. Tokanai et al., "Cold neutron imaging detection with a GSO scintillator", *Nuclear Instruments and Methods in Physics Research Section A: Accelerators, Spectrometers, Detectors and Associated Equipment*, vol. 452, no. 1-2, pp. 266–272, 2000.

[43] L. Ovechkina et al., "Gadolinium loaded plastic scintillators for high efficiency neutron detection", *Physics Procedia*, vol. 2, no. 2, pp. 161–170, 2009, *The 2008 International Conference on Luminescence and Optical Spectroscopy of Condensed Matter* .

[44] K. Watanabe et al., "Neutron-gamma discrimination in a Ce:LiCaAlF6 scintillator based on pulse shape discrimination using digital signal processing", in *2011 IEEE Nuclear Science Symposium and Medical Imaging Conference (NSS/MIC), Conference Record*, Oct. 2011, pp. 436–439.

[45] J. Iwanowska et al., "Thermal neutron detection with Ce^{3+} doped $LiCaAlF_6$ single crystals", *Nuclear Instruments and Methods in Physics Research Section A: Accelerators, Spectrometers, Detectors and Associated Equipment*, vol. 652, no. 1, pp. 319–322, 2011.

[46] K. Watanabe et al., "Wavelength-shifting fiber signal readout from Transparent RUbber SheeT (TRUST) type $LiCaAlF_6$ neutron scintillator ", *Nuclear Instruments and Methods in Physics Research Section A: Accelerators, Spectrometers, Detectors and Associated Equipment*, vol. 784, pp. 260–263, 2015, *Symposium on Radiation Measurements and Applications 2014 (SORMA XV)* .

[47] A. Syntfeld et al., "^{6}LiI(Eu) in neutron and γ-ray spectrometry – a highly sensitive thermal neutron detector", *IEEE Transactions on Nuclear Science*, vol. 52, no. 6, pp. 3151–3156, Dec. 2005.

[48] M. B. Smith et al., "Fast neutron spectroscopy using Cs_2LiYCl_6:Ce (CLYC) scintillator", *IEEE Transactions on Nuclear Science*, vol. 60, no. 2, pp. 855–859, Apr. 2013.

[49] C. Giles and D. Ramsden, "Radiation detector", Jan. 2012, WO Patent App. PCT/GB2011/051,236.

[50] R. T. Kouzes et al., "Neutron detector gamma insensitivity criteria", Tech. Rep., Pacific Northwest National Laboratory, Oct. 2009.

[51] R. T. Kouzes, "Lithium and zinc sulfide coated plastic neutron detector test", Tech. Rep., Pacific Northwest National Laboratory, 2010.

[52] D. Stromswold et al., "Specifications for radiation portal monitor systems", Tech. Rep., Pacific Northwest National Laboratory, Richland, Washington, 2003.

[53] D. L. Chichester et al., "The API 120: A portable neutron generator for the associated particle technique", *Nuclear Instruments and Methods in Physics Research Section B: Beam Interactions with Materials and Atoms*, vol. 241, no. 1–4, pp. 753–758, 2005.

[54] P. A. Hausladen et al., "An alpha particle detector for a portable neutron generator for the Nuclear Materials Identification System (NMIS)", *Nuclear Instruments and Methods in Physics Research Section B: Beam Interactions with Materials and Atoms*, vol. 241, no. 1–4, pp. 835–838, 2005.

[55] H. R. Bowman et al., "Velocity and angular distributions of prompt neutrons from spontaneous fission of ^{252}Cf', *Physical Review*, vol. 126, pp. 2120–2136, Jun. 1962.

[56] J. W. Meadows, "^{252}Cf fission neutron spectrum from 0.003 to 15.0 MeV", *Physical Review*, vol. 157, pp. 1076–1082, May 1967.

[57] J. P. Lestone et al., "Uranium and plutonium average prompt-fission neutron energy spectra (PFNS) from the analysis of NTS NUEX data", *Nuclear Data Sheets*, vol. 119, pp. 213–216, 2014.

[58] C. P. Sargent et al., "Prompt neutrons from thorium photofission", *Physical Review*, vol. 137, pp. 89–101, Jan. 1965.

[59] J. T. Caldwell et al., "Prompt and delayed neutron yields from low energy photofission of ^{232}Th,^{235}U, ^{238}U, and ^{239}Pu", *3rd Symposium on Physics and Chemistry of Fission*; Rochester, New York, USA, 1974, Los Alamos report LAUR-73-968, 1973.

[60] J. M. Mueller et al., "Measurement of prompt neutron polarization asymmetries in photofission of ^{235,238}U, ^{239}Pu, and ^{232}Th", *Physical Review C*, vol. 85, pp. 014605, Jan. 2012.

[61] T. Gozani et al., "Neutron threshold activation detectors (TAD) for the detection of fissions", *Nuclear Instruments and Methods in Physics Research Section A: Accelerators, Spectrometers, Detectors and Associated Equipment*, vol. 652, no. 1, pp. 334–337, 2011, *Symposium on Radiation Measurements and Applications (SORMA) XII 2010.*

[62] T. Gozani, "The investigation of fast neutron Threshold Activation Detectors (TAD)", in *2nd Iinternational Workshop on Fast Neutron Detetctors and Applications,* November 6–11, 2011, Ein Gedi, Israel, 2012.

[63] J. Stevenson et al., "Linac based photofission inspection system employing novel detection concepts", *Nuclear Instruments and Methods in Physics Research Section A: Accelerators, Spectrometers, Detectors and Associated Equipment*, vol. 652, no. 1, pp. 124–128, 2011.

[64] K. A. Jordan et al., "Improving differential die-away analysis via the use of neutron poisons in detectors", *Nuclear Instruments and Methods in Physics Research Section A: Accelerators, Spectrometers, Detectors and Associated Equipment*, vol. 579, no. 1, pp. 404–406, 2007.

[65] A. Danagoulian et al., "Prompt neutrons from photofission and its use in homeland security applications", in *2010 IEEE International Conference on Technologies for Homeland Security (HST)*, Nov. 2010, pp. 379–384.

[66] W. Klamra, P. Sibczynski, et al., "Extensive studies on light yield non-proportional response of undoped CeF_3 at room and liquid nitrogen temperatures", *Journal of Instrumentation*, vol. 8, pp. P06003, 2013.

[67] W. Klamra, P. Sibczynski, et al., "Light yield nonproportionality of doped CeF_3 scintillators", *Journal of Instrumentation*, vol. 9, pp. P07013, 2014.

[68] EJ-313 datasheet, website: *http://www.eljentechnology.com/index.php/products/liquid-scintillators/74-ej-313* (last accessed: 13.07.2015).

[69] National Institute of Standards and Technology (NIST), "ESTAR Database, website: *http://physics.nist.gov/PhysRefData/Star/Text/ESTAR.html* (last accessed 13.07.2015)".

[70] S. Agarwal et al., "Synthesis, characterization and properties evaluation of copolymers of 2,3,4,5,6-pentafluorostyrene and N-phenylmaleimide", *Polymer International*, vol. 54, no. 12, pp. 1620–1625, 2005.

[71] L. Lou et al., "Synthesis and properties of copolymers of methyl methacrylate with 2,3,4,5,6-pentafluoro and 4-trifluoromethyl 2,3,5,6-tetrafluoro styrenes: An intrachain interaction between methyl ester and fluoro aromatic moieties", *Journal of Polymer Science Part A: Polymer Chemistry*, vol. 48, no. 22, pp. 4938–4942, 2010.

[72] R. Hofstadter, "The detection of gamma-rays with thallium-activated sodium iodide crystals", *Physical Review*, vol. 75, pp. 796–810, Mar. 1949.

[73] M. Moszyński et al., "Intrinsic energy resolution of NaI(Tl)", *Nuclear Instruments and Methods in Physics Research Section A: Accelerators, Spectrometers, Detectors and Associated Equipment*, vol. 484, no. 1-3, pp. 259–269, 2002.

[74] P. Sibczynski et al., "Study of NaI(Tl) scintillator cooled down to liquid nitrogen temperature", *Journal of Instrumentation*, vol. 7, no. 11, pp. P11006, 2012.

[75] Canberra Industries, "Neutron detection and counting", 2010.

[76] S. Korolczuk et al., "Digital approach to high count rate gamma-ray spectrometry", *Submitted to IEEE Trans. Nucl. Sci.*, 2015.

[77] D.C. Radford, "Radware software, website: *http://radware.phy.ornl.gov/main.html* (last accessed 13.07.2015)", 2000.

[78] J. Kowalczyk, "mult2d software, Heavy Ion Laboratory, University of Warsaw", Unpublished, 2001.

[79] A. Sonzogni, "National Nuclear Data Center (NNDC), Chart of Nuclides, website: *http://www.nndc.bnl.gov/chart/* (last accessed 13.07.2015)", 2012.

[80] F. Carrel et al., "Detection of high-energy delayed gammas for nuclear waste packages characterization", *Nuclear Instruments and Methods in Physics Research Section A: Accelerators, Spectrometers, Detectors and Associated Equipment*, vol. 652, no. 1, pp. 137–139, 2011.

[81] Hamamatsu R2059 PMT manual, website: *http://www.hamamatsu.com/us/en/R2059.html* (last accessed 13.07.2015.).

[82] M. Bertolaccini et al., "A technique for absolute measurement of theeffective photoelectron per keV yield in scintillation counters", in *Nuclear Electronics Symposium,* Versailles, France, 1968.

[83] M. Moszyński et al., "Absolute light output of scintillators", *IEEE Transactions on Nuclear Science*, vol. 44, no. 3, pp. 1052–1061, Jun. 1997.

[84] L. Swiderski et al., "Measurement of Compton edge position in low-Z scintillators", *Radiation Measurements*, vol. 45, no. 3–6, pp. 605–607, 2010, *Proceedings of the 7th European Conference on Luminescent Detectors and Transformers of Ionizing Radiation (LUMDETR 2009).*

[85] M. Moszyński et al., "Characterization of scintillators by modern photomultipliers - a new source of errors", *IEEE Transactions on Nuclear Science*, vol. 57, no. 5, pp. 2886–2896, Oct. 2010.

[86] Z. Guzik et al., "TUKAN-an 8K pulse height analyzer and multi-channel scaler with a PCI or a USB interface", *IEEE Transactions on Nuclear Science*, vol. 53, no. 1, pp. 231–235, Feb. 2006.

[87] Ortec Detective EX series HPGe radioisotopes finder, website: *http://www.ortec-online.com/Products-Solutions/Hand-Held-Radioisotope-Identifiers-Detective.aspx* (last accessed 13.07.2015).

[88] identiFINDER radio-isotope identification, website: *http://www.flir.com/threatdetection/display/?id=65349* (last accessed 13.07.2015).

[89] A. Luca et al., "Experimental determiantion of the uranium enrichment ratio", *Romanian Journal of Physics*, vol. 53, pp. 35–39, 2008.

[90] M. Garcia-Talavera et al., "Coincidence summing corrections for the natural decay series in γ-ray spectrometry", *Applied Radiation and Isotopes*, vol. 54, pp. 769–776, 2001.

[91] T. W. Burrows, "Nuclear data sheets update for A = 95", *Nuclear Data Sheets*, vol. 68, no. 3, pp. 635–746, 1993.

[92] G. C. Carlson et al., "Half-lives of some short-lived mass-separated gaseous fission products and their daughters", *Nuclear Physics A*, vol. 125, no. 2, pp. 267–275, 1969.

[93] E. Monnand et al., "Desintegration de ^{138}Xe", *Nuclear Physics A*, vol. 195, pp. 192–206, 1972.

[94] L. C. Carraz et al., "Isomerie nucleaire dans ^{138}Cs et ^{138}Ba", *Nuclear Physics A*, vol. 171, no. 1, pp. 209–224, 1971.

[95] J. H. Hubbell et al., "Radiation and Biomolecular Physics, PML, NIST", 2011.

[96] R. B. Firestone et al., *WWW Table of Radioactive Isotopes*, 2004.

[97] H. Rennhofer et al., "Detection of SNM by delayed gamma rays from induced fission ", *Nuclear Instruments and Methods in Physics Research Section A: Accelerators, Spectrometers, Detectors and Associated Equipment*, vol. 652, no. 1, pp. 140–142, 2011, *Symposium on Radiation Measurements and Applications, SORMA XII, 2010.*

[98] M. Gmar et al., "Detection of nuclear material by photon activation inside cargo containers", *SPIE Defense and Security Symposium,* Orlando, Florida, 2006.

[99] H.W. Schmitt et al., "Total neutron cross section of ^{10}B in the thermal neutron energy range", *Nuclear Physics*, vol. 17, pp. 109–115, 1960.

[100] A. Sari et al., "Characterization of the photoneutron flux emitted by an electron accelerator using an activation detector", *IEEE Transactions on Nuclear Science*, vol. 60, no. 2, pp. 693–700, Apr. 2013.

[101] K. Wincel et al., "Monte Carlo simulation of high-pressure ^{3}He detector response to ^{252}Cf neutron source", *NCBJ Annual Report*, 2014.

[102] R. Reifarth et al., "Background identification and suppression for the measurement of (n,γ) reactions with the DANCE array at LANSCE", *Nuclear Instruments and Methods in Physics Research Section A: Accelerators, Spectrometers, Detectors and Associated Equipment*, vol. 531, no. 3, pp. 530–543, 2013.

[103] G. Knoll, *Radiation Detection and Measurements*, John Wiley & Sons, Inc., 1999.

[104] L. Swiderski et al., "Electron response of some low-Z scintillators in wide energy range", *Journal of Instrumentation*, vol. 7, no. 06, pp. P06011, 2012.

[105] Z. Y. Wei et al., "Light yield and surface treatment of barium fluoride crystals", *Nuclear Instruments and Methods in Physics Research Section B: Beam Interactions with Materials and Atoms*, vol. 61, pp. 61 – 66, 1991.

[106] M. Laval et al., "Barium fluoride - inorganic scintillator for subnanosecond timing", *Nuclear Instruments and Methods in Physics Research*, vol. 206, no. 1–2, pp. 169–176, 1983.

[107] P. Dorenbos et al., "Absolute light yield measurements on BaF_2 crystals and the quantum efficiency of several photomultiplier tubes", *IEEE Transactions on Nuclear Science*, vol. 40, pp. 424–430, Aug. 1993.

[108] "International standard ISO 8529, reference neutron radiations - part 1: Characteristics and methods of production, ISO 8529-1:2001".

[109] L. A. Wall et al., "Solid polyperfluorostyrene and method of preparation, US Patent no US3546191 A", 1970.

[110] M. Hamel et al., "Preparation and characterization of highly lead-loaded red plastic scintillators under low energy X-rays", *Nuclear Instruments and Methods in Physics Research Section A: Accelerators, Spectrometers, Detectors and Associated Equipment*, vol. 660, no. 1, pp. 57–63, 2011.

[111] G. Turk et al., "Development of an x-ray imaging system for the Laser Megajoule (LMJ)", *Review of Scientific Instruments*, vol. 81, no. 10, pp. 10E509, Oct. 2010.

[112] EJ-200 plastic scintillator data sheet, website: *http://www.eljentechnology.com/index.php/products/plastic-scintillators/48-ej-200* (last accessed 13.07.2015).

[113] J. B. Birks, *The Theory and Practice of Scintillation Counting*, International Series of Monographs in Electronics and Instrumentation. Pergamon, 1964.

[114] A. Nassalski et al., "Non-proportionality of organic scintillators and BGO", *IEEE Transactions on Nuclear Science*, vol. 55, no. 3, pp. 1069–1072, Jun. 2008.

[115] I.V. Khodyuk et al., "Trends and patterns of scintillator nonproportionality", *IEEE Transactions on Nuclear Science*, vol. 59, no. 6, pp. 3320–3331, Dec. 2012.

[116] J. Iwanowska et al., "Neutron/gamma discrimination properties of composite scintillation detectors", *Journal of Instrumentation*, vol. 6, no. 07, pp. P07007, 2011.

[117] J. Iwanowska-Hanke et al., "Comparative study of large samples (2" × 2") plastic scintillators and EJ309 liquid with pulse shape discrimination (PSD) capabilities", *Journal of Instrumentation*, vol. 9, no. 06, pp. P06014, 2014.

[118] S. A. Pozzi et al., "Pulse shape discrimination in the plastic scintillator EJ-299-33", *Nuclear Instruments and Methods in Physics Research Section A: Accelerators, Spectrometers, Detectors and Associated Equipment*, vol. 723, pp. 19–23, 2013.

[119] H. P. Martinez et al., "Pulse shape discrimination in non-aromatic plastics", *Nuclear Instruments and Methods in Physics Research Section A: Accelerators, Spectrometers, Detectors and Associated Equipment*, vol. 771, pp. 28–31, 2015.

[120] P. Blanc et al., "Neutron/gamma pulse shape discrimination in plastic scintillators: Preparation and characterization of various compositions", *Nuclear Instruments and Methods in Physics Research Section A: Accelerators, Spectrometers, Detectors and Associated Equipment*, vol. 750, pp. 1–11, 2014.

[121] P. Blanc et al., "Intrinsic evaluation of n/γ discrimination in plastic scintillators", *IEEE Transactions on Nuclear Science*, vol. 61, no. 4, pp. 1995–2005, Aug. 2014.

[122] N. Zaitseva et al., "Scintillation properties of solution-grown trans-stilbene single crystals", *Nuclear Instruments and Methods in Physics Research Section A: Accelerators, Spectrometers, Detectors and Associated Equipment*, vol. 789, pp. 8–15, 2015.